



國立臺灣大學理學院化學系

博士論文

Department of Chemistry

College of Science

National Taiwan University

Doctoral Dissertation

以胜肽探針研究漸凍人症中聚甘胺酸-丙胺酸雙肽蛋白質
以及 TDP-43 蛋白質之病理現象

Induction of Glycine-alanine Dipeptide Repeats and TDP-43
Proteinopathies by Peptide Probes for ALS Studies

簡鴻名

Hung-Ming Chien

指導教授： 陳玉如 博士 (Yu-Ju Chen, Ph.D.)

黃人則 博士 (Jen-Tse Huang, Ph.D.)

中華民國一百一十年八月

August 2021

國立臺灣大學博士學位論文

口試委員會審定書

(論文中文題目) 以胜肽探針研究漸凍人症中聚甘胺酸-丙胺酸雙肽蛋白質以及 TDP-43 蛋白質之病理現象

(論文英文題目) Induction of Glycine-alanine Dipeptide Repeats and TDP-43 Proteinopathies by Peptide Probes for ALS Studies

本論文係 簡鴻名 君 (學號 D04223206) 在國立臺灣大學化學系完成之博士學位論文, 於民國 110 年 8 月 4 日承下列考試委員審查通過及口試及格, 特此證明。

口試委員:

黃人則 陳玉如

(簽名)

(指導教授)

黃中化

陳儀莊

吳昌峰

梁文傑

系主任、所長

(簽章)

Acknowledgement



First, I would like to thank my advisor **Dr. Joseph Jen-Tse Huang** and **Dr. Yu-Ru Chen** for their substantial assistance and valuable suggestions in regard to scientific research, career counseling, and life philosophy. Thank Joseph for always treating me as a true friend, encouraging my creativity, and further allowing me to improvise. Thank **Dr. Yijuang Chern**, **Dr. Eric Hwang**, and **Dr. Kuen-Phon Wu** for enlightening me on the road of science research and sincerely pointing out the insufficiency of my work for the further improvements.

Along the way, I have to thank many people in the lab for providing me a wide scope in chemical biology and generously giving me plentiful advice to overcome experimental difficulties. Thanks **Dr. Jye-Chian Hsiao**, **Dr. Ruei-Yu He**, **Dr. Chi-Chang Lee**, and **Dr. Yung-An Huang** for all constructive suggestions and experimental supports. Thank **Po-Wen Chen**, **Yu-Ju Tsai**, **Chu-Yi Yu**, **I-Ju Hung**, **Zhao-Wei Peng**, **Kai-Ting Hou**, **Po-Chao Lu**, **Shih-Ying Cheng**, and **Diksha Agnihotri** for your significant contribution to my research work. I also received many favors from people in other institutes, including **Dr. Po-Yen Lin** and **Yao-Kwan Huang** from institute of cellular and organismic biology, **Sue-Ping Lee** and **Shu-Mei Huang** from institute of molecular biology, and **Dr. Hao Ho** from institute of statistics. I sincerely appreciated all your help.

Finally, I would like to express my deep gratitude to Betty for the great favors on everything. Your wholehearted support is always the beacon of belief to me in the stressed time. It is my tremendous honor to have you around.



摘要

在腦中所發現之蛋白質包含體為漸凍人症候群中的主要病徵，其亦被懷疑與疾病的發展有關。而 TDP-43 蛋白質作為病患組織中蛋白質包含體的主要成分，其經常被發現具有過度磷酸化、過度泛素化之現象，同時此蛋白質亦可進一步遭受裁剪而成具類澱粉蛋白性質之片段。除了 TDP-43 蛋白質以外，近期的研究發現自第九號染色體之第七十二號開放閱讀框突變基因轉譯之甘胺酸-丙胺酸雙肽蛋白質 (Glycine-alanine dipeptide repeats) 亦沉積於病患之神經元中，且其亦具類澱粉蛋白質之特性。隨著越來越多的研究表明 TDP-43 蛋白質與甘胺酸-丙胺酸雙肽蛋白質於疾病中可能扮演著重要的角色，針對這些蛋白質的定性實驗亦顯得更加重要。然而，這些蛋白質的生物物理與生物化學性質之研究卻由於其溶解度與快速聚集等因素而備受阻礙。

為了克服這些困難以研究這些蛋白質之特性，我們設計並利用固相化學方法合成了一系列的胜肽探針，其由甘胺酸-丙胺酸雙肽蛋白質片段、八離胺酸肽片段 (Octalysine)、與甲氧基硝基苯 (Methoxynitrobenzene) 衍生物作為橋接所組成。這些探針可有效的增進甘胺酸-丙胺酸雙肽蛋白質片段之溶解度、預防其片段自我聚集、並能夠於細胞中藉由紫外光照實行可控制之釋放。利用此探針並結合顯微鏡技術，我們發現甘胺酸-丙胺酸雙肽蛋白質片段會先行組裝成類澱粉蛋白質寡聚物 (Amyloid oligomer) 並進一步聚集成類澱粉蛋白質纖維；此胜肽探針亦可幫助釐清甘胺酸-丙胺酸雙肽蛋白質片段之詳細生物物理與生物化學特性。另外，藉由表達可於核質穿梭之螢光蛋白質於細胞系統內，我們發現到甘胺酸-丙胺酸雙肽蛋白質片段會導致細胞內之核質運輸功能異常。而利用電子顯微鏡觀察探針處理過後之細胞切片，我們亦注意到此片段會引起細胞核膜之內陷與不正常之折疊；另一方面，於進一步的免疫染色與生物化學實驗中，我們亦證實了甘胺酸-丙胺酸雙肽蛋白質片段類澱粉蛋白質寡聚物可引起脂質膜之穿透性增加。我們亦於後續的細胞實驗

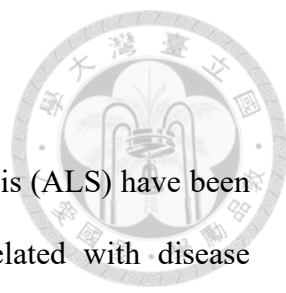
中發現甘胺酸-丙胺酸雙肽蛋白質片段可引起 TDP-43 蛋白質於細胞質內之不正常堆積，其現象與先前文獻所報導之病理特徵相似。

事實上，除了甘胺酸-丙胺酸雙肽蛋白質外，亦有研究證明了 TDP-43 蛋白質羧基端之裁剪片段亦可於細胞內引起 TDP-43 之蛋白質病理。因此，我們設計並合成了於還原環境中藉由雙硫鍵觸發之自釋放胜肽探針以研究 TDP-43 蛋白質羧基端之裁剪片段之堆疊。我們於此研究中仔細地觀測其胜肽探針裂解過程與釋放出之 TDP-43 片段之類澱粉蛋白質特性。

總結來說，我們成功利用甲氧基硝基苯或雙硫鍵之化學以設計並製備了一系列之胜肽探針。我們更進一步於其相對應之系統中，詳細觀測了 TDP-43 蛋白質裁剪片段與甘胺酸-丙胺酸雙肽蛋白質片段之生物物理與生物化學性質。我們期許在未來可藉由這些蛋白質片段之定性研究成果來幫助釐清漸凍人疾病發生之病因。

關鍵詞：漸凍人症、C9orf72、類澱粉蛋白質、胜肽探針、甘胺酸-丙胺酸雙肽蛋白質、TDP-43 蛋白質

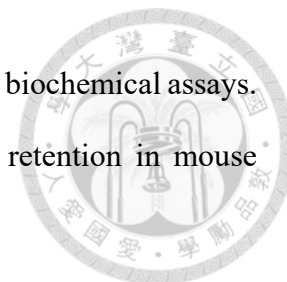
Abstract



Protein inclusions in the brains with amyotrophic lateral sclerosis (ALS) have been suggested as the most common pathological hallmark and correlated with disease progression. As a major component of pathological inclusions, transactive response DNA binding protein 43 (TDP-43) was hyperphosphorylated, hyperubiquitinated, and further truncated into fragments with amyloid properties in patient. In addition to TDP-43, glycine-alanine dipeptide repeats (GA DPRs) translated from the mutated chromosome 9 open reading frame 72 (*C9orf72*) gene has been recently identified in the cytoplasm of neurons with amyloid properties. Though collective evidence has demonstrated that both TDP-43 and GA DPRs inclusions may play pivotal roles in the disease pathology, their detailed biophysical and biochemical characterization were impeded due to poor solubility and rapid polymerization nature.

To overcome these difficulties, we have synthesized a series of chemical probes composed of a GA DPRs fragment and a octalysine sequence linking by a methoxynitrobenzene photolinker. These probes could efficiently enhance the solubility of GA DPRs, prevent them from self-assembly, and enable the controllable liberation in cells upon irradiation of UV light. By employing these probes and advanced microscopies, we have shown GA DPRs first assemble into amyloid oligomers and then evolve into amyloid fibrils. The detailed biophysical and amyloid properties of GA DPRs were characterized. By the ectopic expression of shuttling reporter protein in neuron-like cells, we demonstrated GA DPRs cause the nucleocytoplasmic transport dysregulation. In this regard, we also noticed GADPRs have caused the nuclear depletion of Ran protein and cytosolic diffusion of importin- β . Additionally, GA DPRs released from the probe were found to cause the invagination of nuclear envelope by transmission electron microscopy observation. We further identified it is the GA DPRs amyloid oligomers rather than fibrils

permeabilize the lipid membrane through immunohistochemistry and biochemical assays. Moreover, we noticed GA DPRs could lead to TDP-43 cytosolic retention in mouse cortical neurons, which is consistent with the previous studies.



In fact, it has also been shown that TDP-43 C-terminal peptide fragments could initiate TDP-43 proteinopathy in addition to GA DPRs. Therefore, we also prepared a disulfide bond triggering auto-releasing probe designed for the liberation of TDP-43 fragment upon reducing environment. The detailed cleavage process and the amyloidogenesis properties were monitored in this study and the following cellular studies are still ongoing now.

Conclusively, we have successfully designed and synthesized peptide probes on the basis of either methoxynitrobenzene photochemistry or disulfide bond chemistry. By applying these probes on suitable platforms, we explored the biophysical properties and detailed proteinopathy of GA DPRs and TDP-43 C-terminal fragment, which may eventually shed light on ALS pathology in the future.

Keywords : Amyotrophic lateral sclerosis, C9orf72, Amyloid, Peptide probe, Glycine-alanine dipeptide repeats, TDP-43

Table of Contents



Acknowledgement	ii
摘要	iii
Abstract.....	v
Table of Contents	vii
List of Figures	ix
List of Tables	x
List of Abbreviations.....	xi
<i>Chapter 1 : Photoinduced GA DPRs Oligomers Disrupted the Nuclear Membrane and Caused TDP-43 Cytosolic Retention</i>	1
I. Introduction.....	1
1-1 Amyotrophic lateral sclerosis.....	1
1-2 <i>C9orf72</i> gene mutation in ALS	3
1-3 The roles of GA DPRs in ALS pathology	13
1-4 Correlations between GA DPRs and TDP-43	14
1-5 Research aims and experimental design	15
II. Material and Methods	21
2-1 Material and instruments list.....	21
2-2 Probe preparation and identification.....	23
2-3 General sample preparation for <i>in vitro</i> measurements	25
2-4 Circular dichroism spectroscopy.....	25
2-5 Dye-binding assay	26
2-6 Turbidity measurements	26
2-7 Dot-blot assay	26
2-8 Infrared Spectroscopy.....	27
2-9 Transmission electron microscopy	27
2-10 Dynamic light scattering	28
2-11 Fluorescence-lifetime imaging microscopy.....	28
2-12 Direct stochastic optical reconstruction microscopy.....	30
2-13 Cell maintenance, Transfection, and Probe treatment.....	31
2-14 Cell lysate staining.....	32
2-15 Immunohistochemistry and Confocal microscopy.....	33
2-16 Total internal reflection fluorescence microscopy.....	33
2-17 <i>Ex vivo</i> antibody accessibility assay	34
2-18 Calcein-leakage assay	34
2-19 Seeding assay	35
2-20 Primary cortical neurons culture, Probe treatment and Neurite	

Fragmentation Analysis	36
2-21 Imaging quantification and Statistical analysis	37
III. Results	41
3-1 Preparation of photoinducible GA DPRs probes	41
3-2 Biophysical & biochemical characterization of GA DPRs	43
3-3 GA DPRs formed amyloid oligomers and turned into fibrils.	46
3-4 GA DPRs caused nucleocytoplasmic transport defects.....	50
3-5 GA DPRs compromised nuclear membrane	59
3-6 GA DPRs induced endogenous TDP-43 mislocalized to cytoplasm	67
3-7 Introduction of GA DPRs promote degeneration in mouse cortical neurons.....	70
IV. Discussion	73
4-1 ADP-1 as a feasible tools for <i>C9orf72</i> pathology studies	73
4-2 GA DPRs amyloid oligomers and their toxicities.....	74
4-3 Comparison between GA and PR DPRs in nuclear transport defect	75
4-4 Conclusion and prospect	76
V. Reference	78
<i>Chapter 2 : Developing the Auto-releasing Peptide Probe for Protein Fragment Aggregation Studies</i>	
I. Introduction.....	86
1-1 Amyloidogenic sequence of TDP-43 in ALS.....	86
1-2 Delivery of peptides and proteins into cytoplasm	87
1-3 Research aim and experimental design.....	88
II. Material and Methods	90
2-1 Material and instruments list.....	90
2-2 Synthesis and characterization of auto-releasing probe	91
2-3 General sample preparation for in vitro measurements.....	93
2-4 UV-Vis spectroscopy	93
2-5 Transmission electron microscopy	93
III. Results	94
3-1 Preparation of probe JJS-4 & JJS-5	94
3-2 <i>In vitro</i> characterization of auto-releasing probes	97
IV. Discussion	99
4-1 Comparison between photoinducible probe and auto-releasing probe	99
4.2 Conclusion and prospect	100
V. Reference	101

List of Figures

Figure 1. C9orf72 RNA transcript variants	4
Figure 2. Potential mechanism of C9orf72 mutation in ALS.....	6
Figure 3. Design of photoinducible probe ADP-1 and its cleavage mechanism	18
Figure 4. The HPLC and mass spectra of ADP-1 and its photoinitiated products.	41
Figure 5. HPLC and Mass spectra of ADP-2, ADP-3, and ADP-4	42
Figure 6. Biophysical characterization of the GA DPRs from ADP-1	44
Figure 7. GA DPRs formed amyloid fibrils after photoinitiation	47
Figure 8. Fluorophore-labeled GA DPRs formed compact fibrillar structure	49
Figure 9. GA DPRs oligomerized in cells	51
Figure 10. GA DPRs cause mislocalization of nuclear transport relevant proteins	54
Figure 11. GA DPRs disrupted the nucleocytoplasmic transport	57
Figure 12. GA DPRs compromised nuclear membrane.....	60
Figure 13. GA DPRs oligomers permeabilized nuclear membrane	63
Figure 14. GA DPRs permeabilized lipid membrane.....	66
Figure 15. GA DPRs induced mislocalization of endogenous TDP-43.....	68
Figure 16. GA DPRs induced cytosolic retention of TDP-43 and degeneration in mouse cortical neurons	72
Figure 17. Model of auto-releasing probe and its anticipated reaction in cells	89
Figure 18. Synthesis scheme of JJS-4 and JJS-5.....	95
Figure 19. Disulfide bond exchange reaction monitoring and identification of JJS-4 and JJS-5	96
Figure 20. GSH mediated reductive cleavage of JJS-4	98

List of Tables

Table 1. Sequence of peptides used in this study and their molecular mass.....	24
--	----



List of Abbreviations



<i>Abbreviation</i>	<i>Full Name</i>
DNA	Deoxyribonucleic Acid
RNA	Ribonucleic Acid
mRNA	Messenger Ribonucleic Acid
ALS	Amyotrophic Lateral Sclerosis
SOD1	Superoxide Dismutase-1
TDP-43	TAR DNA-binding Protein 43
HRE	Hexanucleotide Repeat Expansion
C9orf72	Chromosome 9 Open Reading frame 72
DPRs	Dipeptide Repeats
iPSC	Induced Pluripotent Stem Cells
RAN translation	Repeat Associated non-ATG Translation
GA	Glycine-Alanine
GR	Glycine-Arginine
GP	Glycine-Proline
PA	Proline-Alanine
PR	Proline-Arginine
GFP	Green Fluorescence Protein
HPLC	High-performance Liquid Chromatography
MALDI	Matrix-assisted Laser Desorption Ionization
PBS	Phosphate-buffered Saline
CD	Circular Dichroism
TEM	Transmission Electron Microscopy
FLIM	Fluorescence-lifetime Imaging Microscopy
dSTORM	Direct Stochastic Optical Reconstruction Microscopy
N-C ratio	Nuclear-to-cytoplasmic Ratio
LMB	Leptomycin B
IPZ	Importazole
Ran	RAs-related Nuclear Protein
mCNs	Mouse Cortical Neurons

Chapter 1 : Photoinduced GA DPRs Oligomers Disrupted the Nuclear Membrane and Caused TDP-43 Cytosolic Retention




I. Introduction

1-1 Amyotrophic lateral sclerosis

Amyotrophic lateral sclerosis (ALS) is a progressive disease that primarily affects the motor system and subsequently causes the death of motor neurons.¹ Typically, ALS patients present with muscle stiffness, progressive muscular atrophy, and eventually die of breathing difficulty. The onset of the disease is commonly found between the age of 55 to 75, and the average survival from onset to death is 2 to 5 years.² Judging by the family history of the disease, ALS can be classified as sporadic (occur at random) or familial (patients have first-degree or second-degree relatives who also have ALS).¹ The majority of ALS cases (90 to 95 %) are sporadic. Despite several drugs (Riluzole, Edaravone, and Creatine) have been developed to delay the disease progression, there are yet no effective treatments against ALS.³

Currently, both environmental factors and genetic factors are considered to contribute to ALS pathologies.⁴ Through epidemiological studies, smoking and chronic exposure to heavy metal, such as lead (Pb), mercury (Hg), and selenium (Se), have been identified as possible risk factors for ALS.⁵ However, the detailed pathological mechanism of how these environmental toxins cause ALS is still unknown.⁶



Apart from environmental factors, a number of genetic factors have been associated with ALS. To date, more than 25 genes have been identified in potential association with ALS.^{7,8} Among them, *SOD1*, encoded superoxide dismutase-1 (SOD1), was the first identified gene correlated with ALS.⁹ SOD1 is an enzyme that catalyzed redox reactions in cells, involving turning toxic superoxide into hydroperoxide and oxygen. Thus, SOD1 plays a significant role in oxidative stress reduction and apoptosis regulation.¹⁰ Collective findings suggested that mutation on SOD1 promote oxidative damage to mitochondria and induce gain-of-function toxicity in motor neurons, which may be a notably etiological factor in ALS.¹¹ Another hallmark discovery is the aberrant cytosolic accumulation of *TARDBP* gene encoded products, transactive response DNA-binding protein 43 (TDP-43), in brains of patients suffering from ALS.¹²⁻¹⁴ TDP-43, primarily resided at the nucleus, has versatile physiological functions, including mRNA transcription, splicing, transport and translation, non-coding RNAs processing, and stress granule formation.^{15,16} Remarkably, the majority of ALS patients (more than 95 %) share a common feature: TDP-43 deposition in the inclusion bodies, suggesting its critical role in the ALS pathology.^{17,18} Known proteinopathy of TDP-43 in ALS includes mislocalization from the nucleus to the cytoplasm, inclusion bodies comprised of hyperphosphorylated and hyperubiquitinated TDP-43, and toxic truncated C-terminal products.^{14,19,20} Genetic mutations of TDP-43 have been identified to promote the cytosolic accumulation,

accelerated aggregation rate, alter protein stability, and interfere with the protein-protein interactions.²¹⁻²³ Apart from *SOD1* and *TARDBP*, a characteristic mutation in chromosome 9 open reading frame 72 (*C9orf72*) gene has been recently identified to associate with ALS.

1-2 *C9orf72* gene mutation in ALS

The GGGGCC (G₄C₂) hexanucleotide repeat expansion (HRE) in *C9orf72*, discovered at 2011,^{24,25} is the most frequently found genetic cause in familial ALS from Europe and North American.²⁶ The *C9orf72* gene is comprised of 11 exons, has three RNA transcript variants, and produces two *C9orf72* protein isoforms, respectively short-form and long-form *C9orf72* proteins (*C9orf72*-S and *C9orf72*-L).²⁷ The *C9orf72* mutation is located at the first intron within the *C9orf72* gene (Figure 1). While the most of neurologically healthy individuals generally have ≤ 11 G₄C₂ hexanucleotide repeats in the *C9orf72* gene,²⁸⁻³⁰ longer hexanucleotide expansions from hundreds to thousands of repeats are frequently observed in the patients with *C9orf72*-ALS (C9-ALS).^{31,32} As a common genetic cause, *C9orf72* mutation accounts for 45 % in the cases with familial ALS, comparing to 20 % from *SOD1* mutation and 10 % from *TARDBP* mutation.¹ Apart from ALS, G₄C₂ expansion in *C9orf72* has also been found to associate with other

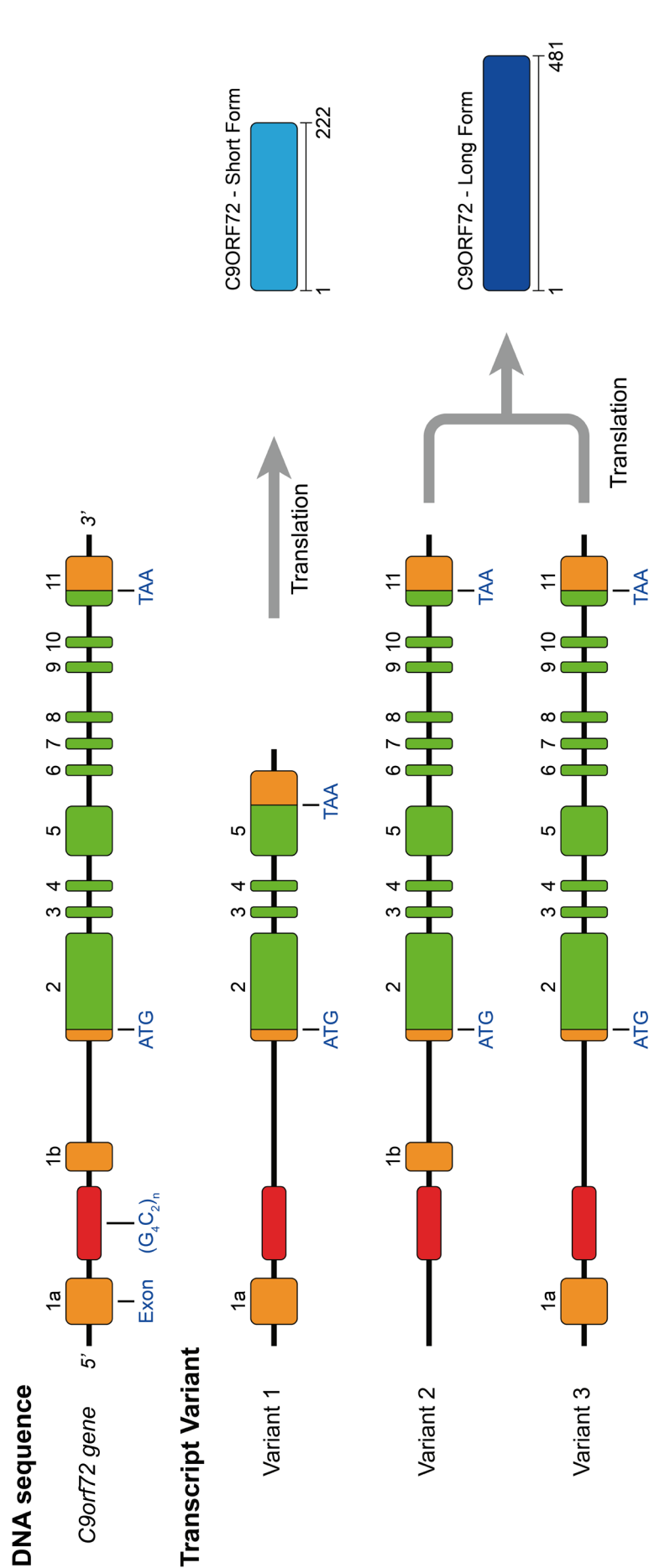


Figure 1. *C9orf72* RNA transcript variants.



neurodegenerative diseases,³³ suggesting its significant role in disease progression. Thus far, three major mechanisms have been proposed to explain how *C9orf72* mutation contributes to neurotoxicity, namely *C9orf72* loss-of-function, *C9orf72* transcripts gain-of-function, and dipeptide repeats (DPRs) pathology.

Loss-of-function of C9orf72 Protein Mechanism in C9-ALS

The reduced level of *C9orf72* mRNA variants in tissues from patients with C9-ALS³⁴ and the decreased level of the nuclear *C9orf72* proteins in patient-derived fibroblasts²⁴ indicated the loss-of-function mechanism may play a role in *C9orf72*-ALS (Figure 2).³⁵ Three pre-mRNA transcript variants are originated from *C9orf72* gene after alternatively splicing (Figure 1).^{36,37} While the transcript variant 1 translates into *C9orf72*-S protein, both the transcript variants 2 and 3 produce *C9orf72*-L proteins. The translated *C9orf72* protein is abundant in neurons, especially cortex and motor neurons.³⁸ It has been shown that the *C9orf72* proteins primarily localize to early endosomes and lysosomes in neuronal cell lines and induced pluripotent stem cells (iPSC)-derived motor neurons.³⁹ Though the detailed functions remain undetermined, studies have shown *C9orf72* proteins are associated with membrane trafficking and autophagy.⁴⁰ Knockdown of *C9orf72* in human neuron cell-lines reduced the endocytosis, disrupted the lysosomal and

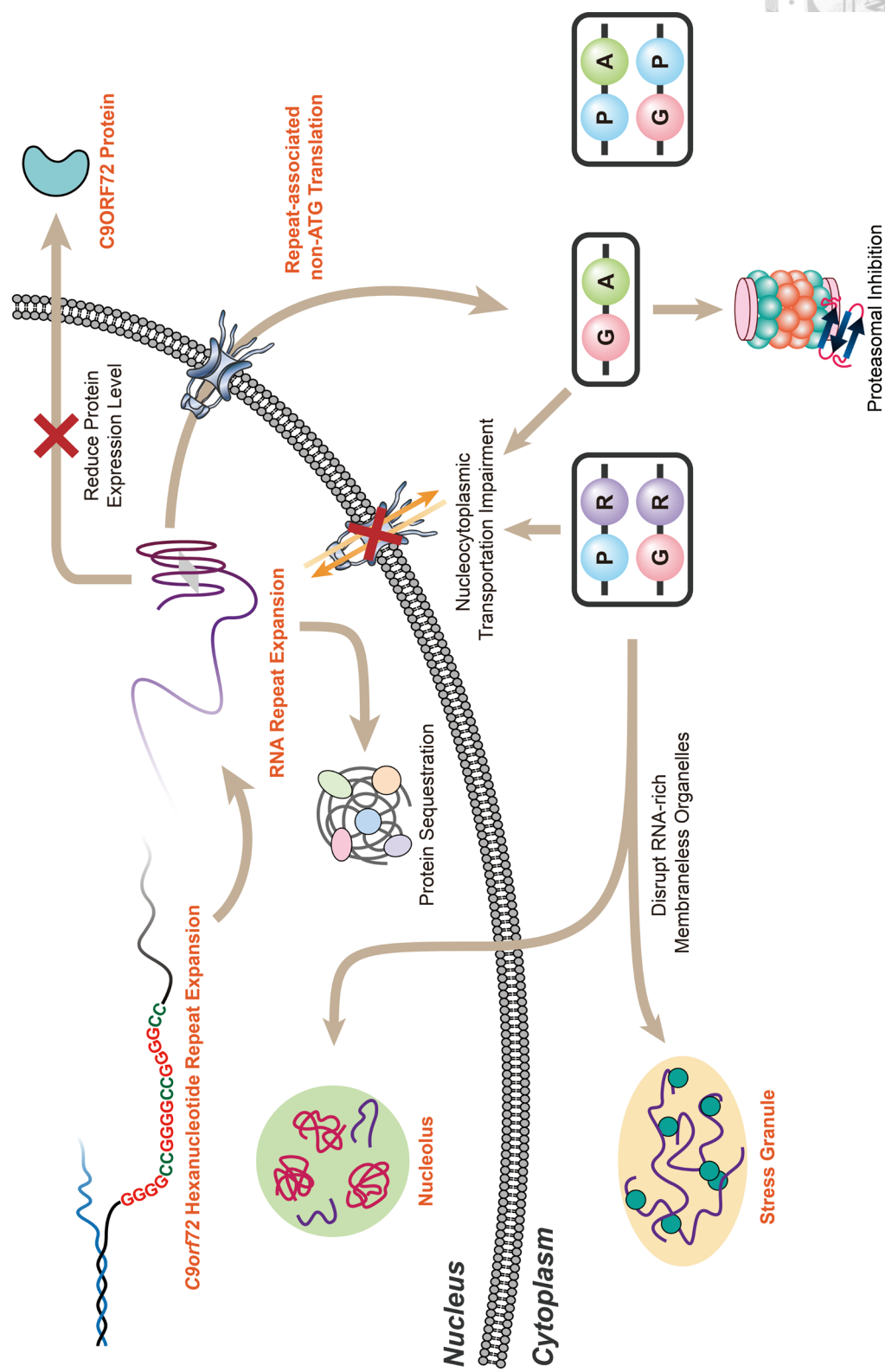
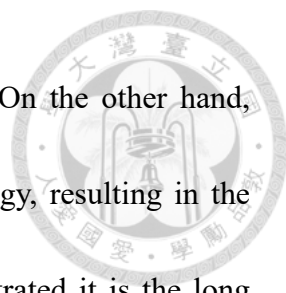


Figure 2. Potential mechanism of C9orf72 mutation in ALS.





endosomal trafficking, and inhibited the autophagy induction.⁴¹⁻⁴⁴ On the other hand, overexpressing of C9orf72 protein in cell model activated autophagy, resulting in the formation of autophagosomes.⁴⁵ Further experiments have demonstrated it is the long isoform rather than short isoform C9orf72 protein that mediates the autophagy via the involvement of Rab proteins.⁴³ Interestingly, reduction of long C9orf72 protein isoform level and increase of short C9orf72 protein isoform level were detected in the brain affected by C9-ALS.⁴⁶ Systematic studies revealed mutated C9orf72 G4C2 HRE can disrupt the polymerase process during transcription, and thereby result in aberrant C9orf72 expression level.⁴⁷⁻⁴⁹ Moreover, increasing evidence suggested that cells can epigenetically silence the mutant *C9orf72* allele by hypermethylation of CpG islands in the promoter region upstream of the G4C2 repeats in order to respond to the presence of *C9orf72* HRE.^{50,51} As the pathogenic G4C2 repeat length increased, the hypermethylation level in CpG island rises, and thereby *C9orf72* transcription reduces.^{52,53} Furthermore, analysis of tissue samples from C9-ALS patients revealed G4C2 repeat expansion is also methylated;⁵² however, the influence of G4C2 methylation on disease progression is yet inconclusive. Taken together, these results highlighted the important role of C9orf72 in cellular trafficking and autophagy, and the loss of C9orf72 in neuronal or glial cells might cause cellular stress and further contribute to neurotoxicity.

Toxicities from C9orf72 G₄C₂ Hexanucleotide Expansion

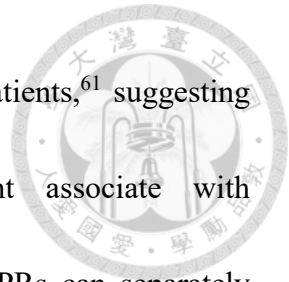


The accumulation of G₄C₂ repeat expansion foci in brain tissues from patients with C9-ALS hints the RNA gain-of-function mechanism may correlate with C9-ALS pathology (Figure 2).⁵⁴⁻⁵⁶ *In vitro* studies demonstrated both sense (G₄C₂) and antisense (C₄G₂) repeat RNA can form secondary structures, such as duplexes, hairpins, i-motifs, and highly stable G-quadruplexes.^{2,57} Moreover, *in vivo* studies suggested these secondary structures could interact and sequester several RNA-binding proteins, including heterogeneous nuclear ribonucleoproteins (hnRNPs), Ran GTPase-activating protein (RanGAP), nucleolins, and THO complexes.^{48,58-60} It is noteworthy to mention the affinity between RNA-binding proteins and *C9orf72* repeat expansion is dependent on the secondary structure of G₄C₂ RNA. For instance, RanGAP1 and nucleolin tended to bind the G-quadruplex structure, while hnRNPs H isoform binds to both RNA G-quadruplex and hairpin structures with no preference.^{48,59} Consequently, sequestration of these RNA-binding proteins would give rise to nucleolar dysfunction, RNA processing (splicing and editing) perturbation, and nucleocytoplasmic trafficking impairment. In brief, along with other neuronal stressors, *C9orf72* G₄C₂ RNA foci might together result in the arrestment of several cellular functions and finally lead to neurodegeneration.

Gain-of-function Mechanism of RAN Translational Product: Dipeptide Repeats

Another proposed gain-of-function mechanism to explain the *C9orf72* pathology in ALS is the toxicities of dipeptides repeats (DPRs) produced by G₄C₂ repeat expansion through repeat associated non-ATG translation (RAN translation) (Figure 2).⁶¹ Normally, initiation of protein translation involves the recruitment of small and large ribosomal subunits, initiation factors, and methionine-charged tRNA on the 5'-end of mRNA. As an initiator, methionine-charge tRNA will recognize the start codon, AUG, on mRNA, so the protein synthesis started. It follows by recruiting the aminoacyl-tRNA positioned at the adjacent site in the ribosome and subsequently formation of the peptidyl bond through the dehydration between primary amine and carboxylic acid. Nevertheless, a study from Zu *et al.* in 2011 discovered that the repeat expansion (CAG) mutations could be translated into poly-glutamine, poly-alanine, and poly-serine proteins by multiple reading frames in the absence of canonical AUG start codon.⁶² Although the detailed mechanism of how translation initiating remained elusive, the fact we learn so far is that the RAN translation yield is largely dependent on the secondary structure and GC content of RNA.⁶³ Through this unconventional translation using all six reading frames from the sense and antisense strand of G₄C₂, five DPRs protein were produced: glycine-alanine (GA), glycine-arginine (GR), glycine-proline (GP), proline-alanine (PA), and proline-arginine (PR). A study published by Mori *et al.* in 2013 reported the detection of these

unnatural DPRs accumulation in the brain tissues from C9-ALS patients,⁶¹ suggesting dipeptide repeat pathology along with other causes might associate with neurodegeneration. Notably, emerging evidence indicated these DPRs can separately contribute to neurotoxicity through distinct mechanisms.⁶⁴

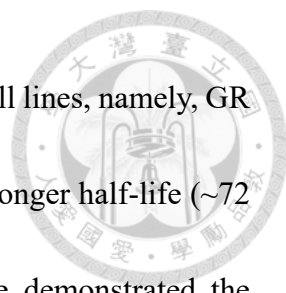


Current Understanding of GP and PA DPRs

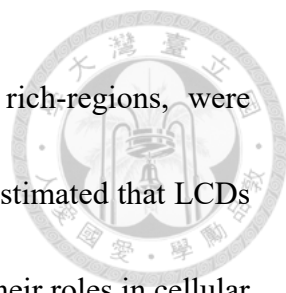
Among these DPRs, uncharged GP and PA DPRs, which mostly adopted random coil conformations, manifest no significant toxicity in cellular and *Drosophila* models.⁶⁵⁻
⁶⁷ Presumption of relatively inert property comparing to other *C9orf72* DPRs was confirmed by mass-based interactome study, which show no substantial interactions between these two DPRs and other proteins in cells.⁶⁷ Given the fact GP DPRs was highly expressed in the brain tissues and remain stable since translation, it has been suggested to serve the purpose of early detection marker for C9-ALS by evaluating its concentration in cerebrospinal fluid.⁶⁸

Toxicities of PR and GR DPRs

Due to their highly charged and polar nature, both PR and GR DPRs tends to form flexible random coil structure, tend to accumulate in the nucleoli where the ribosomes were manufactured, and cause similar toxicity toward neurons.^{65,69} Nevertheless, there is

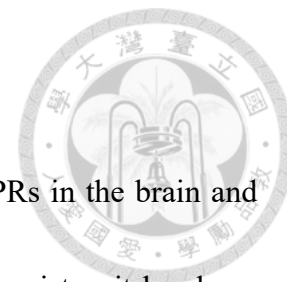


a clear distinction between PR and GR DPRs stabilities in cultured cell lines, namely, GR DPRs has a short (~30 minutes), whereas PR DPRs has a relatively longer half-life (~72 hours).⁶⁹ To assess their roles in pathology, different groups have demonstrated the toxicity of PR and GR DPRs in various model systems using direct peptide treatment or ectopic gene expression. Transfection of GFP-PR₅₀ in human iPSC-derived neurons showed nuclear aggregates of PR DPRs colocalized with nucleolin which is the major component of nucleolus.^{66,67} Moreover, in iPSC-derived induced motor neurons from C9-ALS patients, nuclear aggregates of PR DPRs were extensively found and the survival of neurons was significantly decreased. In addition, tissue-specific expression of PR and GR DPRs in *Drosophila* caused the severe damage to the eyes and neuronal tissues, indicating the toxicity of PR and GR DPRs.⁶⁵ To explain how PR and GR DPRs induce the toxicity in neurons, accumulating studies have pointed the finger at the interaction between these two arginine-rich DRPs and proteins with low-complexity domains (LCDs).^{70,71} Low-complexity domains are amino acid sequences on the proteins which have no preferential folding conformations and hence lack of well-defined three-dimensional structures under physiological conditions.⁷² Usually, LCD sequences are repetitive and highly enriched in nonpolar amino acid: glycine (G), polar amino acids: asparagine (N), glutamine (Q), and serine (S), amino acids with positive charge on sidechain: arginine (R) and lysine (K), and amino acids with aromatic rings on sidechain: phenylalanine (F) and tyrosine (Y).



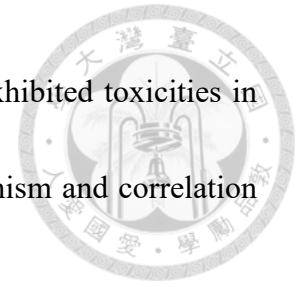
Small motifs, such as FG-, YG/S-, RG-, GY-, SY-, and Q/N rich-regions, were interspersed with alternating charge sequence in LCDs. It has been estimated that LCDs present in up to one-third of human proteome; therefore, dissecting their roles in cellular processes is pivotal to unravel unknown pathology.⁷³ Recent studies revealed the interactions between LCDs and other proteins or RNA are crucial to assembly and disassembly of membrane-less organelle, including stress granule, polysome, processing body, nuclear pore complex, paraspeckle, nucleolus, and Cajal body.⁷² Strikingly, mass-based interactome studies revealed that PR and GR DPRs interacted with proteins containing LCDs, and thereby change the intrinsic properties of these proteins.⁶⁷ For example, Lee *et al.* demonstrated that PR and GR DPRs could impair biophysical properties of nucleophosmin 1 (NMP1) *in vitro* and disrupt nucleolus and stress granule functions.⁶⁷ Also, Shi *et al.* have shown that PR₂₀ can bind to polymeric forms of FG repeat domains within the nuclear pore, and consequently lead to a change in the dynamic equilibrium of FG repeat domain and further cause nuclear transporting defect.⁷⁴ Additionally, in iPSC-derived motor neurons, cytoplasmic GR DPRs are capable of inducing oxidative stress and compromising mitochondrial functions.⁷⁵ In summary, these observations stated the high toxicity of arginine-rich DPRs from *C9orf72* mutation; however, their unstable nature and low abundance in human tissues comparing to other DPRs have raised open questions to their contribution to ALS pathology.

1-3 The roles of GA DPRs in ALS pathology



Comparing to other DPRs, GA DPRs is the most abundant DPRs in the brain and spinal cord from patients with C9-ALS.⁶¹ Through immunohistochemistry, it has been shown that GA DPRs form p62/ubiquitin-positive inclusion bodies in the cytoplasm of neurons. GA DPRs were prone to assemble into the parallel β -sheet structures and have a strong propensity to aggregate, forming planar ribbon-like fibrils in cells.^{76,77} Expressing GFP-(GA)₅₀ in the cultured neurons induced endoplasmic reticulum (ER) stress, impaired neurite outgrowth, and promoted apoptosis through the activation of the caspase-3.^{78,79} Moreover, emerging evidence revealed that GA DPRs would inhibit proteasome activity by direct sequestration of transport factor uncoordinated-119, ubiquilin-1, ubiquilin-2, and several proteasomal subunits (HR23A & HR23B).^{79,80} It has also been shown expressing GFP-(GA)₅₀ partially colocalized with nuclear envelope pore membrane protein 121 and Ran GTPase-activating protein 1, suggesting GA DPRs might disrupt nucleocytoplasmic transport even though the detailed mechanism was under debate. It is worthwhile to mention that expressing GFP-(GA)₅₀ in the male mice model caused a significant decrease in both brain and body weight.⁸⁰ The number of NeuN (known as neuronal nuclei)-positive neurons was significantly dropped in the motor cortex and in the CA3 region of hippocampus in the mice. Furthermore, these GFP-(GA)₅₀-expressed mice developed behavior defects including hyperactivity, anxiety-like behavior, and

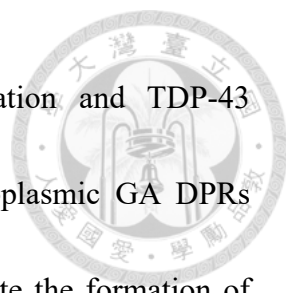
difficulties in learning and memory.⁸⁰ Taken together, GA DPRs exhibited toxicities in cellular, neuronal, and mice model, while the detailed pathomechanism and correlation with disease are still less clear.



During the amyloidogenesis process, amyloid oligomers may serve an important role in the initiation and propagation of the fibrillization process. Not until the last two decades, studies have disclosed that these amyloid oligomers could compromise several cellular functions and further induce inflammation of neurons.⁸¹ As a member of the amyloid family, GA DPRs are suspected to form amyloid oligomers during the amyloidogenesis process. Nevertheless, the GA DPRs oligomers have not yet been reported and characterized and thus their roles in C9-ALS pathology required further investigations.

1-4 Correlations between GA DPRs and TDP-43

As previously mentioned, TAR DNA-binding protein 43 (TDP-43) containing-inclusion bodies have been identified in most ALS patient's brains.^{14,17,18} It has also been reported that TDP-43 deposited in the neuronal cytoplasm in hippocampi from C9-ALS patients; however, the size of TDP-43 inclusions from C9-ALS patients is quantitatively smaller than those from sporadic ALS patients.⁸² Although the reason why TDP-43 mislocalization presenting in most ALS cases is undetermined, a few studies have




attempted to elucidate the relationship between *C9orf72* mutation and TDP-43 proteinopathy. Notably, a study published in 2017 indicated cytoplasmic GA DPRs aggregates would impair the nuclear import of TDP-43 and promote the formation of cytoplasmic TDP-43 granule.⁸³ Along this direction, another study published in 2018 revealed that GA DPRs inclusions could induce intracellular aggregation of endogenous phosphorylated TDP-43 (pTDP-43) in cultured cells.⁸⁴ Interestingly, it has also been shown the formation of pTDP-43 inclusions crucially depended on the repeat number of GA DPRs. Notwithstanding that the GA DPRs had strong propensity to aggregate, the conjugated green fluorescent protein (GFP) might greatly alter the intrinsic property of GA DPRs. Furthermore, detergent-insoluble fraction of lysates from cells co-expressing GA DPRs and TDP-43 was capable of seeding cellular TDP-43 and thereby induced TDP-43 aggregation.⁸⁴ Nevertheless, it was unclear how these insoluble fractions penetrated the plasma membrane and induce protein aggregation.

1-5 Research aims and experimental design

While more and more studies have attempted to investigate the proteinopathy of GA DPRs and their correlation with TDP-43, it is still challenging to clarify how they contribute to neurotoxicity due to the following issues:

- 1) Direct overexpression of DPRs in cell models by genetic transfection may lead to

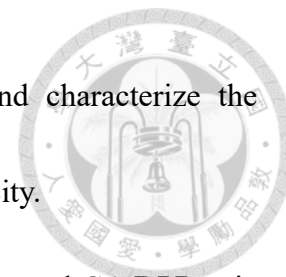
a confusion between G₄C₂ RNA toxicities and DPRs toxicities.

- 
- 2) Common reporters such as GFP may disrupt the intrinsic properties of GA DPRs owing to the difference in size and conformational energy.
 - 3) Due to the poor photostability and dimerization propensity, reporters attached to the transfected GA DPRs proteins can hardly be used in some advanced microscopies, such as single-molecule imaging and fluorescence-lifetime imaging.
 - 4) Through genetic transfection, it is challenging to distinguish the toxicity of GA DPRs intermediate (oligomers) during the aggregation due to rapid polymerization property.
 - 5) Due to the poor solubility and rapid polymerization property of GA DPRs, directly treating the cellular model with synthetic GA DPRs fragments is not feasible.

To overcome aforementioned difficulties in elucidating the pathological role of GA DPRs in C9-ALS, we aimed to design a probe to deliver the GA DPRs into neurons. This probe should fulfill following requests:

- 1) To efficiently enrich GA DPRs in neurons without the interference from G₄C₂ hexanucleotide expansion (HRE).
- 2) The vehicle carrying DPRs should be highly hydrophilic and cell-permeable and can help enhance the solubility of GA DPRs.
- 3) Prevent GA DPRs from polymerization until the onset of release, so we can

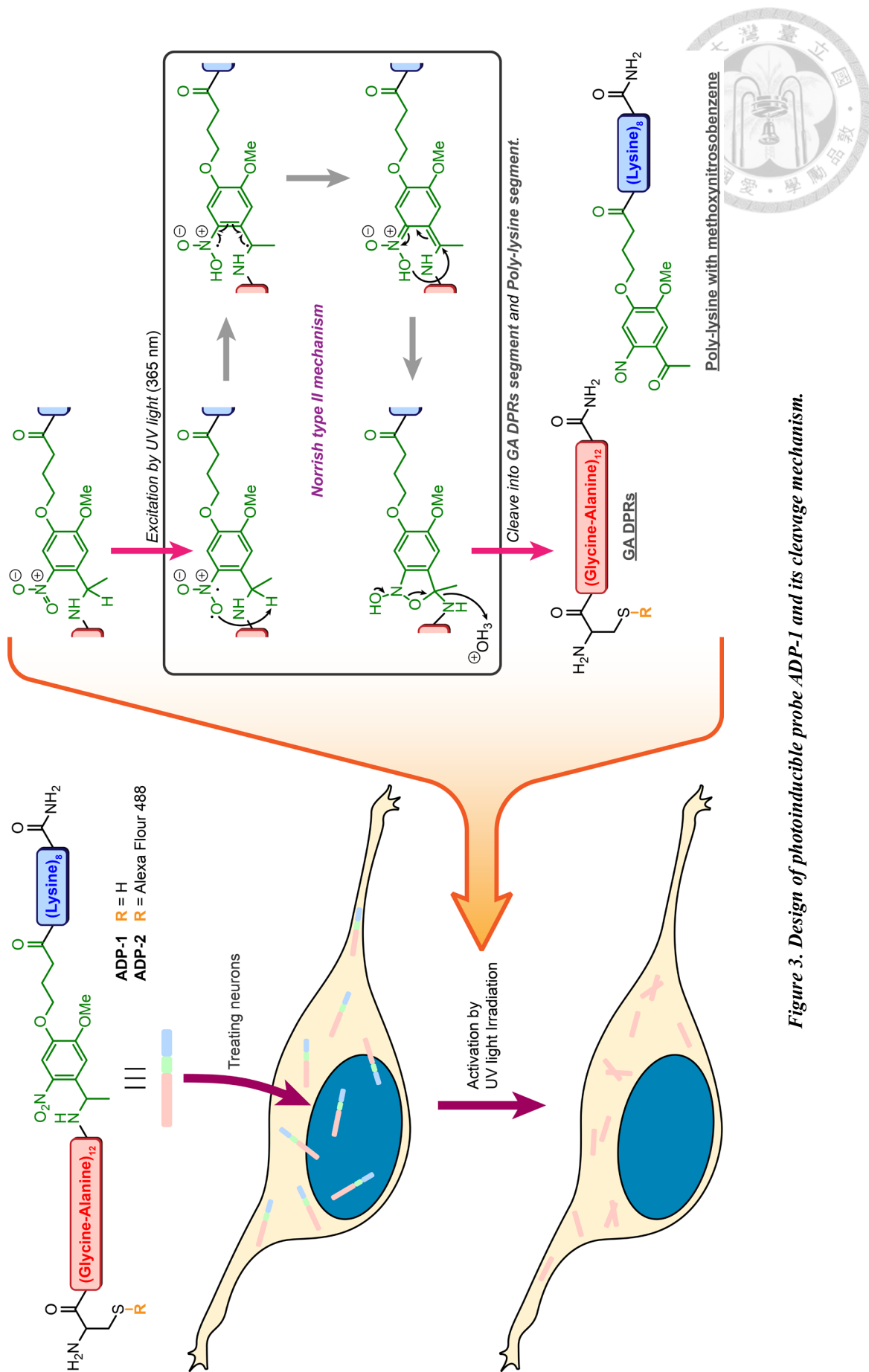
delineate the oligomerization and fibrillization process and characterize the biophysical properties of GA DPRs oligomers and their toxicity.

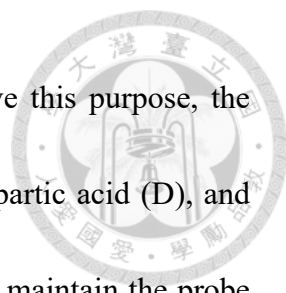


- 4) Released GA DPRs must share similar conformation as expressed GA DPRs via genetic transfection.
- 5) A photostable and pH-insensitive fluorophore should be conjugated to GA DPRs and will not alter the intrinsic properties of GA DPRs.

To avoid the genesis of G₄C₂ HRE, we aimed to directly deliver synthetic GA DPRs fragments into cells. To do so, a hydrophilic and controllable vehicle to carry the GA DPRs was necessary. Here, we applied the *o*-methoxynitrobenzene photolabile linker as a bridge to conjugate GA DPRs fragment to cell-permeable sequence (Figure 3).⁸⁵⁻⁸⁷ Upon the irradiation of UV light (360 nm), methoxynitrobenzene can undergo photolysis reaction involved Norrish type II mechanism (Figure 3).⁸⁵ That is, the incident photo will first excited the electron on π molecular orbital on N-O double bond, which generates nitro radical anion. The excited anion can then abstract the hydrogen at benzylic position, and consequently induce the rearrangement of *aci*-nitro intermediate, and finally release a leaving group. By applying this photochemistry, we were able to not only spatiotemporally control the release of GA DPRs in neurons without the interference from G₄C₂ RNA toxicity but also minimize the cellular damage.

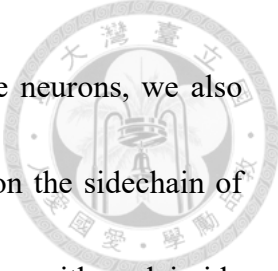
In order to help enhance the solubility of probe and prevent the aggregation of GA





DPRs, we examined the known cell-permeable sequences. To serve this purpose, the content of charged amino acid, such as lysine (K), arginine (R), aspartic acid (D), and glutamic acid (E), in the cell-permeable sequence should be high to maintain the probe solubility. Nevertheless, to achieve higher cellular uptake efficiency of probe, positive-charge amino acids are preferred over negative-charge amino acids due to weak negative charges on plasma membrane. Moreover, poly-(positive-charge amino acid) peptide sequences can provide an additional intermolecular repulsion⁸⁸ for preventing the GA DPRs from self-assemble. As a result, we decided to conjugate poly-arginine or poly-lysine sequences to photolabile linker as the vehicle to carry GA DPRs (Figure 3).

Most important of all, the GA DPRs fragment released by probe should form planar ribbon-like fibrils with β -sheet signature as expressed GA DPRs. Published literatures hypothesized that conformation of GA DPRs greatly depends on the repeats number. Thus, in order to decipher the influence of GA DPRs repeats number on its conformational structure, we have synthesized different repeats number of GA DPRs including (GA)₃, (GA)₁₂, and (GA)₂₀. It turns out that (GA)₁₂ had high propensity to form fibrillar aggregates at micromolar concentration but still exhibited acceptable solubility. By contrast, (GA)₃ formed only trace of aggregates at the same concentration, whereas (GA)₂₀ was mainly insoluble. Therefore, (GA)₁₂ was used as GA DPRs fragment in our probe.



In addition, to enable the visualization of GA DPRs within the neurons, we also installed a cysteine on the N-terminus end of GA DPRs. The thiol on the sidechain of cysteine allows us to attach a fluorophore through Michael addition with maleimide warheads. Considering the issue that fluorophore labeling may impact GA DPR conformation, small molecular fluorophores with high photostability and pH-insensitivity including Alexa Fluor 488, Alexa Fluor 568 and Alexa Fluor 647 were used respectively for the labelling in this study. The fluorophore-tagged GA DPRs will be detected with the advanced microscopy as described below.

II. Material and Methods



2-1 Material and instruments list

Material list

Reagents	CAS no.	Suppliers
Fmoc-Ala-OH	35661-39-3	AnaSpec
Fmoc-Gly-OH	29022-11-5	AnaSpec
Fmoc-Cys(Trt)-OH	103213-32-7	AnaSpec
Fmoc-Lys(Boc)-OH	71989-26-9	AnaSpec
Fmoc-Arg(Pbf)-OH	154445-77-9	AnaSpec
Fmoc-Photolabile Linker	162827-98-7	Advanced ChemTech
Rink Amide AM Resin (200-400 mesh)	None	Merck-Millipore
Acetonitrile	75-05-8	Fisher Scientific
Dichloromethane	75-09-2	Seedchem
Ethanol	64-17-5	J.T. Baker
N,N-Dimethylformamide	68-12-2	ECHO Chemicals
Methyl tert-butyl ether	1634-04-4	TEDIA
2-(1H-Benzotriazole-1-yl)-1,1,3,3-tetramethyluronium hexafluorophosphate	94790-37-1	Alfa Aesar
N,N-Diisopropylethylamine	7087-68-5	Sigma-Aldrich
Piperidine	110-89-4	ECHO Chemicals
Trifluoroacetic Acid	76-05-1	Sigma-Aldrich
Triisopropylsilane	6485-79-6	Sigma-Aldrich
1,2-Ethanedithiol	540-63-6	Sigma-Aldrich
Sodium chloride	7647-14-5	TCI Chemicals
Potassium chloride	7447-40-7	TCI Chemicals
Sodium phosphate dibasic	7558-79-4	Fisher Scientific
Alexa Fluor™ 488 C5 Maleimide	500004-82-0	Thermo-Fisher
Thioflavin T	2390-54-7	Sigma-Aldrich
Uranyl acetate	541-09-3	Provide by IMB,AS
Paraformaldehyde	30525-89-4	Thermo-Fisher
Osmium tetroxide	20816-12-0	Provide by ICOB, AS
Tris(hydroxymethyl)aminomethane	77-86-1	Sigma-Aldrich
Glucose oxidase	9001-37-0	Sigma-Aldrich
Catalase	9001-05-2	Sigma-Aldrich
Glucose	50-99-7	Sigma-Aldrich

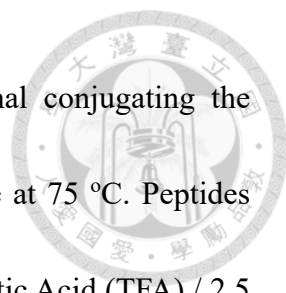
2-Mercaptoethylamine		60-23-1	Sigma-Aldrich
2-Mercaptoethanol		60-24-2	Sigma-Aldrich
Dulbecco's modified Eagle's medium		<i>None</i>	Invitrogen
Glutamine		56-85-9	Thermo-Fisher
Fetal bovine serum		9014-81-7	Thermo-Fisher
Penicillin-Streptomycin		<i>None</i>	Invitrogen
Lipofectamine® 3000 Reagent		<i>None</i>	Thermo-Fisher
Anti-TDP-43 antibody	(ab104223)	<i>None</i>	Abcam
Anti-Ran antibody	(ab155103)	<i>None</i>	Abcam
Anti-importin-β antibody	(ab2811)	<i>None</i>	Abcam
Anti-Lamin B1 antibody	(ab16048)	<i>None</i>	Abcam
Anti-Nup153 antibody	(ab24700)	<i>None</i>	Abcam
Anti-GAPDH antibody	(gtx627408)		GeneTex
1,2-Dimyristoyl-sn-glycero-3-phospho-(1'-rac-glycerol) (sodium salt)		200880-40-6	Avanti Polar Lipid
1,2-Dimyristoyl-sn-glycero-3-phosphocholine		18194-24-6	Avanti Polar Lipid
Cholesterol		57-88-5	Sigma-Aldrich
Calcein		154071-48-4	Sigma-Aldrich
Sepharose CL-4B		61970-08-9	Sigma-Aldrich
AmershamProtran 0.45 NC nitrocellulose Western blotting membranes		<i>None</i>	General Electric
Bovine Serum Albumins		9048-46-8	Sigma-Aldrich
Oligomer A11 antibody	(AHB0052)	<i>None</i>	Thermo-Fisher
Anti-GA repeat antibody	(24492-1-AP)	<i>None</i>	Proteintech
TnT® quick coupled transcription /translation system		<i>None</i>	Promega
Anti-FLAG M2 antibody	(F3165)	<i>None</i>	Sigma-Aldrich
B-27 Supplement	(17504001)	<i>None</i>	Thermo-Fisher
Anti-β-III-tubulin	(ab18207)	<i>None</i>	Abcam

Instrument list

Instruments	Model	Company
Automated peptide synthesizer	Liberty Blue™	CEM Corporation, U.S.A.
High-performance liquid chromatography	1260 Infinity LC System	Agilent, U.S.A.
HPLC Column	Spolar C18	Shiseido, Japan
Lyophilizer	CoolSafe 4-15L	LaboGene, Denmark
Mass spectrometer	New ultrafleXtreme™	Bruker, U.S.A.
Handheld UV lamp	UVP 95000705	Fisher Scientific, U.S.A.
Circular dichroism spectrophotometer	J-815	JASCO, Japan
Fluorescence spectrophotometer	F-4500	Hitachi, Japan
UV-Vis spectrophotometer	DU 800	Beckman, U.S.A.
Fourier-transform infrared spectrometer	FT/IR-6700	JASCO, Japan
Dynamic light scattering detector	DynaPro NanoStar	Wyatt, U.S.A.
Sonicator	UP200S	Hielscher Ultrasonics, Germany
Electron microscope	JEM-2011	JEOL, Japan
Fluorescence-lifetime imaging microscope	Q2 Fast FLIM system	ISS, U.S.A.
Superresolution microscope	ELYRA PS.1	Zeiss, Germany
Confocal microscope	LSM 880	Zeiss, Germany
Total internal reflection fluorescence microscope	Eclipse Ti2	Nikon, Japan
Mini-Extruder	Extruder Set	Avanti Polar Lipid, U.S.A.
Eppendorf mixer/ incubator	Thermomixer	Eppendorf, Germany

2-2 Probe preparation and identification

Probe ADP-1 and other peptides [*i.e.*, ADP-3, (GA)₃, (GA)₁₂, (GA)₂₀] were synthesized by the Fmoc-protecting polyamide chemistry on Rink Amide AM resin using the microwave-assisted automated peptide synthesizer Liberty Blue™ [*Activator*: 2-(1H-Benzotriazole-1-yl)-1,1,3,3-tetramethyluronium hexafluorophosphate (HBTU) ; *Activator base*: N,N-Diisopropylethylamine (DIEA) ; *Deprotection*: 20% Piperidine in



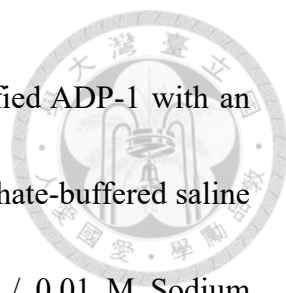
N,N-Dimethylformamide (DMF) ; *Main solvent*: DMF]. Additional conjugating the Fmoc-photolabile linker to peptides required double coupling cycle at 75 °C. Peptides were cleaved from the resin by cleavage cocktail [90 % Trifluoroacetic Acid (TFA) / 2.5 % water / 2.5 % Triisopropylsilane (TIPS) / 5 % 1,2-Ethanedithiol (EDT)], then purified by high-performance liquid chromatography (HPLC) equipped with a C18 reverse-phase semi-preparative column (Shiseido, Japan). Gradient separation of peptides was accomplished by mixing buffer A (5 % Acetonitrile (ACN) / 0.1 % TFA / 94.9 % water) and buffer B (0.1 % TFA / 99.9 % acetonitrile). Collecting purified peptides was analyzed and identified by matrix-assisted laser desorption/ionization - time of flight (MALDI-TOF) mass spectroscopy (New ultrafleXtreme™) (Table 1).

Name	Sequence*	Calc. Mass	Observed Mass
(GA)₃	(GA) ₃ -NH ₂	401.4	424.2 (M+Na) ⁺ (420 ppm)
(GA)₁₂	(GA) ₁₂ -NH ₂	1554.6	1576.8 (M+Na) ⁺ (480 ppm)
(GA)₂₀	(GA) ₂₀ -NH ₂	2578.2	2601.5 (M+Na) ⁺ (120 ppm)
ADP-1	C-(GA) ₁₂ -#PL-K ₈ -NH ₂	2963.4	2963.7 (M) ⁺ (67 ppm)
ADP-2	AF 488 C5 Maleimide-C-(GA) ₁₂ - #PL-K ₈ -NH ₂	3661.0	3661.2 (M) ⁺ (54 ppm)
ADP-3	C-(GA) ₃ -#PL-K ₈ -NH ₂	1809.9	1811.0 (M+H) ⁺ (55 ppm)
ADP-4	AF 488 C5 Maleimide-C-(GA) ₃ - #PL-K ₈ -NH ₂	2507.5	2509.1 (M+H) ⁺ (240 ppm)

Table 1. Sequence of peptides used in this study and their molecular mass.

* Sequences were written following the N-terminus to C-terminus order.

X represents photoabile linker which conjugates with nearby amino acid residues through amide bond.



Fluorescent probe ADP-2 was synthesized by mixing the purified ADP-1 with an equivalent amount of Alexa Fluor™ 488 C5 Maleimide in the phosphate-buffered saline (PBS; 0.137 M Sodium chloride / 0.0027 M Potassium chloride / 0.01 M Sodium phosphate dibasic / 0.002 M Monopotassium phosphate, pH = 8.0) for 2 hours. Resulting solution was further purified through gradient separation by HPLC to obtain the ADP-2.

2-3 General sample preparation for *in vitro* measurements

Peptides (50 μ M) was prepared in the low salt phosphate-buffered saline (PBS, 0.05 M Sodium chloride / 0.0027 M Potassium chloride / 0.01 M Sodium phosphate dibasic / 0.002 M Monopotassium phosphate, pH = 7.4). For photoinitiation of probe, samples were irradiated with light (Wavelength: 365 nm, Lighting intensity: 1200 μ w/cm², Duration: 1 minute). Resulting peptide samples were incubated at 37 °C for following *in vitro* characterization.

2-4 Circular dichroism spectroscopy

The circular dichroism (CD) spectra were collected by measuring the peptide containing samples with 1 mm quartz cuvette on CD spectrometer (Wavelength: 195-260 nm, Scan rate: 200 nm/min, Accumulation: 10). Peptides with different incubation time were recorded individually.



2-5 Dye-binding assay


Thioflavin T (ThT) working solution (50 μ M in low salt PBS as aforementioned, filtered with 0.22 μ m Millipore PVDF filter) was freshly prepared for dye-binding assay. 50 μ L aliquot of peptide solution was mixed with 50 μ L aliquot of ThT working solution first, and then incubates at room temperature for 5 minutes. The fluorescence emission spectra of resulting mixture solution were recorded in a 3 mm path length rectangular fluorescence quartz cuvette on fluorescence spectrophotometer (Excitation wavelength: 440nm, Emission wavelength: 460-600 nm, Scan speed: 1200 nm/min) Peptides with different incubation time were recorded individually. Resulting fluorescence intensity of peptide-ThT mixture solution was compared to the fluorescence intensity of blank solution (50 μ L of low salt PBS mixed with 50 μ L aliquot of ThT working solution).

2-6 Turbidity measurements

Turbidity of peptide samples were measured with 1 cm quartz cuvette on UV-Vis spectrophotometer. The absorbance of each samples at 600 nm of wavelength were recorded.

2-7 Dot-blot assay

ADP-1 solution (100 μ M) was fresh prepared in low salt PBS, photoinitiated and,



incubated at 37 °C. 2 μ L of peptide solution was applied on the nitrocellulose membrane and the resulting membrane was rest till it dried. 5 % bovine serum albumins (BSA) in tris-buffered saline-tween [20 mM Tris(hydroxymethyl)aminomethane(Tris) / 150 mM Sodium chloride / 0.1 % Tween 20] was used to block free site on the membrane. Oligomer A11 Polyclonal Antibody (AHB0052) and anti-GA repeat antibody (24492-1-AP) was used to stain amyloid oligomer and GA DPRs on the membrane.

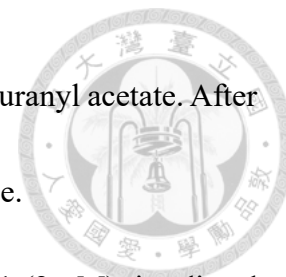
2-8 Infrared Spectroscopy

For infrared spectroscopy measurements, the photoinitiated ADP-1 was incubated for 48 hours at 37 °C, and then centrifuged at 16000 g for 30 minutes to collect the pellet. The resulting pellet was washed with ethanol and then dried in vaccum for overnight. The attenuated total reflectance fourier-transform infrared spectrometer was used to measure the infrared specrum of GA DPRs. The deconvolution of IR spectrum was achieved by Origin 2021 with Peak Deconvolution App. The Lorentzian spectrrum were deconvoluted by second derivative method and smoothed by Savitzky Golay with 2 polynomial order and 9 points of window.

2-9 Transmission electron microscopy

5 μ L aliquot of peptides solution was applied on the grow-charged 300 mesh

Formvar- and carbon-coated copper grids, and then stained with 2 % uranyl acetate. After drying overnight, grid samples were analyzed by electron microscope.



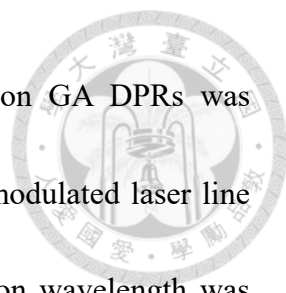
For cellular sample preparation, cos-7 cells treated with ADP-1 (2 μM), irradiated with UV light (mercury lamp with 345-385 nm bandpass filter; average power: 8.24 mW/cm²; duration: 1 minute) and then fixed with 4 % paraformaldehyde in PBS. Cells were firstly stained with 1 % osmium tetroxide in PBS. Dehydration of cells was achieved by adding ethanol solution. Cells were ultracuted using diamond knife to acquired thin section. Thin cell sections were then fixed on the grid and stained with 1 % uranyl acetate. After drying overnight, samples were analyzed by electron microscope.

2-10 Dynamic light scattering

To measure the size distribution of GA DPRs oligomers, ADP-1 (100 μM in low salt PBS buffer was UV-irradiated followed by 2 hours incubation at 37 °C. Samples were measured at 25 °C, and more than 15 times measures were averaged to acquire correlation function curve. The correlation function curve was later fitted with regularization fitting. The results with sum of squares (SOS) larger than 100 will be excluded.

2-11 Fluorescence-lifetime imaging microscopy

Fluorescent ADP-2 (1 μM) solution was freshly prepared, illuminated, and incubated



for different time. Fluorescence-lifetime of Alexa Fluor™ 488 on GA DPRs was analyzed by nanometer resolution Z-piezo objective. The 488 nm modulated laser line with 20 MHz repetition rate was used for excitation. The excitation wavelength was connected by optical fiber and a band-pass filter to improve wavelength selection. Fluorescence emission from the sample went through a band-pass filter (FF05-500/25-25 for Alexa 488, Semrock) before being sent to the confocal unit with single photon counting module avalanche photodiodes APDs detectors. A water objective (PlanApo 60x, N.A. 1.2, Nikon) was used for the imaging. To avoid any perturbation to the sample, optical sectioning was achieved by the XY galvo mirror scanning and the Z sectioning by moving Piezo encoded motorized device.

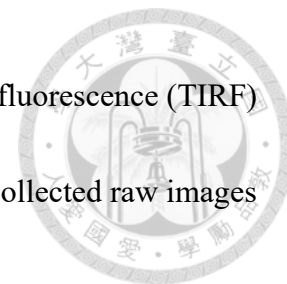
For the cellular FLIM images, SH-SY5Y cells were cultured on a sterilized 35 mm μ -Dish. After ADP-2 (1 μ M) treatment and photoinitiation as described above, cells were incubated for an additional 24 hours and then fixed with 4 % paraformaldehyde. Fluorescence-lifetime imaging microscopy (FLIM) analysis was carried out with nanometer resolution Z-piezo objective. The fluorescence-lifetime of Alexa Fluor 488-labeled GA DPRs in the cells will be monitored and compared. The sample will be excited by modulated laser with 20 MHz repetition rate. The excitation wavelength will be connected with optical fiber and a band-pass filter to improve wavelength selection. Fluorescence emission from the sample will go through a band-pass filter (FF05-500/25-

25 for Alexa 488, Semrock) before being sent to the confocal unit with single photon counting module avalanche photodiodes APDs detectors. A water objective (PlanApo 60x, N.A. 1.2, Nikon) will be used for the imaging. To avoid any perturbation to the sample, optical sectioning is achieved by the XY galvo mirror scanning and the Z sectioning by moving Piezo encoded motorized device.

2-12 Direct stochastic optical reconstruction microscopy

Irradiated ADP-2 (1 μ M) solution was freshly prepared in a 35mm glass-bottom dish and further incubated. Blinking buffer [50 mM Tris(hydroxymethyl)aminomethane (Tris) / 10 mM Sodium chloride / 160 mg/mL Glucose oxidase / 0.5 mg/mL Catalase / 10 wt% Glucose / 750 mM 2-Mercaptoethylamine / 1000 mM 2-Mercaptoethanol] was prepared for optimizing blinking duty cycles and duration and also avoiding oxygen-induced photolysis of excited dyes. Direct stochastic optical reconstruction microscopy (dSTORM) images were capture with the ELYRA PS.1 superresolution microscope. The regions of interest were selected with the 100 x, NA 1.46, plan-APO objective. An EMCCD AndoriXon 897 (pixel size 16 μ m; Optovar lens, magnification 1.6 x, was used, along with the 100x objective lens yielded a final pixel size of 100 nm) was used as the camera detector. With laser excitation at 488 nm and emission filter adjustments matched to Alexa Fluor 488 emission spectrum, we acquired 30000-50000 raw images of blinking

fluorophores under epifluorescence (EPI) or total internal reflection fluorescence (TIRF) microscopy mode dSTORM images were reconstructed from these collected raw images with a pixel size of 10 nm.



For cellular dSTORM images, SH-SY5Y, Cos-7 and, ST14a cells were cultured, treated with ADP-2, photoinitiated, and fixed with 4 % paraformaldehyde. Fixed cells were further stained with antibodies for interested protein. Cell sample were immersed in the blinking buffer [50 mM Tris(hydroxymethyl)aminomethane(Tris) / 10 mM Sodium chloride / 160 mg/mL Glucose oxidase / 0.5 mg/mL Catalase / 10 wt% Glucose / 75 mM 2-Mercaptoethylamine / 100 mM 2-Mercaptoethanol]. 30000-50000 raw images were collected and reconstructed through aforementioned methods.

2-13 Cell maintenance, Transfection, and Probe treatment

Human neuroblastoma SH-SY5Y and monkey kidney COS-7 cells were cultured in Dulbecco's modified Eagle's medium (DMEM) supplemented with 2 mM glutamine, 10% heat-inactivated fetal bovine serum, and 100 U/mL penicillin-streptomycin antibiotics at 37°C in a humidified atmosphere with 5 % CO₂.

To treat the cells with probes, lyophilized peptide powder were dissolved in the medium. After 24 hours of incubation in probe-containing medium, cells were irradiated with light (mercury lamp with 345-385 nm bandpass filter; average power: 8.24 mW/cm²;

duration: 1 minute) and then washed with medium. Washed cells were next incubated for 24 hours for experimental observation.

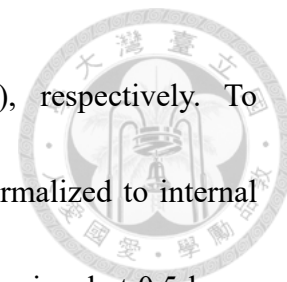


For nucleocytoplasmic shuttling experiments, SH-SY5Y cells were transfected with 1.5 μg shuttling-GFP (pcDNA3.1-NES-eGFP-NLS) DNA, using Lipofectamine® 3000 Reagent according to the manufacturer's protocol. After 24 hours, cells were harvested for further probe (ADP-1: 1 μM) or inhibitors (Importazole: 40 μM ; Leptomycin B: 20 nM) treatment.

2-14 Cell lysate staining

1.6×10^6 of SH-SY5Y cells were treated with ADP-1 or ADP-3 (1 μM) for 24 hours and then exposed to UV light (mercury lamp with 345-385 nm bandpass filter; average power: 8.24 mW/cm²; duration: 1 min). After washing with culture medium (DMEM/F12 supplemented with 10 % FBS), cells were further incubated and collected the cell lysates in RIPA buffer at different time points. Cells lysates was first sonicated by UP200S (Hielscher Ultrasonics, Germany) and the total protein concentration in the resultant lysates were measured by detergent compatible (Dc) protein assay (Bio-Rad, U.S.A.). 50 μg of proteins were loaded onto nitrocellulose membrane (0.1 μm , GE healthcare, U.S.A.) adopted with the PR648 Slot Blot Blotting Manifold. Collected membranes were blocked by 2 % bovine serum albumin, and then stained with A11 antibody (AHB0052,

ThermoFisher) and GAPDH antibody (GTX627408, GeneTex), respectively. To quantitate the A11 kinetics, the collected A11 signals were first normalized to internal control GAPDH and the resultant signals were then compared to the signal at 0.5-hour-incubation to learn the relative fold value.



2-15 Immunohistochemistry and Confocal microscopy

To observe the proteins of interest, 2×10^5 of SH-SY5Y or COS-7 cells on a 30 mm square coverslip were first treated with probe according to the aforementioned protocol, fixed with 4 % paraformaldehyde, and then stained with corresponding antibody. For immunostaining, anti-TDP-43 antibody (Abcam, ab104223), anti-Ran antibody (Abcam, ab155103), anti-importin- β antibody (Abcam, ab2811), anti-lamin B1 antibody (Abcam, ab16048) and anti-Nup153 antibody (Abcam, ab24700) were used, respectively. Images of the resulting samples were captured with confocal microscope.

2-16 Total internal reflection fluorescence microscopy

The epifluorescence images of shuttling-GFP distribution were carried out using a total internal reflection fluorescence microscope, where samples were illuminated with an ultra-high-pressure 130 W mercury lamp for the excitation.




2-17 *Ex vivo* antibody accessibility assay

SH-SY5Y cells (2×10^6) were first treated with digitonin (0.001 %) on the ice for 2 minutes to deprive the cytoplasm membrane. Remaining of cells were further treated with either 100 μ M GA DPRs oligomers (2-hours-incubation), fibrils (24-hours-incubation) or triton X-100 at 37 °C for 2 hours, followed by fixation with 2 % paraformaldehyde. Fixed cells were then stained with DAPI and lamin B1 antibody. Images were captured by confocal microscopy. Permeabilized nuclear compartments in the cell remaining were manually counted, analyzed and compared.

2-18 Calcein-leakage assay


To prepared the calcein-containing liposome for membrane leakage evaluation, 3.3 mg of 1,2-Dimyristoyl-sn-glycero-3-phospho-(1'-rac-glycerol) (sodium salt) (DMPG), 5.0 mg of 1,2-Dimyristoyl-sn-glycero-3-phosphocholine, and 2.5 mg of Cholesterol were first dissolved in 1:1 chloroform/methanol solution. Nitrogen gas and lyophilizer was then used to remove the solvent. The dried lipid was rehydrated by 1 ml of 50 mM calcein-containing phosphate buffered saline which titrated with potassium hydroxide to adjust the pH value to 7.0. The mixture was sonicated for 1 hour to ensure all lipids were dissolved in the solution. The lipid-containing solution was treated with freeze-thaw process cycle in liquid nitrogen and a 70 °C hot plate for 7 times. Resulting suspension



solution then passed tens of times continuously through an Avanti Mini-Extruder with two stacked 100 nm polycarbonate membranes. Unencapsulated calcein was removed by self-packed size-exclusion column with Sepharose CL-4B gel filtration medium. To evaluate the influence of GA DPRs on lipid membrane, peptides (100 μ M) were fresh prepared and then added into the liposome solution to a final concentration of 0.7 mM lipid and 50 μ M peptide. The GA DPRs fibrils were collected by incubating the irradiated ADP-1(100 μ M in low salt PBS) for 1 day and then harvested by centrifugation (16000g-force). The pellet was re-suspended before adding to liposome solution. The liposome and peptide mixtures were incubated at 37 °C with 1400 rpm shaking in an eppendorf mixer/ incubator for 2 hours. Fluorescence intensity of leak calcein was measured at Excitation/Emission = 490/520 nm. The percentage of fluorescence intensity is defined as $(FP-FL)/(FT-FL)$, where FP is the fluorescence signal after the peptide is added, FL is the fluorescence for liposome only, and FT is the fluorescence signal obtained after 5 % of Triton X-100 added.

2-19 Seeding assay

TnT® quick coupled transcription/translation system was used to express human TDP-43 proteins *in vitro* according to the manufacturer's instruction. Reagents was mixed with human TDP-43 plasmid (pIVEX2.3d FLAG-TDP-43-His), RNase-free water, and

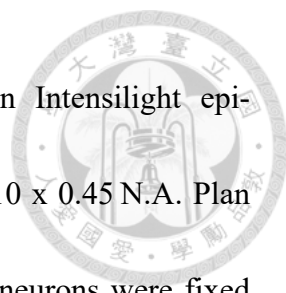


methionine. Resulting solution was agitated by eppendorf mixer/ incubator at 30 °C for 16 hours. After 4 hours since the reaction starting, collected GA DPRs pellets were subjected to the mixed solution and continued to agitate. While the reaction finish, the supernatant and pellet of reaction was separated by centrifugation (16000 g-force) and respectively analyzed by western blot stained with Anti-FLAG M2 monoclonal antibody (F3165).

2-20 Primary cortical neurons culture, Probe treatment and Neurite

Fragmentation Analysis

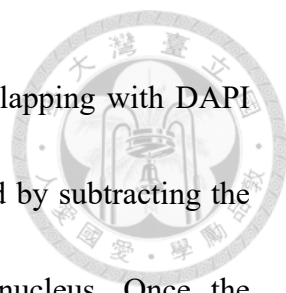
All animal experimental procedures were approved by the Institutional Animal Care and Use Committee (IACUC) and in accordance with the Guide for the Care and Use of Laboratory Animals of National Chiao Tung University. Primary culture of dissociated mouse cortical neurons isolated from the brains of E17.5 (embryonic 17.5) mouse pups was carried out as previously described.⁸⁹ The ADP-1 peptide (final concentration 1 μ M) was dissolved in the pre-equilibrated B27-supplemented neurobasal medium containing 50 % of the old cultured medium. The 21 days in vitro (21DIV) cortical neurons were incubated with null or ADP-1-containing medium for 8 hours. To completely remove ADP-1 from the culture medium, the washing process, involving replacement with 500 μ L of pre-equilibrated B27-supplemented neurobasal medium, was applied once. Cortical



neurons were then UV irradiated for 2 minutes using a Nikon Intensilight epi-fluorescence light source, a Semrock filter FF01-357/44-25, and a 10 x 0.45 N.A. Plan Apochromat objective lens. 24 hours after UV irradiation, cortical neurons were fixed with 3.7 % formaldehyde in 1× PBS at 37 °C for 15 min, followed by membrane permeabilization with 0.25 % Triton X-100 for 5 min at room temperature. Cells were then blocked with 10 % bovine serum albumin (BSA) in 1× PBS for 30 min at 37 °C followed by 1 hour of incubation at 37 °C with primary antibodies (anti-TDP-43, 1:1000, Abcam, ab104223; anti- β -III-tubulin, 1:200, Abcam, ab18207) in 2 % BSA. Cells were washed 3 times with 1× PBS and subjected to 1 hour of incubation with AlexaFluor 488-labeled (anti-mouse) and 568-labeled (anti-rabbit) secondary antibodies (1:1000, Thermo Fisher Scientific) at 37 °C in the dark. Immunofluorescence stained neurons were acquired on a Nikon Eclipse-Ti inverted microscope equipped with a 60× 1.49 N.A. Plan Apochromat objective lens, an Intensilight epi-fluorescence light source, a Photometrics CoolSNAP HQ2 camera, and Nikon NIS-Elements software 4.13.05.

2-21 Imaging quantification and Statistical analysis

To evaluate the ratio of nuclear Ran depletion in treated or untreated SH-SY5Y cells, the fluorescence intensity from Ran antibody immunohistochemistry in cytoplasm and nucleus were analyzed by ImageJ (<http://imagej.nih.gov/ij/>). The fluorescence intensity

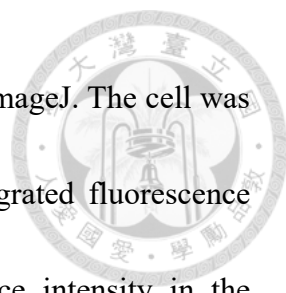


in nucleus was acquired by isolating the nuclear area through overlapping with DAPI staining, while the fluorescence intensity in cytoplasm was acquired by subtracting the total fluorescence intensity with the fluorescence intensity in nucleus. Once the fluorescence intensity in cytoplasm was three times higher than fluorescence intensity in nucleus, that cell was determined as nuclear Ran depletion.

To evaluate the ratio of importin- β diffusion in treated or untreated SH-SY5Y cells, the fluorescence intensity from importin- β antibody immunohistochemistry in cytoplasm and perinucleus region were analyzed by ImageJ. The cell was determined as cell with importin- β diffusion if the integrated fluorescence intensity in the cytoplasm is two times higher than the integrated fluorescence intensity in the perinucleus region via fluorescence intensity profiling.

The quantification of sGFP distribution was carried out using ImageJ for evaluation fluorescence intensity in cytoplasm and nucleus. The sGFP fluorescence intensity in nucleus was acquired by isolating the nuclear area through overlapping with DAPI staining channel, while the sGFP fluorescence intensity in cytoplasm was acquired by subtracting the total fluorescence intensity with the fluorescence intensity in nucleus. The resulting nuclear-to-cytoplasmic ratio of sGFP for each cells was acquired by fluorescence intensity in nucleus over the fluorescence intensity in cytoplasm.

The quantification of nuclear diffusion of Lamin B1 in treated or untreated SH-



SY5Y cells was achieved by fluorescence intensity profiling using ImageJ. The cell was determined as cell with Lamin B1 staining in nucleus if the integrated fluorescence intensity in the nucleus is higher than the integrated fluorescence intensity in the perinucleus region via fluorescence intensity profiling.

To evaluate the antibody penetrance level, ImageJ was employed. The nuclear remains will be determined as Lamin B1 staining positive if the fluorescence signals in perinuclear region were noticed.

The cytosolic retention ratio of TDP-43 in SH-SH5Y cells was carried out by analyzing the fluorescence distribution of TDP-43 antibody immunohistochemistry in cytoplasm and nucleus using ImageJ. The fluorescence intensity in nucleus was acquired by isolating the nuclear area through overlapping with DAPI staining channel, while the fluorescence intensity in cytoplasm was acquired by subtracting the total fluorescence intensity with the fluorescence intensity in nucleus. The cell will be determined as TDP-43 cytosolic retention positive if the fluorescence intensity in cytoplasm is higher than 20% of total fluorescence.

To quantify the degeneration area of neurites, ImageJ was used to process and analyze the neurite signal in the β -III-tubulin channel. Briefly, the total neurite area was obtained from the original β -III-tubulin image using Subtract Background \rightarrow Gaussian Blur \rightarrow Phansalkar auto local threshold. The fragmented neurite area was obtained using

the analyze particles function with a particle size less than 50 pixels. The degeneration area percentage (%) of neuron is quantified as fragemnted neurite area / total nerutite area.

For the analysis of TDP-43 nuclear to cytoplasmic ratio in neurons, we first used the fluorescence signal from TUJ1 staining to manually select the total soma area. The DAPI staining was used to select the nuclear area. The cytoplasmic area was selected by subtracting the nuclear area from the soma area. The TDP-43 intensity in nuclei was quantified from the signal in nuclear area, and the TDP-43 intensity in cytoplasm was then quatified from the signal in cytoplasmic area. The nuclear to cytoplasmic ratio was achieved by dividing the fluorescence intentisty of nuclear TDP-43 over fluorescence intentisty of cytoplasmic TDP-43 (fluorescence intentisty of nuclear TDP-43 / fluorescence intentisty of cytoplasmic TDP-43). More than 50 neurons were counted from three individual experiments ($n = 3$).

All experimental comparisons were analyzed using two-sided Welch's T test. The Bonferroni correction was used for multiple comparison correction.

III. Results

3-1 Preparation of photoinducible GA DPRs probes

To synthesize photoinducible probe ADP-1, automated microwave peptide synthesizer (Liberty Blue, CEM Corporation, U.S.A.) was employed. Amino acids and F-moc-photolabile linker solutions were prepared in DMF as manufacturer's instruction. Polypeptide were synthesized through HBTU (2-(1H-Benzotriazole-1-yl)-1,1,3,3-tetramethyluronium hexafluorophosphate) / DIEA (N,N-Diisopropylethylamine) coupling reagent. In particular, due to the steric hindrance, incorporating photolabile

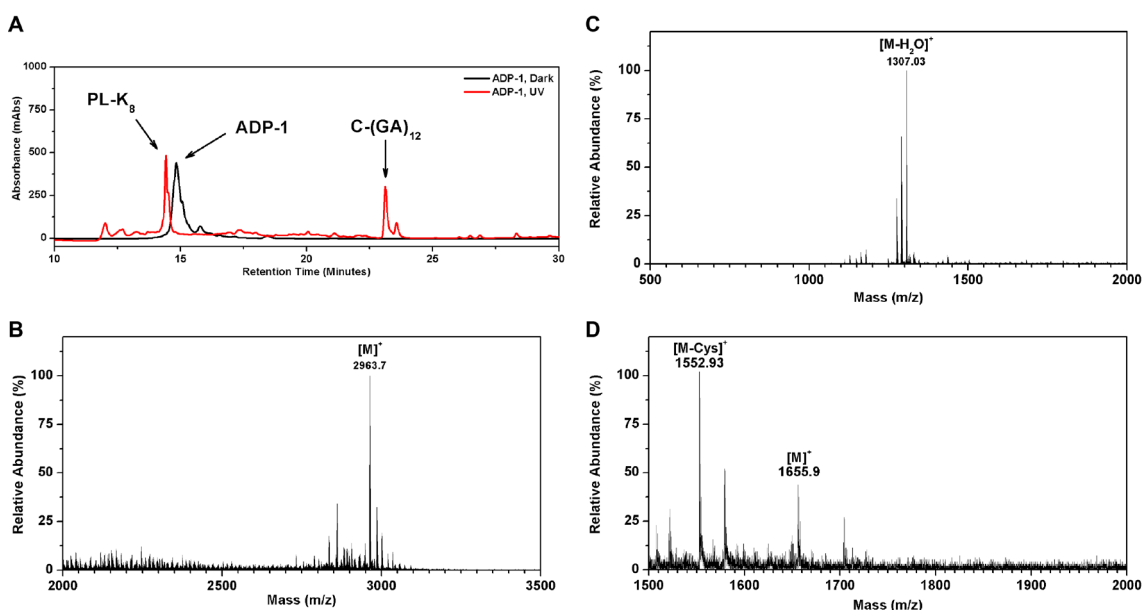


Figure 4. The HPLC and mass spectra of ADP-1 and its photoinitiated products. (A) HPLC spectra of unirradiated and irradiated ADP-1. The first red peak with retention time around 14 minute is the photolinker-octalysine segment as we confirmed by mass in Figure 4C, whereas the other red peak with retention time about 23 minute is the GA DPRs fragment as we identified by mass in Figure 4D. **(B)** MALDI-TOF mass spectrum of ADP-1, calc. mass: 2963.7; observed: 2963.7 ($[M]^+$). **(C)** MALDI-TOF mass spectrum of GA DPRs fragment from the photoinitiated ADP-1, calc. mass: 1657; observed: 1655.9 ($[M]^+$). **(D)** MALDI-TOF mass spectrum of octalysine fragment from the photoinitiated ADP-1, calc. mass: 1324.3; observed: 1307.03 ($[M-H_2O]^+$).

linker on the peptide chain with higher yield requires double coupling at aforementioned condition. High-performance liquid chromatography (HPLC) was used to purified the peptides (Black curve in Figure 4A), further identification and characterization were accomplished by matrix-assisted laser desorption ionization-time of flight (MALDI-TOF) mass spectroscopy (Figure 4B). The calculated yield for ADP-1 is around 85 %.

In order to enable visualization of GA DPRs in neurons, the purified ADP-1 was then labeled with commercial fluorescence dye Alexa FlourTM 488 (AF-488) C₅ maleimide through Michael addition reaction. HPLC was used to purify fluorescent ADP-

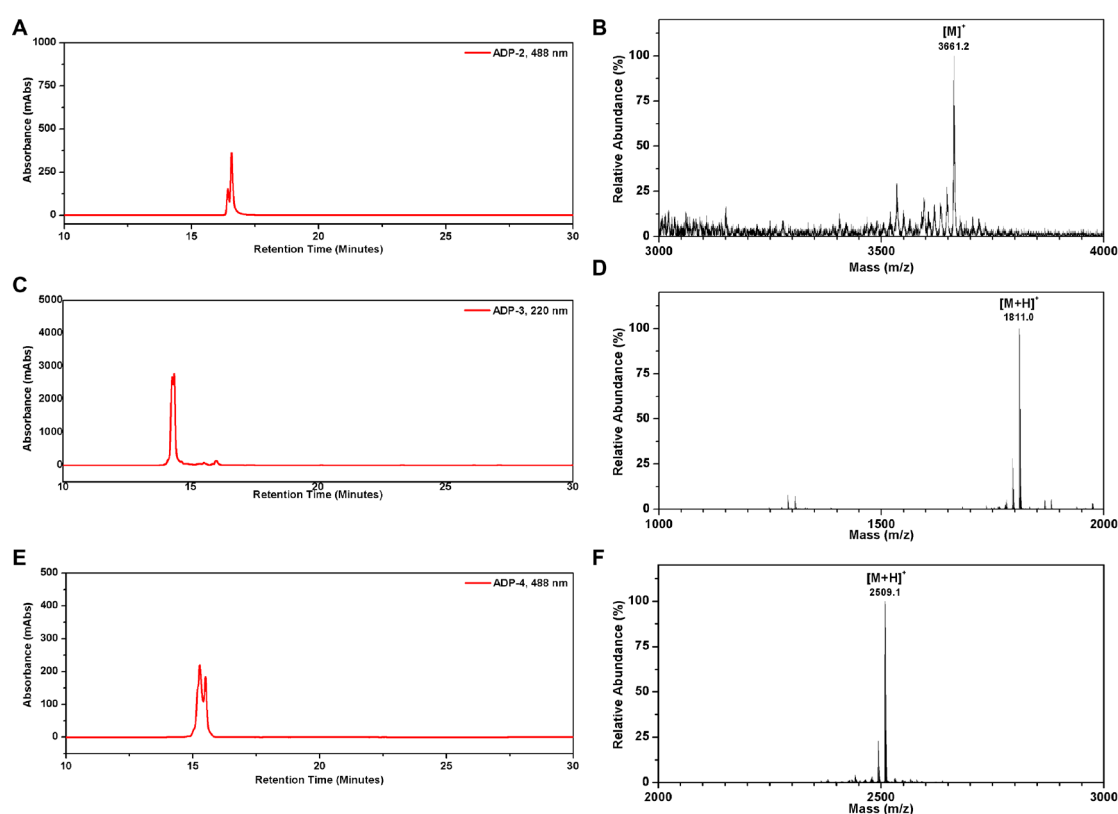


Figure 5. HPLC and Mass spectra of ADP-2, ADP-3, and ADP-4. (A) HPLC spectrum of ADP-2. (B) MALDI-TOF mass spectrum of ADP-2, calc. mass: 3661.0; observed: 3661.2 ($[M]^+$). (C) HPLC spectrum of ADP-3 (D) MALDI-TOF mass spectrum of ADP-3, calc. mass: 1809.9; observed: 1811.0 ($[M+H]^+$). (E) HPLC spectrum of ADP-4 (F) MALDI-TOF mass spectrum of ADP-4, calc. mass: 2507.5; observed: 2509.1 ($[M+H]^+$).

2 (Figure 5A) which was later identified by MALDI-TOF mass spectroscopy (Figure 5B).

The labeling yield is around 60 %.

As a control, we also prepared a probe with a shorter GA dipeptide repeat length, ADP-3, and the corresponding fluorophore-labeled probe ADP-4 (Figure 5C-F). On the basis of our experimental design, these probes will be cleaved into GA DPRs [(GA)₃] and octalysine (PL-K₈) fragments after photoinitiation.

3-2 Biophysical & biochemical characterization of GA DPRs

Since ADP-1 probe was successfully synthesized, we first attempted to assess the photolysis efficiency of ADP-1. The lyophilized ADP-1 was prepared in the PBS buffer solution and then irradiated with UV light (355-365 nm). The resulting solution was then analyzed by HPLC and mass spectrometer. As shown in Figure 4A, the octalysine (retention time ~ 15 minutes) and GA DPRs (retention time ~ 23 minutes) fragments were separated and then identified (Figure 4C-D), validating our design of photoinducible probe.

Previous studies have showed that GA DPRs might adopt β -sheet conformation and form ribbon-like amyloid in cells.⁷⁷ Therefore, we next aimed to understand whether GA DPRs fragments released from photoinitiated ADP-1 would also form β -sheet-rich amyloid fibrils. To learn the secondary structure of GA DPRs fragments, we applied

circular dichroism spectroscopy which provides structural information based on the differential absorption of left- and right-handed polarized light. As depicted in Figure 6A, GA DPRs fragments developed enhanced β -sheet signature as incubation extended.

However, because glycines on the GA DPRs fragments are lack of chirality, the resulting

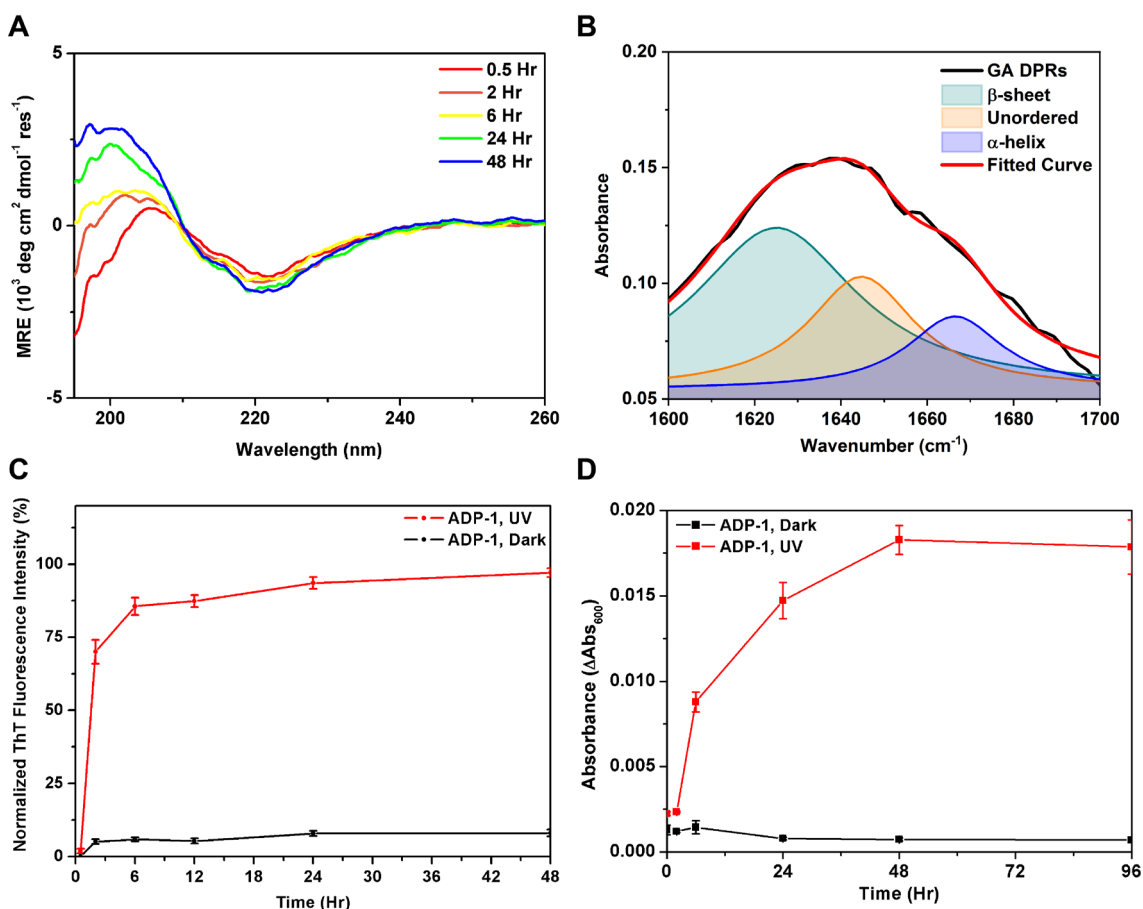


Figure 6. Biophysical characterization of the GA DPRs from ADP-1. (A) Time-course circular dichroism spectrum of photoinitiated ADP-1 (50 μM) in low salt PBS (0.05 M NaCl, 0.0027 M KCl, 0.01 M Na_2HPO_4 , 0.002 M KH_2PO_4 , pH = 7.4). (B) Attenuated total reflectance Fourier-transform infrared spectrum of GA DPRs fibrils. The irradiated and incubated (48 hours) ADP-1 were centrifuged (16000 g) for 30 minutes to collect the GA DPRs fibrils in pellet. Black line indicated the raw IR spectrum of GA DPRs. Red line indicated the fitted curve of GA DPRs IR spectrum. (C) Normalized fluorescence intensity (484 nm) of Thioflavin-T (ThT) mixed with either irradiated or unirradiated ADP-1 (50 μM) in the low-salt PBS. Both ThT and ADP-1 concentration equals to 25 μM in the solution. (D) Time-course turbidity measurements of irradiated (wavelength: 365 nm, power density: 32 mW/cm^2 , duration: 1 minute) (red) and unirradiated (black) ADP-1 (50 μM). Data are collected at 0.5th, 2nd, 6th, 12th, 24th, 48th, and 96th hour (Standard deviation, $n=3$).

circular dichroism spectra were atypical. To further confirm the secondary structure of GA DPRs fibrils, we employed infrared spectroscopy to monitor the vibration and stretch frequencies of Amide I. The resulting IR spectrum (Figure 6B) indicated that GA DPRs fibrils had higher content of β -sheet, which was in line with our circular dichroism observation.

As the vast majority of GA DPRs fragments tended to adopt β -sheet structure, we were intrigued by question of whether they could form amyloid fibrils; therefore, dye-binding assay was applied here. Several dyes, such as thioflavin T, congo red, and NIAD-4, are capable of visualizing and characterizing the presence of amyloid through the intercalation of dye molecules between the β -strand. Once dye molecules bind to the β -sheet-rich structure such as amyloid, these dyes exhibit enhancement in fluorescence and red-shift of their emission spectrum, which provides us a preliminary insight into amyloidogenesis. The enhancement of fluorescence at 490 nm (Figure 6C) from Thioflavin T revealed the formation of amyloid fibrils of GA DPRs fragments overtime. Along this direction, we also surveyed the turbidity change of ADP-1 solution either irradiated with UV light or not by optical density measurements at 600 nm. As shown in Figure 6D, the increase of turbidity in irradiated ADP-1 samples suggesting the formation of GA DPRs aggregates overtime. Moreover, we noticed both enhanced fluorescence and increased turbidity reached the saturation after 48-hours-incubation, indicating most of

released GA DPRs fragments formed Thioflavin T-positive amyloid aggregates.



3-3 GA DPRs formed amyloid oligomers and turned into fibrils.

One of the features in amyloidogenic proteins is that they form fibrillar structures stacking by β -sheet. To examine the physical morphology of GA DPRs amyloid aggregates, we employed transmission electron microscopy (TEM). As the micrograph shown in Figure 7A, GA DPRs promptly formed spheroid structures with size ranging from 20 nm to 50 nm after 2 hours of incubation since photoinitiation. Extending the incubation time gave the result to show GA DPRs gradually formed fibrils. By contrast, unirradiated ADP-1 formed only trace nonfibrillar structures, suggesting the positive-charged octalysine fragment could prevent the GA DPRs from polymerization. In addition, no significant structures could be found in the irradiated or unirradiated ADP-3, evincing that neither octalysine nor (GA)₃ fragments can form fibrils (Figure 7A). To verify if the spheroid structure observed in TEM were also existing in the aqueous solution, we used dynamic light scattering to measure 2-hour incubated photoinitiated ADP-1 samples. Judged from the size distribution diagram (Figure 7B), the average diameter of spheroid structures in aqueous solution ranged from 60 to 130 nm. On the contrary, unirradiated ADP-1 formed only trace amount of amorphous aggregates that could be hardly detected by dynamic light scattering, similar to what we have observed in TEM micrographs.

In order to resolve our doubts on the correlation between spheroids we found in TEM and putative GA DPRs oligomers, we next utilized dot-blot analysis on GA DPRs by immunostaining with A11 antibody, a polyclonal antibody recognized amyloid oligomers. Our result (Figure 7C) revealed GA DPRs released from ADP-1 might form amyloid oligomers after 2 hours incubation. As we extended the incubation time, the signals from A11 staining gradually decreased, hinted GA DPRs amyloid oligomers might turn into

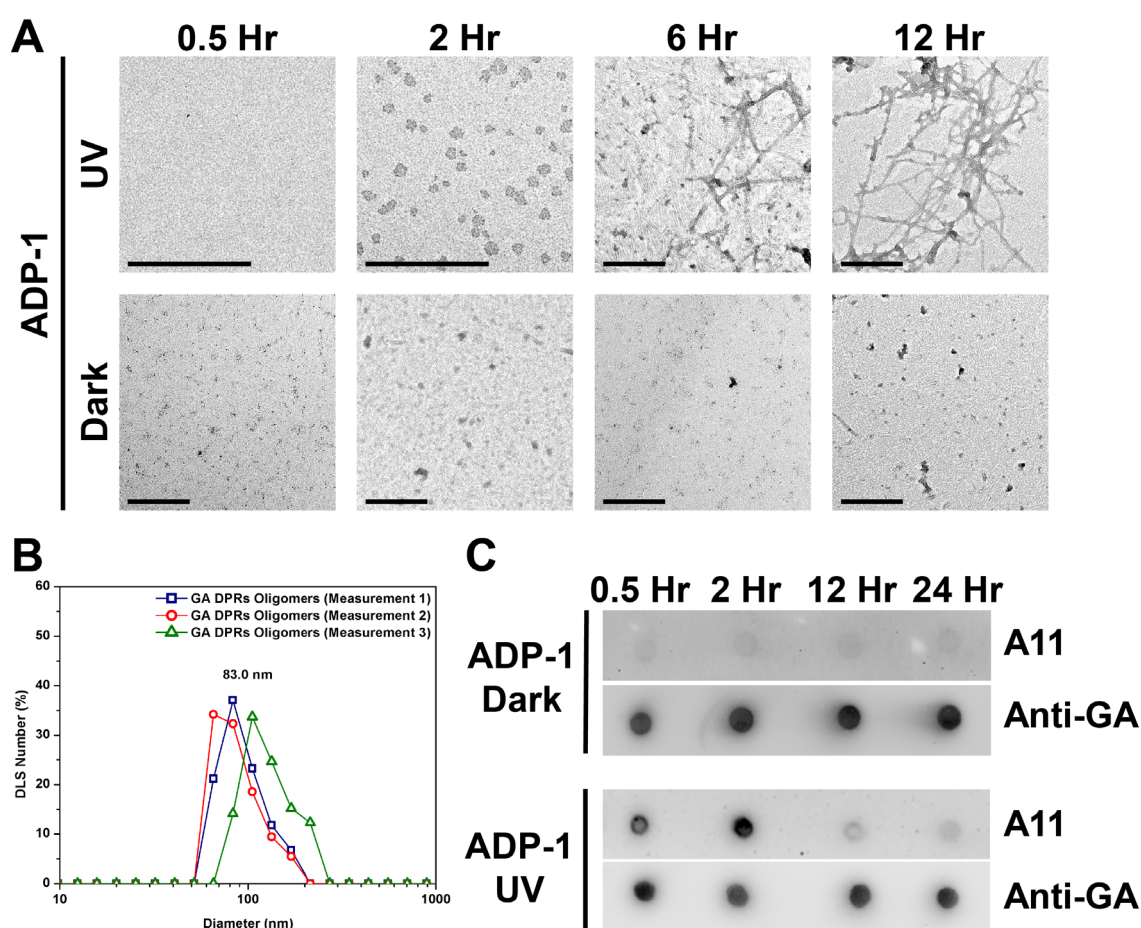


Figure 7. GA DPRs formed amyloid fibrils after photoinitiation. (A) Time-course transmission electron microscope analysis of ADP-1 (50 μ M). Scale bars indicate 200 nm. (B) Size distribution diagram of GA DPRs oligomers measured by DLS. ADP-1 (100 μ M) were irradiated with UV light and incubated for 2 hours before measurements. (C) Dot blot analysis of ADP-1-induced GA DPRs over time. The Sample were incubated until the indicated time and applied on PVDF membrane. After drying, membranes were stained with anti-GA DPRs antibody and A11 antibody.

fibrils overtime. The A11 staining kinetic is in accordance with our previous observation in TEM, together highlighting the transient oligomerization process of GA DPRs. By contrast, the unirradiated ADP-1 showed no signal enhancement in A11 staining, again demonstrating the ability of octalysine on suppressing the GA DPRs oligomerization and fibrillization.

Meanwhile, we also performed fluorescence-lifetime imaging microscopy (FLIM) to acquire further structural information of GA DPRs during oligomerization and fibrillization. FLIM is a powerful imaging technique that provides information with images by monitoring the difference in fluorescence decay rate (lifetime). The fluorescence lifetime greatly depends on the local environments, such as molecular binding, energy acceptors, ion or oxygen concentration, and pH value, but not excitation intensity or absorption of the sample. Chen *et al.* have demonstrated the application of FLIM on informing the aggregation kinetics and structural density of K18 protein fragments in Alzheimer's disease based on the fluorescence self-quenching property.⁹⁰ As the structural compactness of amyloid proteins increased, the fluorescence lifetime of the attached fluorophore decreased. On the basis of this principle, we aimed to investigate the compactness change of GA DPRs after photoinitiation by monitoring the fluorescence lifetime change of synthetic fluorophore attached to GA DPRs. Solution of fluorescent ADP-2 was prepared, photoinitiated, and then incubated at 37 °C. After photolysis, the

fluorescence-lifetime of *AF-488* decreased overtime from 4.1 ns of lifetime in the beginning, to slightly decrease of lifetime in the middle (2-6 hours), and finally drop to 3.7 ns of lifetime (Figure 8A). We have also performed the TEM observation on irradiated or unirradiated ADP-2 to confirm whether if small fluorophore had impacts on GA DPRs oligomerization. As shown in Figure 8B, the fluorescent GA DPRs released from ADP-2

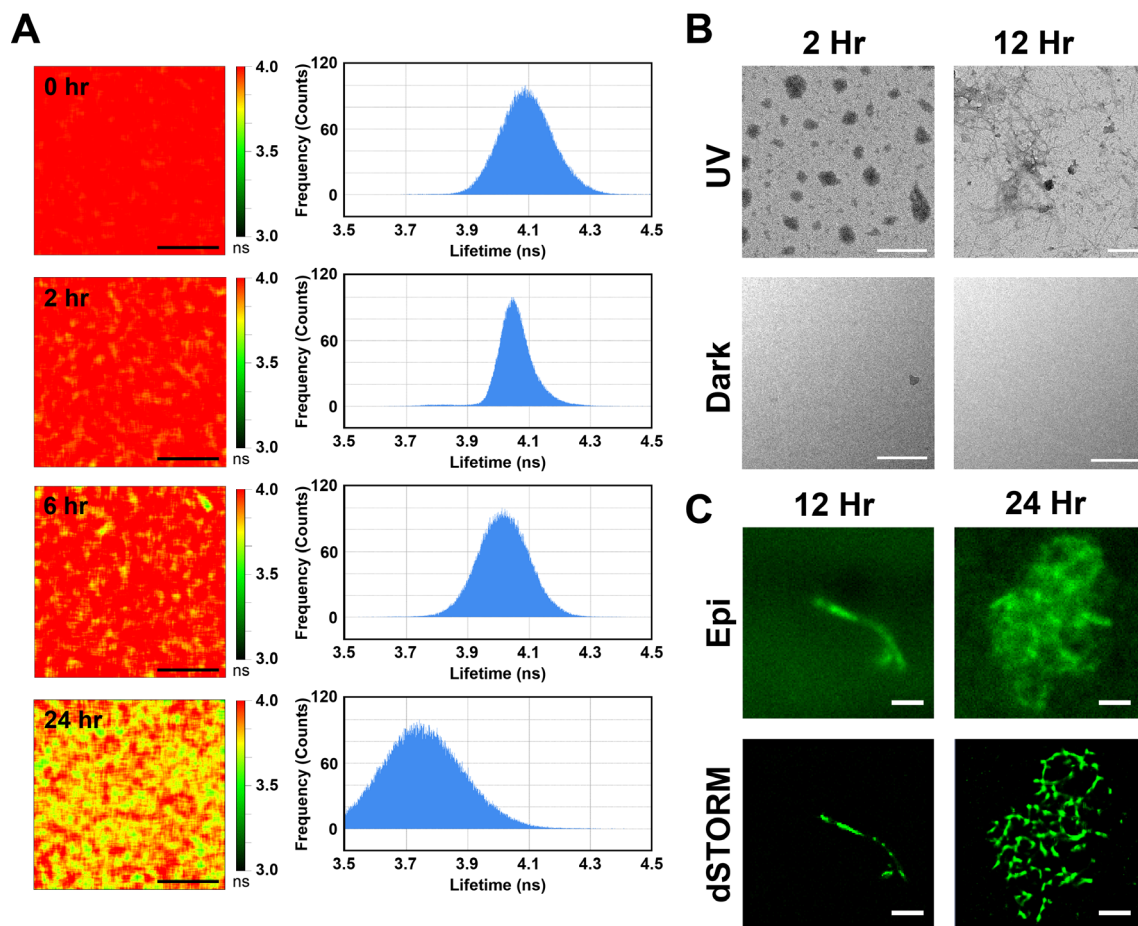


Figure 8. Fluorophore-labeled GA DPRs formed compact fibrillar structure. (A) Fluorescence lifetime images and the histogram of the photoinitiated ADP-2 (5 μ M). Images were taken at the 0.5th, 2nd, and 24th hour of incubation; scale bars indicate 5 μ m. (B) Transmission electron microscopy images of ADP-2. ADP-2 (100 μ M) were prepared in the low salt phosphate buffer saline and incubated at 37 $^{\circ}$ C for different periods. Scale bar indicated 100 nm. (C) Epi-fluorescence and direct stochastic optical reconstruction microscopy (dSTORM) images of the photoinitiated ADP-2 (50 μ M). Images were acquired at the 12th and 24th hours of incubation; scale bars indicate 10 μ m.

share similar kinetics with unlabeled GA DPRs released from ADP-1. Collectively, our result evinced GA DPRs formed more compact structures from the monomers, to oligomers, and finally fibrils as time evolved.



In addition to TEM and FLIM, we also applied direct stochastic optical reconstruction microscopy (dSTORM) to observe the fibrillar network of fluorescent GA DPRs. As illustrated in (Figure 8C), linear fibrils were documented with an average size of 10-20 μm after 12 hours incubation. By extending the incubation time to 24 hours, we noticed cluster fibrils with planar ribbon-like structure.

3-4 GA DPRs caused nucleocytoplasmic transport defects

Since biophysical and biochemical properties of GA DPRs fragments released from ADP-1 have been delineated *in vitro*, our next aim was to learn whether if ADP-1 can deliver GA DPRs fragments into cells and release them upon photoinitiation. Therefore, human neuroblastoma SH-SY5Y, a frequently used neuronal-like cell model, was first treated with 1 μM of ADP-2, then illuminated by UV light (wavelength: 335-379 nm; power density: $\leq 8.24 \text{ mW/cm}^2$; duration: 1 minute), and incubated. Monitored by FLIM, GA DPRs evenly distributed in the cell bodies in the beginning (Figure 9A). The fluorescence lifetime of *AF-488* attached on the GA DPRs is around 4.2 ns. As we extended the incubation time to 12 hours, GA DPRs monomers gradually assembled and

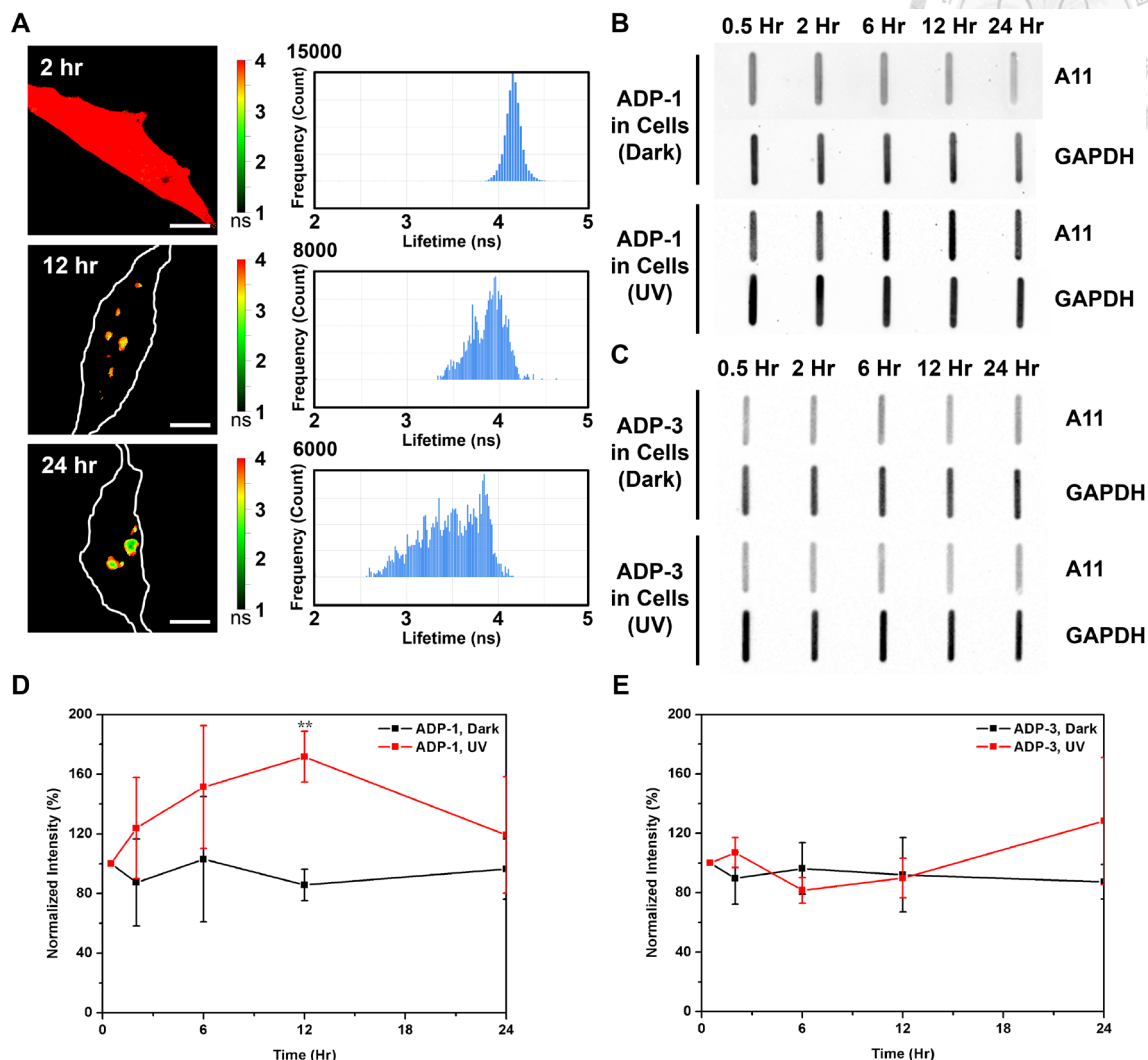
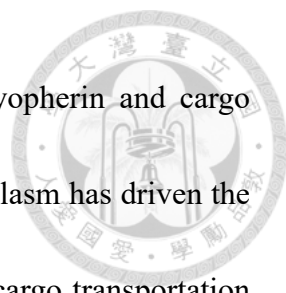


Figure 9. GA DPRs oligomerized in cells. (A) Time-course fluorescence-lifetime images and histograms of ADP-2 in SH-SY5Y cells. 1 μ M ADP-2 were treated to cells and photoinitiated by UV light (wavelength: 335-379 nm, power density: ≤ 8.24 mW/cm², duration: 1 minute). Cell periphery was contoured with white line in 12th and 24th hour, respectively. Images were taken at 2nd, 12th, 24th hour after UV illumination; scale bars indicate 5 μ m. (B) (C) A11 immunoblotting with cell lysates from SH-SY5Y cells received ADP-1 or ADP-3 (1 μ M) treatment with or without photoinitiation. After photoinitiation, Cell lysates at different time points were harvested and analyzed. (D)(E) Quantification analysis of A11 immunoblot of SH-SY5Y total cell lysates. The signal of A11 staining was first normalized to GAPDH staining and then compared to signal at 0.5 hour incubation. Three biological replicates were carried out ($r = 3$). Mean and standard deviation for ADP-1, UV = 171.7 ± 17.0 ; ADP-1, Dark = 85.8 ± 10.6 . ** indicates statistical significance where p value < 0.01 (analyzed by two-sided Welch's T test, p -value = 0.005, degree of freedom = 3, t -value = 3.18).

formed several small puncta in the cytoplasm with a slightly decreased lifetime (3.5-4.2 ns). After 24 hours of incubation, huge cytosolic puncta were recorded and the lifetime in the center of puncta is around 2.5 ns. The drop of *AF-488* fluorescence-lifetime indicated GA DPRs are capable of forming compact structures in cells overtime after photolysis from ADP-2 probes.

To further delineate whether GA DPRs fragments formed amyloid oligomers in cells, we loaded the ADP-1-treated SH-SY5Y cell lysate that collected at different time points on the nitrocellulose membrane for immunoblotting with A11 antibody. The resulting A11 signal would be normalized with internal control, GAPDH, and then compared with the signal collected at 0.5-hour time point. The A11 signal peaked around 12-hour incubation in the photoinitiated ADP-1-treated-cell lysate and then decreased afterward, revealing the transient existing of GA DPRs amyloid oligomers in cells (Figure 9B and 9D). On the contrary, neither unirradiated nor ADP-3-treated cell lysates showed significant enhancement of A11 signal, suggesting they failed to induce the GA DPRs oligomerization (Figure 9C and 9E).

Since accumulating studies have pointed out the nucleocytoplasmic transport defects may play a critical role in ALS,^{71,80,91} we thus were intrigued to investigate whether GA DPRs impair nucleocytoplasmic transport. Nuclear transportation, the entry and exit of biomacromolecule, is tightly regulated by nuclear pore complexes (NPCs), Ras-related



nuclear protein (Ran) gradient, and specific binding between karyopherin and cargo proteins. RanGTP concentration gradient between nucleus and cytoplasm has driven the transportation machinery, while importin and exportin mediate the cargo transportation into and out of nucleus via binding to signal sequence on proteins. On the account of the importance of Ran and importin to nuclear transport, we next attempted to delineate whether transport-relevant proteins were under the influence of GA DPRs. To dispel our doubts, ADP-2 treated SH-SY5Y cells were stained with Ran protein and importin- β antibody for immunofluorescence analysis. Under normal circumstance, Ran protein is more abundant in the nucleus due to RanGTP gradient, whereas importin- β is relatively rich in the perinuclear area because of weak binding affinity between importin and FG repeat domain of nucleoporins. Nevertheless, our results (Figure 10) demonstrated GA DPRs would lead to nuclear depletion of Ran and diffusion of importin- β to cytoplasm only in the group that received both ADP-2 treatment and photoinitiation. It is worthwhile to mention that GA DPRs are barely colocalized with Ran or importin- β , implying that GA DPRs did not instigate nuclear transport impairment through direct sequestration to transport-relevant proteins.

As the Ran gradient disruption was noticed, we sequentially doubted whether GA DPRs induced nucleocytoplasmic transport dysregulation. In order to evaluate the transport function, we have established a functional assay based on the imaging analysis

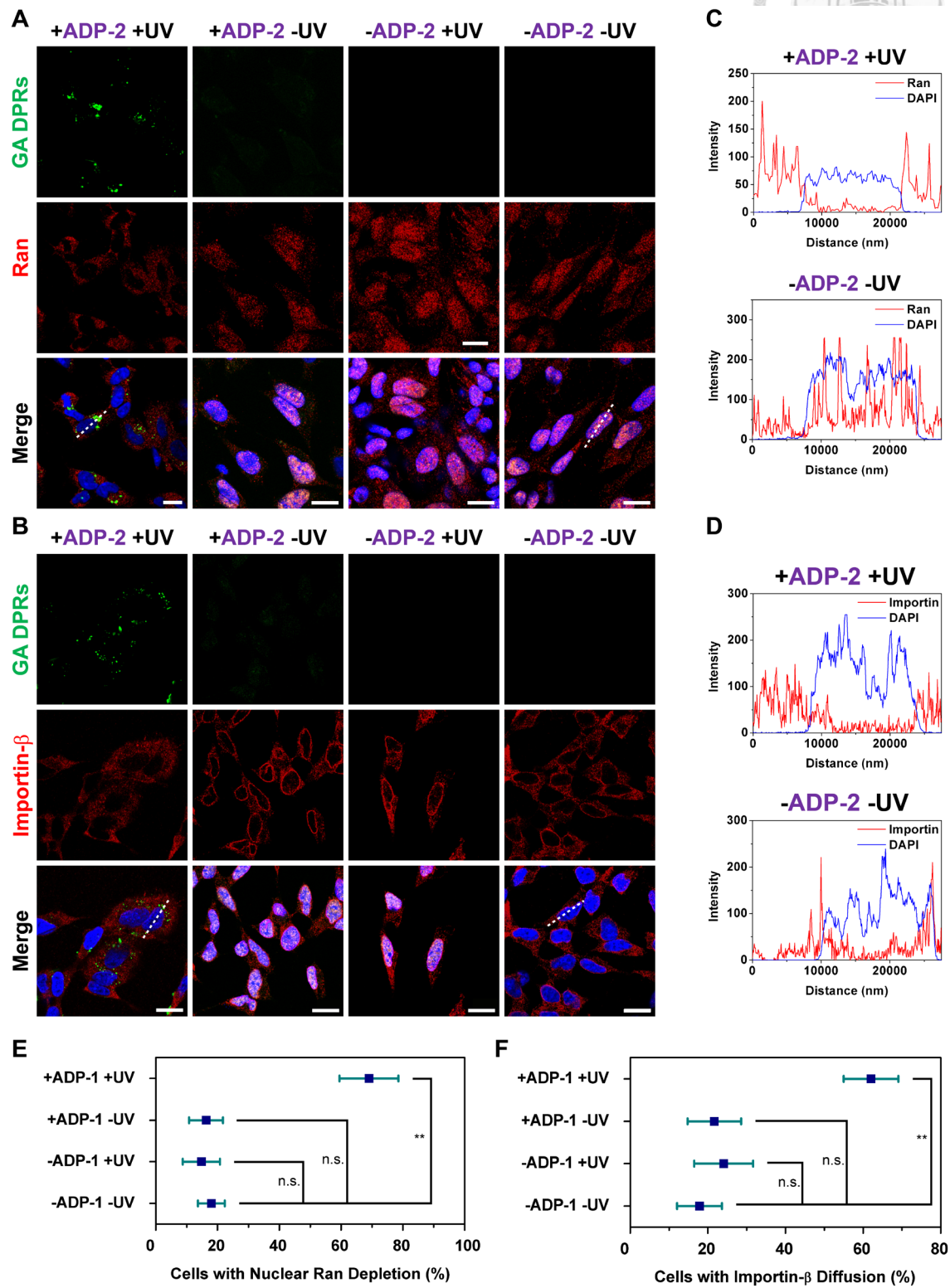
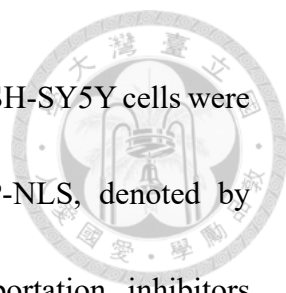


Figure 10. GA DPRs cause mislocalization of nuclear transport relevant proteins.

Figure 10. GA DPRs cause mislocalization of nuclear transport relevant proteins. (continued) (A) Immunofluorescence images of Ran protein (red) in ADP-2 photoinitiated (+ADP-2 +UV) or control SH-SY5Y cells. GA DPRs aggregates were shown in green color. Cells were treated with ADP-2 (1 μ M) and then exposure to UV light and incubated for 24 hours. Yellow arrows indicate the cells with nuclear Ran depletion. White dash line indicated the region for fluorescence intensity profiling. Scale bars indicate 10 μ m. (B) Immunofluorescence images of importin- β (red) in SH-SY5Y after ADP-2 (1 μ M) and irradiation treatment. GA DPRs aggregates were shown in green color. Yellow arrows indicate the cells with importin- β mislocalization. White dash line indicated the region for fluorescence intensity profiling. Scale bars indicate 10 μ m. (C) Fluorescence intensity profile of selected cells in Figure 10A. Blue curve indicated DAPI channel and red curve indicated Ran channel. (D) Fluorescence intensity profile of selected cells in Figure 10B. Blue curve indicated DAPI channel and red curve indicated importin- β channel. (E) Quantification analysis of SH-SY5Y cells with nuclear ran protein depletion. Three biological replicates were carried out ($r = 3$). More than 55 cells were counted and analyzed in each groups ($n \geq 55$). Mean and standard deviation for +ADP-1 +UV = 69.0 ± 9.6 ; +ADP-1 -UV = 16.2 ± 5.5 ; -ADP-1 +UV = 14.7 ± 6.0 ; -ADP-1 -UV = 18.0 ± 4.4 . ** indicate statistical significance where p value < 0.01 (analyzed by two-sided Welch's T test with Bonferroni correction, test statistic in group comparision between +ADP-1 +UV and -ADP-1 -UV: p -value = 0.0011, degree of freedom = 3, t -value = 3.18), and n.s. indicated not significant. (F) Quantification analysis of SH-SY5Y cells with importin- β diffusion. Three biological replicates were carried out ($r = 3$). More than 37 cells were counted and analyzed in each groups ($n \geq 37$). Mean and standard deviation for +ADP-1 +UV = 62.0 ± 7.0 ; +ADP-1 -UV = 21.7 ± 6.9 ; -ADP-1 +UV = 24.1 ± 7.6 ; -ADP-1 -UV = 17.8 ± 5.8 . *** indicates statistical significance where p value < 0.001 (analyzed by two-sided Welch's T test with Bonferroni correction, test statistic in group comparision between +ADP-1 +UV and -ADP-1 -UV: p -value = 0.0004, degree of freedom = 4, t -value = 2.78), and n.s. indicates not significant.



of reporter cargoes that shuttled between the nucleus and cytoplasm. SH-SY5Y cells were transfected with shuttling green-fluorescence protein (NES-eGFP-NLS, denoted by sGFP), then treated with either importation (Importazole), exportation inhibitors (Leptomycin B), or ADP-1 (Figure 11A). Epifluorescence microscopy equipped with total internal reflection fluorescence (TIRF) was used to collect the cellular image and Image J was applied to analysis the ratio of sGFP in the nucleus and cytoplasm. The nuclear-to-cytoplasmic ratio (N to C ratio = fluorescence intensity of sGFP in the nucleus / fluorescence intensity of sGFP in the cytoplasm) was used to evaluate the transport function. In the mock (treated with 1 % of dimethyl sulfoxide), the nuclear-to-cytoplasmic ratio (N-C ratio) is around 0.98, indicating sGFP the evenly distributed in the nucleus and cytoplasm (Figure 11B-C). When cells were treated with leptomycin B (LMB), which was known to target chromosomal maintenance 1(CRM1, also referred to as exportin 1), exporting function was severely inhibited and the resulting N-C ratio was increased to 2.18. On the other hand, when cells were treated with importazole (IPZ), a known importing inhibitor that targets the importin- β 1, most of sGFP retained in the nucleus and the corresponding N-C ratio was decreased to 0.54. Notably, with the ADP-1 treatment and photoinitiation, the majority of sGFP also retained in the cytoplasm and the calculating N-C ratio dropped to 0.4, suggesting transport function was severely sabotaged, especially the importation of proteins, by GA DPRs.

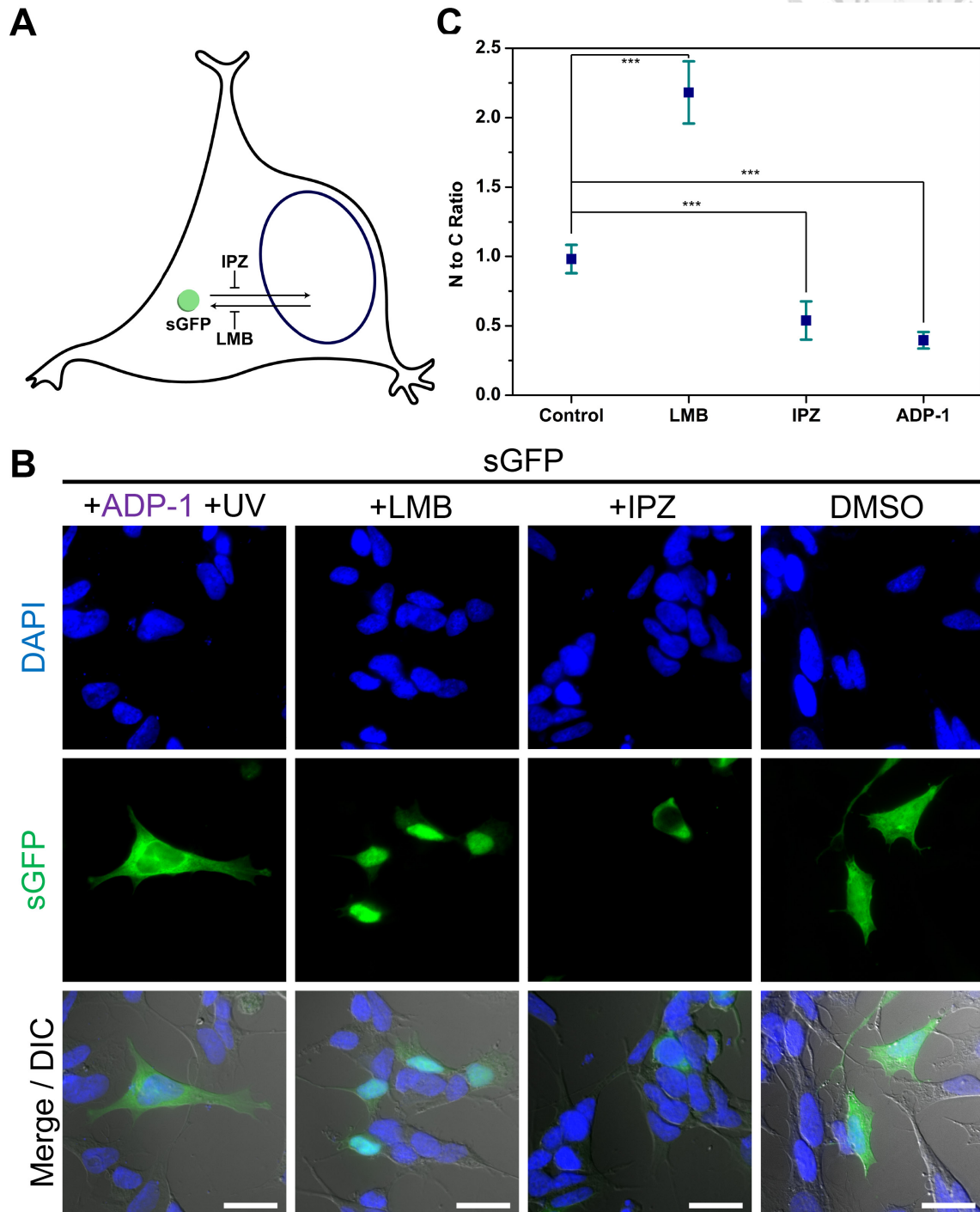


Figure 11. GA DPRs disrupted the nucleocytoplasmic transport.

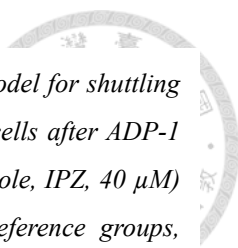


Figure 11. GA DPRs disrupted the nucleocytoplasmic transport. (continue) (A) Model for shuttling GFP experiments. (B) Immunofluorescence images of sGFP-transfected SH-SY5Y cells after ADP-1 treatment (1 μ M) and UV-irradiation. Corresponding nuclear importation (Importazole, IPZ, 40 μ M) and exportation (Leptomycin B, LMB, 20 nM) inhibitors were used here as reference groups, respectively. Scale bars indicate 10 μ m. (C) Quantification analysis of nuclear-to-cytoplasmic ratio of sGFP reporter in SH-SY5Y. One biological replicates were carried out ($r = 1$). Cell counting number (n) in each group: Control = 38, LMB = 36, IPZ = 31, ADP-1 = 38. Mean and standard deviation for Control = 0.98 ± 0.10 ; LMB = 2.18 ± 0.22 ; IPZ = 0.54 ± 0.14 ; ADP-1 = 0.40 ± 0.06 . *** indicates statistical significance where p value < 0.001 , (analyzed by two-sided Welch's T test with Bonferroni correction, test statistic in group comparision between Control and LMB: p -value = 7.6×10^{-33} , degree of freedom = 48, t -value = 2.01; group comparision between Control and IPZ: p -value = 3×10^{-21} , degree of freedom = 54, t -value = 2.00; group comparision between Control and ADP-1: p -value = 2.6×10^{-38} , degree of freedom = 59, t -value = 2.00).

3-5 GA DPRs compromised nuclear membrane



Previous studies have stated that the nucleocytoplasmic transport defects along with nuclear membrane disruption have been correlated with neurodegenerative diseases.⁹²⁻⁹⁵

Given the fact that the expression of *C9orf72* HRE mutations in the cell model was reported to disrupt the nuclear membrane,⁹⁶ we were thus intrigued to investigate whether GA DPRs compromise the nuclear membrane integrity. We employed TEM on sliced Cos-7 cells stained with osmium tetroxide to confirm whether nuclear morphology were disrupted by GA DPRs. Cos-7 cells were used here for better attachment to the coverslip. As depict in Figure 12A, ADP-1 treated and photoirradiated cells exhibited invaginated nuclear morphology. Moreover, the boundary of nuclear membrane structure, namely the inner and outer membrane, in ADP-1 treated and irradiated cells were getting considerably blurred and crossed; while the membrane boundary in control cells could be easily distinguished, hinting that GA DPRs may have impinged upon the nuclear membrane.

In addition, we further employed two-color direct stochastic optical reconstruction microscopy (dSTORM) to examine the nuclear lamina, the protein networks that support membrane structure, of illuminated Cos7 cells in the presence of photoinitiated ADP-2. Cells were stained with lamin B1, a marker protein for nuclear lamina. Comparing to the

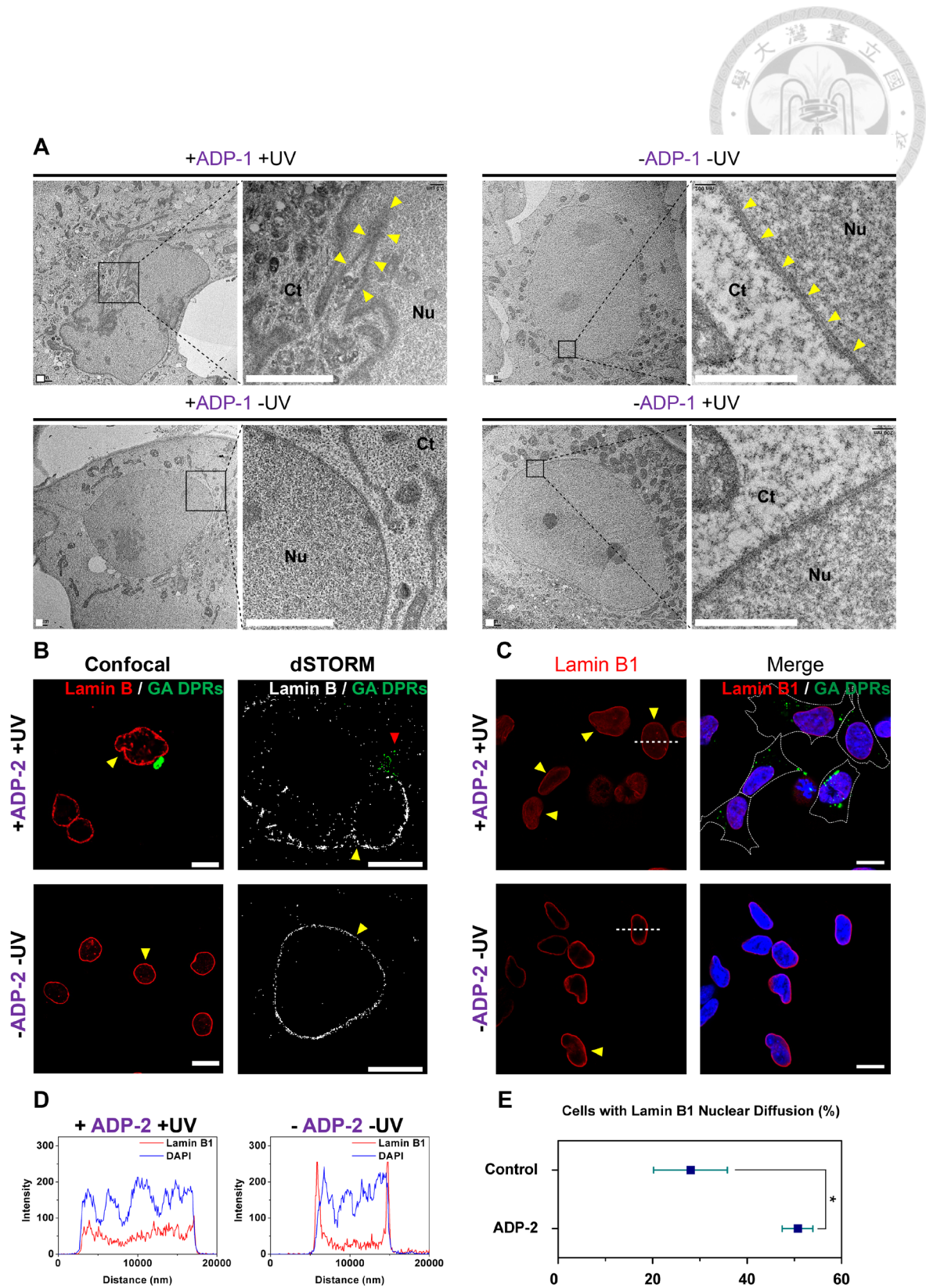


Figure 12. GA DPRs compromised nuclear membrane.

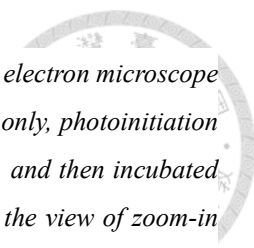
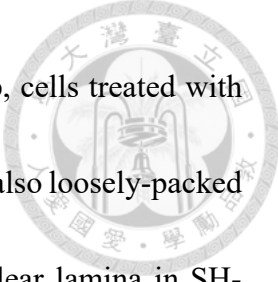


Figure 12. GA DPRs compromised nuclear membrane. (continue) (A) Transmission electron microscope images of in Cos-7 cells with ADP-1 treatment and photoinitiation, ADP-1 treatment only, photoinitiation only, and not treatment. Cos-7 cells were treated with ADP-1 (1 μ M), photoinitiated, and then incubated for 24 hours. Yellow arrows indicate the nuclear membrane. Black squares indicate the view of zoom-in images. Scale bar indicates 1 μ m. (B) Immunofluorescence images of lamin B1 in Cos-7 cells treated with ADP-2 and photoinitiation under confocal microscopy or dSTORM. Cells were treated with ADP-2 (1 μ M), photoinitiated and then incubated for 24 hours. Yellow arrows indicate the lamin B1 staining. Scale bars indicate 10 μ m. (C) Immunofluorescence images of lamin B1 (red) in GA DPRs (green)-rich SH-SY5Y. Cells were treated with ADP-2 (1 μ M), photoinitiated and then incubated for 24 hours. Yellow arrows indicate the lamin B1 nuclear diffusion. White dash line in the lamin B1 channel indicated the region for fluorescence intensity profiling. Scale bars indicate 10 μ m. (D) Fluorescence intensity profile of the cells in Figure 4B. Red curve indicated Lamin B1 channel and the blue curve indicated DAPI channel. (E) Quantification analysis demonstrated majority of cells with lamin B1 nuclear diffusion after ADP-2 treatment and photoinitiation (+ADP-2 +UV). Three biological replicates were carried out ($r = 3$). More than 53 cells were counted and analyzed in each groups ($n \geq 53$). Mean and standard deviation for group Control = 28.0 ± 7.8 ; ADP-2 = 50.7 ± 3.3 . * indicates statistical significance where p value < 0.05 (p -value = 0.019, analyzed by two-sided Welch's T test, degree of freedom = 3, t -value = 3.18).



round-shape and tightly-packed lamina structure in the control group, cells treated with ADP-2 and photoinitiation displayed not only severe invagination but also loosely-packed lamina (Figure 12B). Meanwhile, we also paid attention to the nuclear lamina in SH-SY5Y cells after photoinitiated ADP-2 treatment. Consistent to what we observed in Cos-7 cells, photoinitiated ADP-2-treated SH-SY5Y cells showed abnormal invagination of nuclear envelope (Figure 12C). By contrast, nuclear envelope in the untreated cells remained intact and round-shape. Through the quantifying the percentage of cells with abnormal nuclear morphology (Figure 12C-E), we found that GA DPRs could cause higher nuclear diffusion of lamin B (51 %) comparing to controls did (23 %).

Since we have identified the GA DPRs oligomers *in vitro* as aforementioned, we thus wondered whether GA DPRs amyloid oligomers may be the prime suspect in nuclear membrane disruption. To investigate if GA DPRs oligomers damage nuclear membrane, we herein employed *ex vivo* antibody penetrance assay on SH-SY5Y cells. Digitonin was used to selectively remove the plasma membrane but leave intact nuclear membrane for subsequent GA DPRs oligomers / fibrils treatment. The integrity of the nuclear membrane was evaluated by the level of lamin B antibody penetrance using immunohistochemistry. Normally, antibodies cannot penetrate lipid membranes to bind with target proteins without surfactant-assistant permeabilization. Therefore, the positive staining of nuclear lamina may evince that GA DPRs can interact with and permeabilize the nuclear

membrane, which allow antibody penetrating for immunohistochemistry. SH-SY5Y cells were first treated with digitonin (0.001%) on the ice for 2 minutes to remove the plasma membrane, followed by treating the cellular remains (nucleus + some cytosolic contents) with GA DPRs oligomers or fibrils (100 μ M) for 2 hours at 37 °C. Next, these cellular

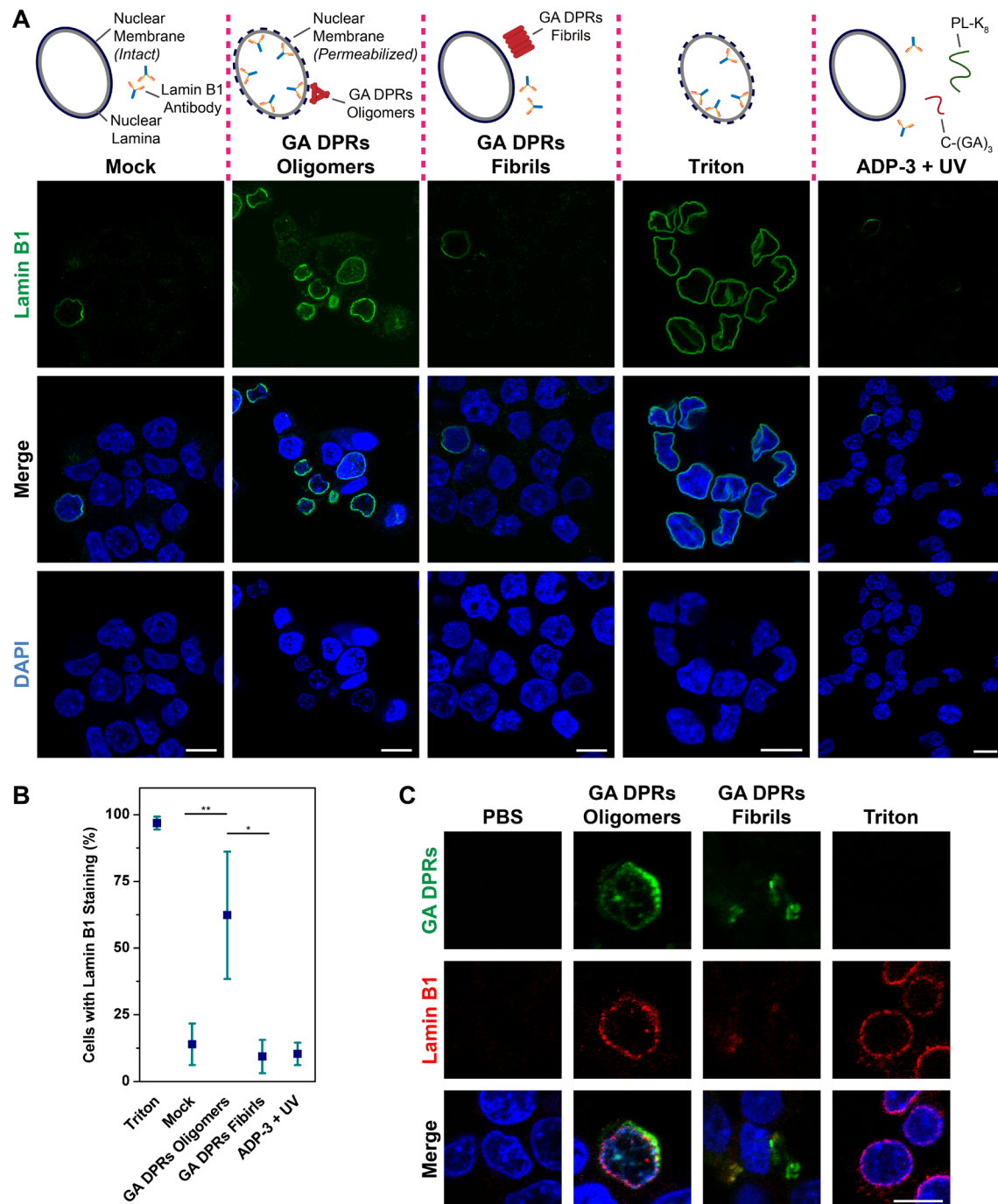
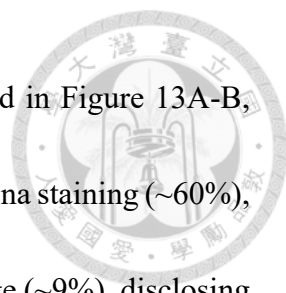


Figure 13. GA DPRs oligomers permeabilized nuclear membrane.

Figure 13. GA DPRs oligomers permeabilized nuclear membrane. (continue) (A) Representative images of lamin B1 staining on digitonin-treated SH-SY5Y cells in the presence of GA DPRs oligomers, fibrils, triton, photoinitiated ADP-3, or mock (buffer only). The nuclei was counterstained with DAPI. Scale bars indicate 10 μ m. (B) Quantification analysis of SH-SY5Y cell nuclei with lamin B1 staining. Three biological replicates were carried out ($r = 3$). More than 27 cells were counted and analyzed in each groups ($n \geq 27$). Mean and standard deviation for Mock = 13.9 ± 7.8 ; Triton = 96.9 ± 2.4 ; GA DPRs Oligomers = 62.3 ± 23.9 ; GA DPRs fibrils = 9.5 ± 6.2 ; ADP-3 + UV = 10.6 ± 4.2 . * indicates statistical significance where p value < 0.05 and ** indicate statistical significance where p value < 0.01 (analyzed by two-sided Welch's T test with Bonferroni correction, test statistic in group comparision between Mock and GA DPRs Oligomers: p -value = 0.009, degree of freedom = 4, t -value = 2.77; group comparison between GA DPRs Oligomers and GA DPRs Fibrils: p -value = 0.011, degree of freedom = 3, t -value = 3.18). (C) Representative images of lamin B1 staining on digitonin-treated SH-SY5Y cells in the presence of fluorescent GA DPRs oiligomers, fibrils, triton or mock (buffer only). The nuclei was counterstained with DAPI. Scale bars indicate 10 μ m.



remains were fixed and stained with lamin B1 antibody. As depicted in Figure 13A-B, GA DPRs oligomers-treating-group showed higher percentage of lamina staining (~60%), while GA DPRs fibrils-treating group had minimal staining percentage (~9%), disclosing that it is the GA DPRs oligomers rather than the fibrils that caused the nuclear membrane disruption. We further utilized ADP-2-derived fluorescent GA DPRs oligomers / fibrils to treat the digtonin-treated SH-SY5Y cell remains. Our results (Figure 13C) pointed out that GA DPRs had close contacts with the nuclear membrane, implying GA DPRs oligomers may disrupt the nuclear membrane through direct interaction.

On the basis of our findings, we next aim to clarify if GA DPRs oligomers can directly interact with the lipid membrane. Calcein-leakage assay was applied here to examine the interaction between GA DPRs and the synthetic lipid liposome. Fluorescent calcein molecules were encapsulated in the cholesterol-containing lipid liposomes, and their fluorescence was self-quenched within the liposome but restored when leaking out (Figure 14A). By monitoring the fluorescence intensity change of calcein-encapsulated liposomes in the presence or absence of peptides, one can learn if peptides interact with lipid membranes and enhance their permeability. The resulting fluorescence readouts, obtained by subtracting the background signal (liposome + buffer) from the signal of encapsulated liposome in the presence of peptide, were normalized to the signal of totally permeabilized liposome (liposome + Triton X100). GA DPRs oligomers or fibrils were

mixed with calcein-encapsulated liposome-containing solution and agitated at 37 °C for 1 hour. As shown in Figure 14B, GA DPRs oligomers resulted in fluorescence enhancement, whereas GA DPRs fibrils and photoinitiated ADP-3 have a minimal enhancement in fluorescence, revealing that GA DPRs can interact with synthetic liposomes and cause the permeability change. In addition, we have further employed

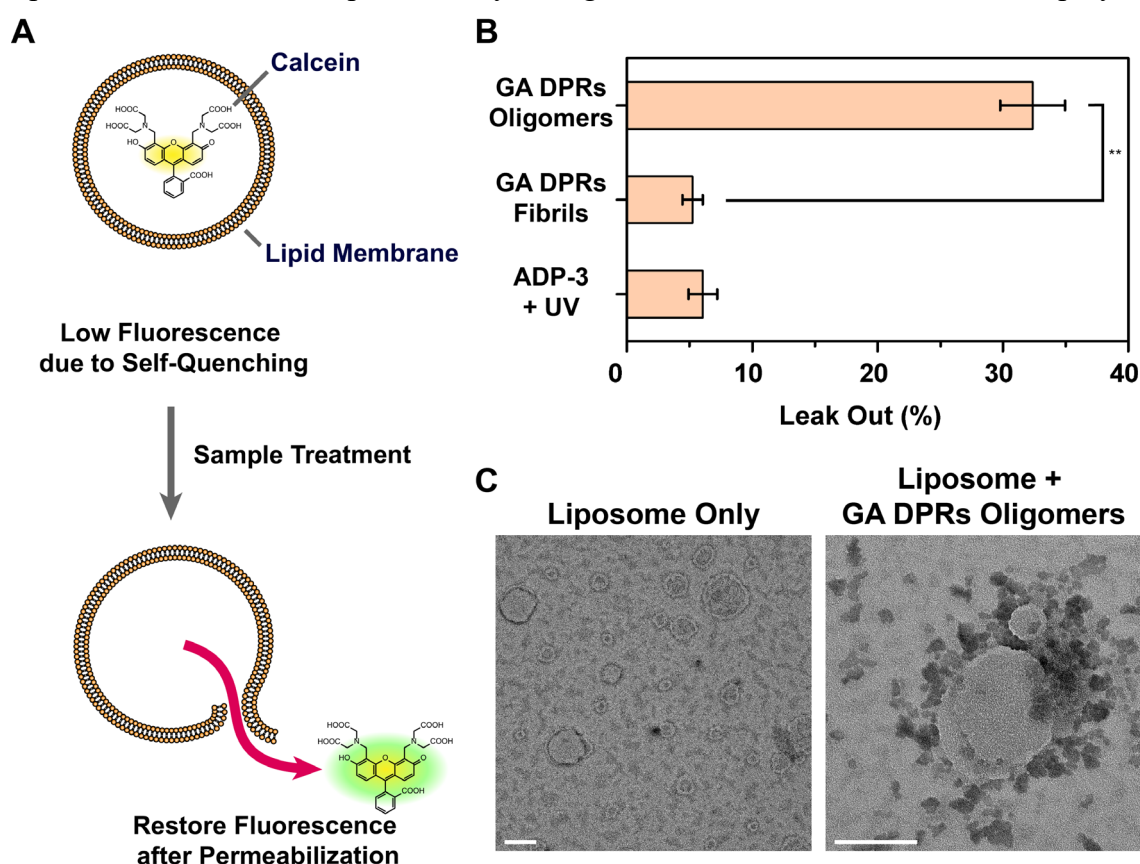


Figure 14. GA DPRs permeabilized lipid membrane. (A) Model of calcein-leakage assay. (B) Ratio of the calcein (emission at 520 nm) leak-out from lipid-based liposome based on the fluorescence measurement. Fluorescence intensity was measured for each sample, and then subtracts the background (liposome only) and normalized to the signal from the Triton X100 treatment (lysed liposome). Three experiment replicates were carried out ($r = 3$), Mean and standard deviation for GA DPRs Oligomers = 32.4 ± 2.6 ; GA DPRs Fibrils = 5.2 ± 0.8 . ** indicates statistical significance where p value < 0.01 (analyzed by two-sided Welch's T test, p -value = 0.003, degree of freedom = 2, t -value = 4.30). (C) Transmission electron microscopy images of lipid liposome interacting with GA DPRs oligomers. The solution containing calcein-encapsulated liposomes were mixed with GA DPRs oligomers ($100 \mu\text{M}$). The resulting solution were quickly applied on the TEM grids and stained with 1 % phosphotungstic acid. Scale bar indicated 100 nm.

TEM to monitor the interaction between lipid liposomes and GA DPRs oligomers. Our result indicated that GA DPRs oligomers bind to the surface of lipid liposome upon mixing (Figure 14C), hinting GA DPRs could directly interact with lipid membrane while detailed mechanism required further investigation.

3-6 GA DPRs induced endogenous TDP-43 mislocalized to cytoplasm

As we mentioned earlier, GA DPRs are correlated with TDP-43 pathology in the C9-ALS.¹⁴ Therefore, we would like to scrutinize if GA DPRs released from ADP-1 could also result in the TDP-43 proteinopathy in cells. Our result (Figure 15A-B) has demonstrated TDP-43 in photoinitiated ADP-1-treated SH-SY5Y cells (~60%) translocated from the nucleus to cytoplasm. In contrast, the control groups (either with or without probe treatment and UV irradiation) showed minimal mislocalization of TDP-43 (~20%). It is manifesting the close correlation between GA DPRs and TDP-43 as previous studies have found. Accordingly, we surmised that cytosolic accumulation of TDP-43 may be the outcome of nuclear importing dysregulation induced by GA DPRs.

Apart from translocation of TDP-43, we also noticed some cytosolic TDP-43 inclusions after ADP-1 treatment and photoinitiation. We consequently wonder if GA DPRs could seed the TDP-43 protein into large inclusion bodies. To answer the question, we expressed the human TDP-43 via rabbit reticulocyte cell-free protein synthesis system

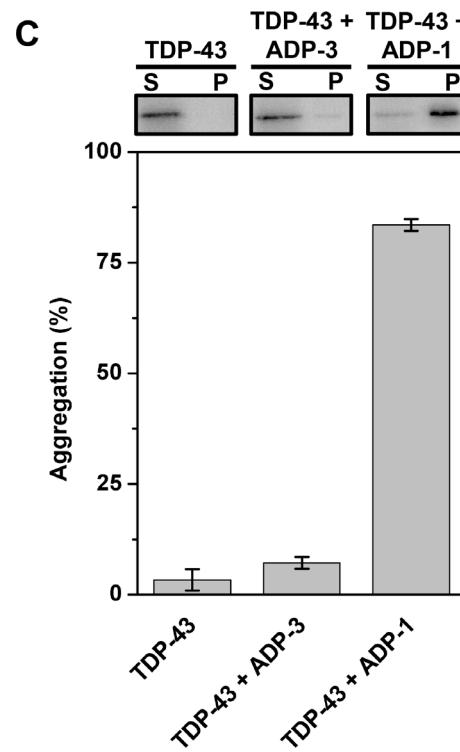
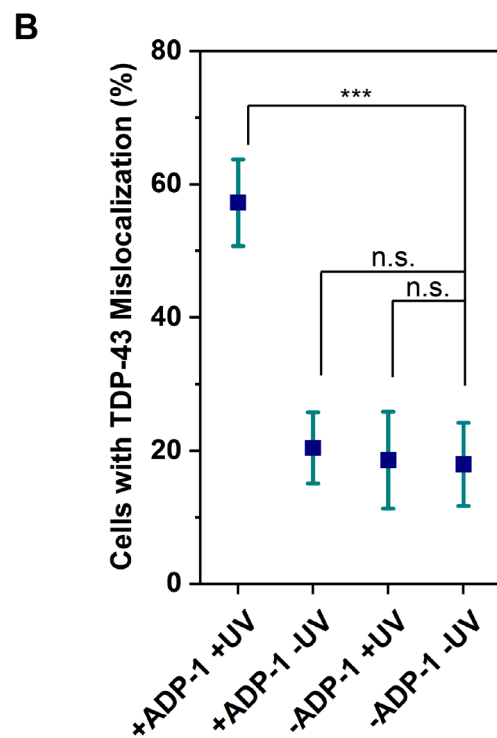
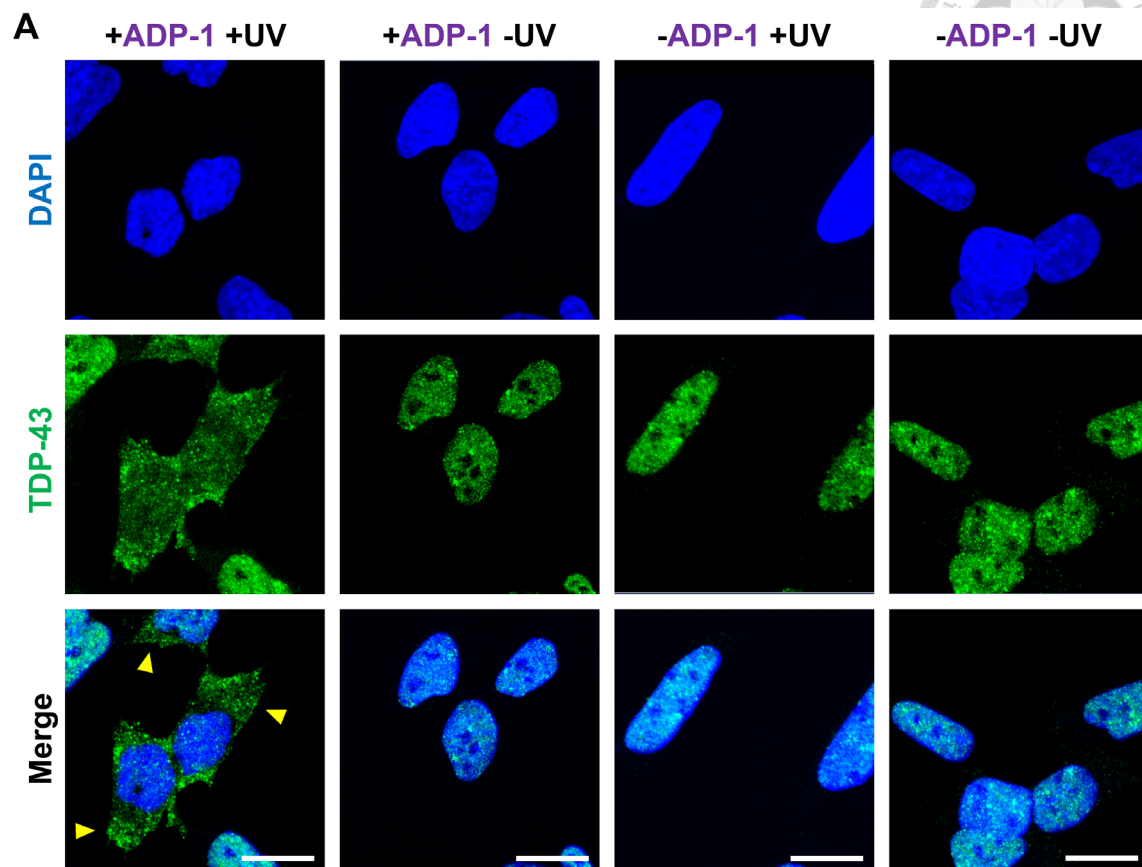
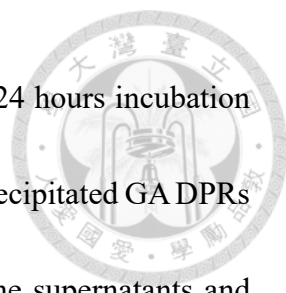


Figure 15. GA DPRs induced mislocalization of endogenous TDP-43.

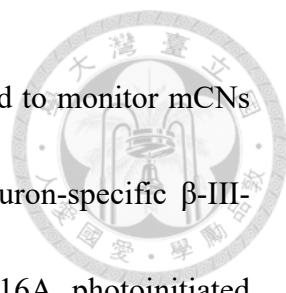
Figure 15. GA DPRs induced mislocalization of endogenous TDP-43. (continue) (A) Representative immunofluorescence of endogenous TDP-43 (Green) in neuroblastoma SH-SY5Y after ADP-1 treatment (1 μ M), photoinitiated, and then incubated for 24 hours. Yellow arrows indicate the cells with mislocalized TDP-43. Scale bars indicate 10 μ m. (B) Quantification analysis of SH-SY5Y cells with TDP-43 mislocalization. Three biological replicates were carried out ($r = 3$). More than 32 cells were counted and analyzed in each groups ($n \geq 32$). Mean and standard deviation for +ADP-1 +UV = 57.2 ± 6.5 ; +ADP-1 -UV = 20.4 ± 5.4 ; -ADP-1 +UV = 18.6 ± 7.3 ; -ADP-1 -UV = 17.9 ± 6.3 . *** indicates statistical significance where p value < 0.001 (analyzed by two-sided Welch's T test with Bonferroni correction, test statistic in group comparision between +ADP-1 +UV and -ADP-1 -UV: p -value = 0.0005, degree of freedom = 4, t -value = 2.78; group comparision between +ADP-1 -UV and -ADP-1 -UV: p -value = 0.21, degree of freedom = 4, t -value = 2.77; group comparision between -ADP-1 +UV and -ADP-1 -UV: p -value = 0.30, degree of freedom = 4, t -value = 2.77), and n.s. indicates not significant. (C) The ratio of aggregation TDP-43 expressed by cell-free system in the presence or absence of ADP-1 and ADP-3. The probes were irradiated with UV light and incubated for 24 hours. Centrifugation (16000 g-force) was used to collect the GA DPRs fibrils from ADP-1.



and spiked with GA DPRs. GA DPRs seeds were obtained through 24 hours incubation of GA DPRs that photocleaved from ADP-1. We coincubated the precipitated GA DPRs fibrils with expressed human TDP-43 for 12 hours and separated the supernatants and pellets from mixture through centrifugation. Both of fractions were subjected to sodium dodecyl sulfate-polyacrylamide gel electrophoresis and Western blotting. It showed that GA DPRs fibrils could seed TDP-43 protein and that transformed soluble TDP-43 into insoluble pellets (Figure 15C). Our result manifested that the GA DPRs fibrils are capable of cross-seeding the TDP-43 protein into insoluble inclusions, hinted at GA DPRs along with TDP-43 may together contribute to the neurotoxicity.

3-7 Introduction of GA DPRs promote degeneration in mouse cortical neurons

Accumulating studies have shown that expressing the GA DPRs in the mouse cortical tissue resulted in cognitive deficits, cerebellar atrophy, and neural toxicity.^{80,97} To characterize the effect of GA DPRs released from our probe on the cortical neurons, ADP-1 was applied to dissociate primary mouse cortical neurons (mCNs). mCNs were isolated from E17.5 (embryonic day 17) mouse embryos and further cultured for 21 days *in vitro* (21DIV) which allowed mCNs to mature and establish synaptic connection between each other. 21DIV mCNs were treated with 1 μ M of ADP-1, irradiated with UV light, and then



incubated for 24 hours. Immunofluorescence staining was performed to monitor mCNs morphology and the localization of endogenous TDP-43 using neuron-specific β -III-tubulin antibody and TDP-43 antibody. As demonstrated in Figure 16A, photoinitiated ADP-1-treated mCNs manifested severe neurite fragmentation (35%, Figure 16B). In comparison, both untreated, probe treatment alone, and UV irradiation alone groups show only minimal neurite fragmentation (15%). In addition, we also performed quantification analysis on the distribution of endogenous TDP-43 in mCNs. While the overall TDP-43 level decreased in photoinitiated ADP-1-treated mCNs was noted, it exhibited a lower TDP-43 nucleus-to-cytoplasm (N to C) ratio (Figure 16C), evincing TDP-43 may translocate from the nucleus to cytoplasm. In summary, our results have demonstrated GA DPRs could induce endogenous TDP-43 mislocalization and cause severe degeneration in the primary cortical neuron, implying the neurotoxicity of GA DRPs may play a role in disease progression.

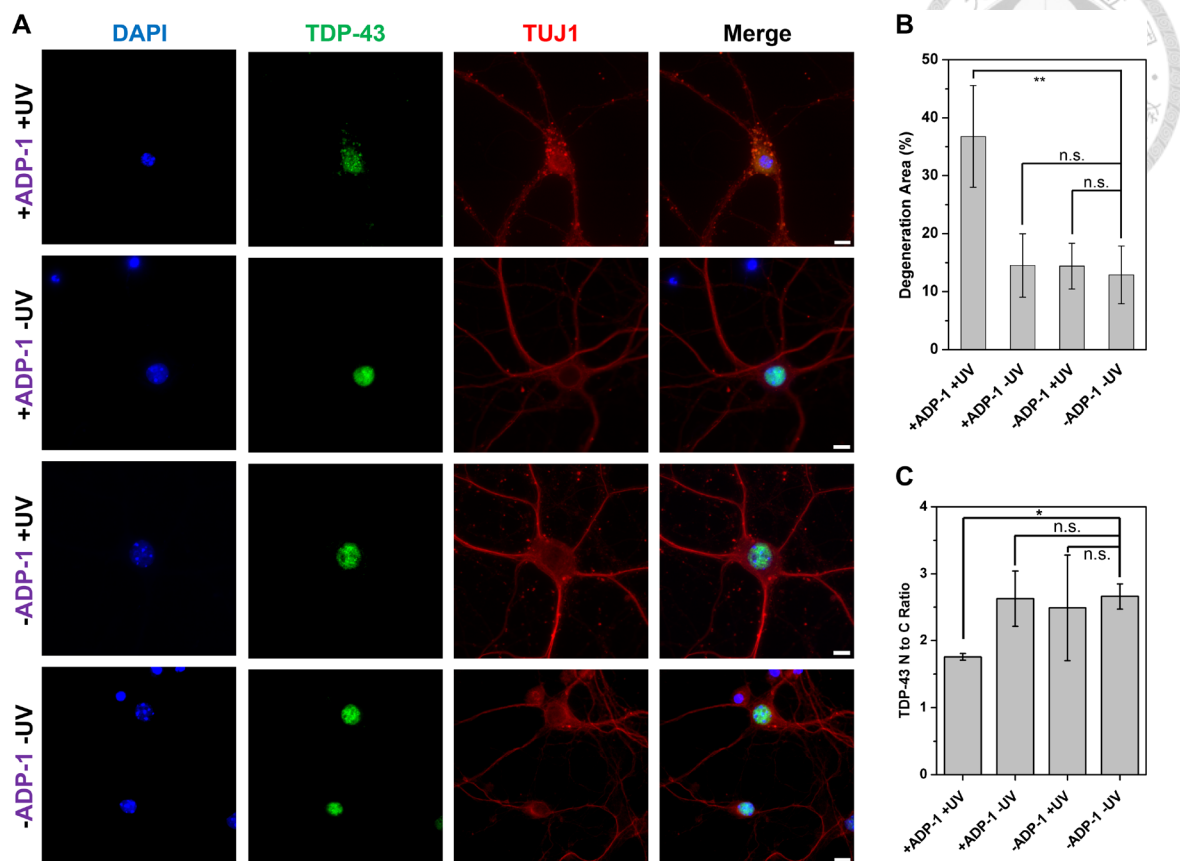


Figure 16. GA DPRs induced cytosolic retention of TDP-43 and degeneration in mouse cortical neurons. (A) Representative immunofluorescence images of 21DIV mouse cortical neurons stained with antibody against β -III-tubulin (red) and TDP-43 (green) treated with or without 1 μ M ADP-1 and/or 2 minutes of UV irradiation. The mouse cortical neurons were further incubated for 24 hours after ADP-1 treatment and/or UV irradiation. The DNA counter stain DAPI (blue) was included to identify the location of the nucleus. Scale bar indicated 10 μ m. (B) Quantification analysis of degeneration area in 21DIV mouse cortical neurons. The degeneration area percentage (%) of neuron is quantified as fragmented neurite area / total neurite area. Three biological replicates were carried out ($r = 3$). Mean and standard deviation for +ADP-1 +UV = 36.8 ± 8.8 ; +ADP-1 -UV = 14.5 ± 5.5 ; -ADP-1 +UV = 14.4 ± 3.9 ; -ADP-1 -UV = 12.9 ± 5.0 . ** indicates statistical significance where p value < 0.01 (analyzed by two-sided Welch's T test with Bonferroni correction, test statistic in group comparison between +ADP-1 +UV and -ADP-1 -UV: p -value = 0.0086, degree of freedom = 3, t -value = 3.18), and n.s. indicated not significant. (C) Quantification analysis nuclear-to-cytoplasmic ratio of TDP-43 in mice cortical neurons. Three biological replicates were carried out ($r = 3$) and counted neuron number (n) in each group: +ADP-1 +UV = 86; +ADP-1 -UV = 55; -ADP-1 +UV = 52; -ADP-1 -UV = 56. Mean and standard deviation for +ADP-1 +UV = 1.75 ± 0.05 ; +ADP-1 -UV = 2.62 ± 0.42 ; -ADP-1 +UV = 2.49 ± 0.79 ; -ADP-1 -UV = 2.66 ± 0.19 . ** indicates statistical significance where p value < 0.01 (analyzed by two-sided Welch's T test with Bonferroni correction, test statistic in group comparison between +ADP-1 +UV and -ADP-1 -UV: p -value = 0.005, degree of freedom = 2, t -value = 4.30), and n.s. indicated not significant.

IV. Discussion

4-1 ADP-1 as a feasible tools for *C9orf72* pathology studies

To study the GA DPRs proteinopathy in living cells, genetic transfection is widely used. However, to transfect a *C9orf72* mutation-derived dipeptide, one cannot properly avoid the interference of RNA toxicities. Inevitably, studying *C9orf72* pathology through genetic transfection of G₄C₂ HRE might lead to a misunderstanding between the toxicity from RNA toxicities and the DPRs toxicities. While alternative codons can be used to replace the G₄C₂ HRE in order to avoid RNA toxicities, it is less clear whether alternative codons contribute to other toxicities or not. Taking advantage of our photoinducible probe, one can differentiate the GA DPRs toxicity in neurons without the interference from G₄C₂ HRE.

Furthermore, genetic transfecting the DPRs protein that conjugated with fluorescent reporter seemed to alter their intrinsic properties. Nonaka *et al.* has shown the fluorescent reporters with relatively large size comparing to the GA DPRs could disrupt the localization and aggregation properties of GA DPRs.⁸⁴ In addition, the poor photostability and dimerization properties of fluorescent proteins would limit the application of fluorescent protein labeled GA DPRs on the advanced microscopy technique, such as dSTORM and FLIM. Our ADP-2 probe was conjugated with photostable and pH-insensitive small-molecule fluorophore, which allowed us to monitor the detailed

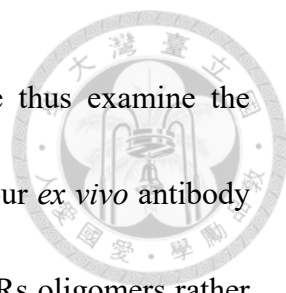
aggregation process of GA DPRs in cells. From our results, it has been shown that the small size of synthetic fluorophore has minimal influence on the intrinsic properties of GA DPRs.



Directly treating dipeptides in the cell cultured medium has been used in previous studies. Synthetic peptides (GA)₁₅ were used to treat N2a cells and monitor their cell-to-cell transmission by Chang *et al.*⁷⁶ however, it has raised our doubts about the peptide treatments. The solubility of GA DPRs in physiological buffer is poor, hence the additional additive was required. In their study, dichloroacetic acid (DCA) was used to pretreat the (GA)₁₅ peptides, and the remaining concentration of DCA in further experiments is about 1%. It is disputable that whether reactive oxygen species (ROS) level increase and cytotoxicity are resulting from (GA)₁₅ peptides or DCA. In our study, we can efficiently deliver GA DPRs by ADP-1 probe without any toxic additives because of its high solubility and cellular permeability.

4-2 GA DPRs amyloid oligomers and their toxicities.

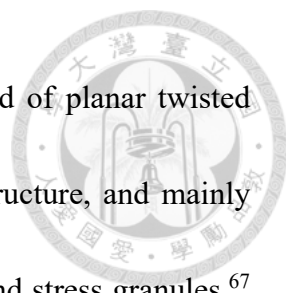
There has never been reported that GA DPRs formed oligomers during the amyloidogenesis process, and yet we have identified the existence of them through our probes. Similar to other amyloid fragments such as amyloid- β , GA DPRs oligomers had a spheroid structure with size ranging from 20-30 nm and A11-staining positivity. Since



amyloid oligomers were known to induce membrane rupture, we thus examine the correlation between membrane disruption and GA DPRs. Through our *ex vivo* antibody penetrance assay and calcein-leakage assay, we noticed it is GA DPRs oligomers rather than fibrils that perturbed the lipid membrane via direct interaction. Previous studies have shown that both α -synuclein and amyloid- β oligomers interacted with membranes by electrostatic force between their charged amino acid residue and the phosphate groups on lipid.⁹⁸ However, GA DPRs fragment has no charged amino acid residue and its predicted net charge at physiological condition is zero for carboxylation modification and one for amidation modification at C-terminus, whereas other amyloidogenic sequences usually carry either multiple positive or negative charges at the same condition. Though the detailed mechanism of how GA DPRs oligomers interact with lipid membranes is yet to be determined, we thus reasoned that this interaction is mainly based on Van der Waals forces and hydrogen bonding due to the hydrophobicity of glycine and alanine and the lack of charge on peptide sequence.

4-3 Comparison between GA and PR DPRs in nuclear transport defect

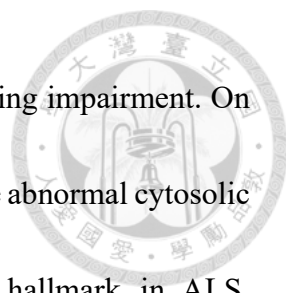
In addition to GA DPRs, both PR and GR DPRs have been previously shown to cause neurotoxicity and impair nuclear transport.⁷⁴ Therefore, it is interesting to compare the proteinopathy of GA DPRs to that of PR/GR DPRs. In neuronal models, GA DPRs



tends to form cytosolic inclusion bodies which is mainly composed of planar twisted ribbon structures,⁷⁷ while PR and GR DPRs have no secondary structure, and mainly localized in the RNA-rich organelle, such as nucleoli, Cajal body, and stress granules.⁶⁷ Moreover, a few studies demonstrated that PR can impair the nuclear transport via directly binding to FG repeat domain in the nuclear pore complexes and thus disrupt their morphological equilibrium.⁷⁴ By contrast, our results revealed GA DPRs might compromise the nuclear membrane via direct interaction and further induce nucleocytoplasmic transport dysregulation though the detailed mechanism required further investigation.

4-4 Conclusion and prospect

In summary, we have developed a photoinducible probe which allows the spatiotemporally controlled release of GA DPRs in cells. We demonstrated that one could study the mechanism of GA DPRs toxicity without the interference from G4C2 HRE by applying our probe. Through the biochemical and microscopical investigation, we comprehensively inspected the GA DPRs inclusion formation process from the monomers, to the oligomers, and finally fibrils. We found that GA DPRs oligomers would compromise the integrity of nuclear membrane and induce nucleocytoplasmic transport defects. Through the distribution analysis of shuttling-GFP and transport-relevant

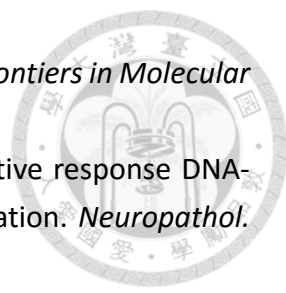



proteins (Ran & importin- β), we have confirmed the nuclear trafficking impairment. On the basis of our findings, we identified GA DPRs would further induce abnormal cytosolic accumulation of both endogenous TDP-43, a key pathological hallmark in ALS. Collectively, we have demonstrated the capability of ADP-1 probe in elucidating the GA DPRs pathology for *C9orf72*-ALS studies.

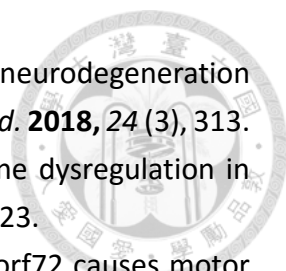
In the future, we expect to apply our probe on multiple DPRs studies to figure out if GA DPRs interacting with other DPRs and their potentially synergistic effects in ALS. Furthermore, it has been suspected that DPRs possess of cell-to-cell transmission properties and thus infected other healthy neurons.⁹⁹ To resolve this issue, we believe our probe can serve as an excellent platform in cellular transmission studies for its controllable property. We hope future application of ADP-1 probe may shed the light on unraveling pathological mechanism of *C9orf72*-ALS.

V. Reference

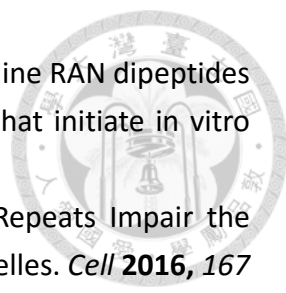
- (1) Brown, R. H.; Al-Chalabi, A. Amyotrophic Lateral Sclerosis. *New England Journal of Medicine* **2017**, 377 (2), 162.
- (2) Balendra, R.; Isaacs, A. M. C9orf72-mediated ALS and FTD: multiple pathways to disease. *Nat. Rev. Neurol.* **2018**, 14 (9), 544.
- (3) Petrov, D.; Mansfield, C.; Moussy, A. *et al.* ALS Clinical Trials Review: 20 Years of Failure. Are We Any Closer to Registering a New Treatment? *Front. Aging Neurosci.* **2017**, 9 (68).
- (4) Al-Chalabi, A.; Hardiman, O. The epidemiology of ALS: a conspiracy of genes, environment and time. *Nat. Rev. Neurol.* **2013**, 9 (11), 617.
- (5) Ingre, C.; Roos, P. M.; Piehl, F. *et al.* Risk factors for amyotrophic lateral sclerosis. *Clin. Epidemiol.* **2015**, 7, 181.
- (6) Al-Chalabi, A.; Calvo, A.; Chio, A. *et al.* Analysis of amyotrophic lateral sclerosis as a multistep process: a population-based modelling study. *The Lancet. Neurology* **2014**, 13 (11), 1108.
- (7) Taylor, J. P.; Brown, R. H.; Cleveland, D. W. Decoding ALS: from genes to mechanism. *Nature* **2016**, 539 (7628), 197.
- (8) Therrien, M.; Dion, P. A.; Rouleau, G. A. ALS: Recent Developments from Genetics Studies. *Curr. Neurol. Neurosci. Rep.* **2016**, 16 (6), 59.
- (9) Rosen, D. R.; Siddique, T.; Patterson, D. *et al.* Mutations in Cu/Zn superoxide dismutase gene are associated with familial amyotrophic lateral sclerosis. *Nature* **1993**, 362 (6415), 59.
- (10) Bosco, D. A.; Morfini, G.; Karabacak, N. M. *et al.* Wild-type and mutant SOD1 share an aberrant conformation and a common pathogenic pathway in ALS. *Nat. Neurosci.* **2010**, 13 (11), 1396.
- (11) Gurney, M. E.; Pu, H.; Chiu, A. Y. *et al.* Motor neuron degeneration in mice that express a human Cu,Zn superoxide dismutase mutation. *Science* **1994**, 264 (5166), 1772.
- (12) Arai, T.; Hasegawa, M.; Akiyama, H. *et al.* TDP-43 is a component of ubiquitin-positive tau-negative inclusions in frontotemporal lobar degeneration and amyotrophic lateral sclerosis. *Biochemical and Biophysical Research Communications* **2006**, 351 (3), 602.
- (13) Neumann, M.; Sampathu, D. M.; Kwong, L. K. *et al.* Ubiquitinated TDP-43 in Frontotemporal Lobar Degeneration and Amyotrophic Lateral Sclerosis. *Science* **2006**, 314 (5796), 130.
- (14) Prasad, A.; Bharathi, V.; Sivalingam, V. *et al.* Molecular Mechanisms of TDP-43

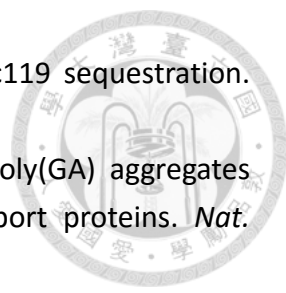
- 
- Misfolding and Pathology in Amyotrophic Lateral Sclerosis. *Frontiers in Molecular Neuroscience* **2019**, 12 (25).
- (15) Gendron, T. F.; Josephs, K. A.; Petrucelli, L. Review: Transactive response DNA-binding protein 43 (TDP-43): mechanisms of neurodegeneration. *Neuropathol. Appl. Neurobiol.* **2010**, 36 (2), 97.
 - (16) Cohen, T. J.; Lee, V. M. Y.; Trojanowski, J. Q. TDP-43 functions and pathogenic mechanisms implicated in TDP-43 proteinopathies. *Trends Mol. Med.* **2011**, 17 (11), 659.
 - (17) Ling, S.-C.; Polymenidou, M.; Cleveland, Don W. Converging Mechanisms in ALS and FTD: Disrupted RNA and Protein Homeostasis. *Neuron* **2013**, 79 (3), 416.
 - (18) Tan, R. H.; Ke, Y. D.; Ittner, L. M. *et al.* ALS/FTLD: experimental models and reality. *Acta Neuropathologica* **2017**, 133 (2), 177.
 - (19) Lee, E. B.; Lee, V. M. Y.; Trojanowski, J. Q. Gains or losses: molecular mechanisms of TDP43-mediated neurodegeneration. *Nat. Rev. Neurosci.* **2012**, 13 (1), 38.
 - (20) Gao, J.; Wang, L.; Huntley, M. L. *et al.* Pathomechanisms of TDP-43 in neurodegeneration. *J. Neurochem.* **2018**, 146 (1), 7.
 - (21) Barmada, S. J.; Skibinski, G.; Korb, E. *et al.* Cytoplasmic Mislocalization of TDP-43 Is Toxic to Neurons and Enhanced by a Mutation Associated with Familial Amyotrophic Lateral Sclerosis. *The Journal of Neuroscience* **2010**, 30 (2), 639.
 - (22) Gendron, T. F.; Rademakers, R.; Petrucelli, L. TARDBP mutation analysis in TDP-43 proteinopathies and deciphering the toxicity of mutant TDP-43. *Journal of Alzheimer's disease* **2013**, 33 (S1), S35.
 - (23) Mutihac, R.; Alegre-Abarategui, J.; Gordon, D. *et al.* TARDBP pathogenic mutations increase cytoplasmic translocation of TDP-43 and cause reduction of endoplasmic reticulum Ca²⁺ signaling in motor neurons. *Neurobiol. Dis.* **2015**, 75, 64.
 - (24) Renton, Alan E.; Majounie, E.; Waite, A. *et al.* A Hexanucleotide Repeat Expansion in C9ORF72 Is the Cause of Chromosome 9p21-Linked ALS-FTD. *Neuron* **2011**, 72 (2), 257.
 - (25) DeJesus-Hernandez, M.; Mackenzie, I. R.; Boeve, B. F. *et al.* Expanded GGGGCC hexanucleotide repeat in noncoding region of C9ORF72 causes chromosome 9p-linked FTD and ALS. *Neuron* **2011**, 72 (2), 245.
 - (26) Gijselinck, I.; Van Langenhove, T.; van der Zee, J. *et al.* A *C9orf72* promoter repeat expansion in a Flanders-Belgian cohort with disorders of the frontotemporal lobar degeneration-amyotrophic lateral sclerosis spectrum: a gene identification study. *Lancet Neurol.* **2012**, 11 (1), 54.
 - (27) Haeusler, A. R.; Donnelly, C. J.; Rothstein, J. D. The expanding biology of the

- 
- C9orf72 nucleotide repeat expansion in neurodegenerative disease. *Nat. Rev. Neurosci.* **2016**, *17*, 383.
- (28) Rutherford, N. J.; Heckman, M. G.; DeJesus-Hernandez, M. *et al.* Length of normal alleles of C9ORF72 GGGGCC repeat do not influence disease phenotype. *Neurobiol. Aging* **2012**, *33* (12), 2950. e5.
 - (29) Van der Zee, J.; Gijselinck, I.; Dillen, L. *et al.* A Pan-European Study of the C9orf72 Repeat Associated with FTL D: Geographic Prevalence, Genomic Instability, and Intermediate Repeats. *Hum. Mutat.* **2013**, *34* (2), 363.
 - (30) Harms, M. B.; Cady, J.; Zaidman, C. *et al.* Lack of C9ORF72 coding mutations supports a gain of function for repeat expansions in amyotrophic lateral sclerosis. *Neurobiol. Aging* **2013**, *34* (9), 2234.e13.
 - (31) Van Blitterswijk, M.; DeJesus-Hernandez, M.; Niemantsverdriet, E. *et al.* Association between repeat sizes and clinical and pathological characteristics in carriers of C9ORF72 repeat expansions (Xpansize-72): a cross-sectional cohort study. *Lancet Neurol.* **2013**, *12* (10), 978.
 - (32) Suh, E.; Lee, E. B.; Neal, D. *et al.* Semi-automated quantification of C9orf72 expansion size reveals inverse correlation between hexanucleotide repeat number and disease duration in frontotemporal degeneration. *Acta Neuropathol* **2015**, *130* (3), 363.
 - (33) Woollacott, I. O. C.; Mead, S. The C9ORF72 expansion mutation: gene structure, phenotypic and diagnostic issues. *Acta Neuropathol* **2014**, *127* (3), 319.
 - (34) Rizzu, P.; Blauwendraat, C.; Heetveld, S. *et al.* C9orf72 is differentially expressed in the central nervous system and myeloid cells and consistently reduced in C9orf72, MAPT and GRN mutation carriers. *Acta Neuropathol Commun* **2016**, *4* (1), 37.
 - (35) Waite, A. J.; Bäumer, D.; East, S. *et al.* Reduced C9orf72 protein levels in frontal cortex of amyotrophic lateral sclerosis and frontotemporal degeneration brain with the C9ORF72 hexanucleotide repeat expansion. *Neurobiol. Aging* **2014**, *35* (7), 1779.e5.
 - (36) Zhang, D.; Iyer, L.; He, F. *et al.* Discovery of Novel DENN Proteins: Implications for the Evolution of Eukaryotic Intracellular Membrane Structures and Human Disease. *Frontiers in Genetics* **2012**, *3* (283).
 - (37) Levine, T. P.; Daniels, R. D.; Gatta, A. T. *et al.* The product of C9orf72, a gene strongly implicated in neurodegeneration, is structurally related to DENN Rab-GEFs. *Bioinformatics* **2013**, *29* (4), 499.
 - (38) Kim, M.-S.; Pinto, S. M.; Getnet, D. *et al.* A draft map of the human proteome. *Nature* **2014**, *509* (7502), 575.

- 
- (39) Shi, Y.; Lin, S.; Staats, K. A. *et al.* Haploinsufficiency leads to neurodegeneration in C9ORF72 ALS/FTD human induced motor neurons. *Nat. Med.* **2018**, 24 (3), 313.
 - (40) Lai, J. D.; Ichida, J. K. C9ORF72 protein function and immune dysregulation in amyotrophic lateral sclerosis. *Neurosci. Lett.* **2019**, 713, 134523.
 - (41) Ciura, S.; Lattante, S.; Le Ber, I. *et al.* Loss of function of C9orf72 causes motor deficits in a zebrafish model of amyotrophic lateral sclerosis. *Ann. Neurol.* **2013**, 74 (2), 180.
 - (42) Amick, J.; Roczniak-Ferguson, A.; Ferguson, S. M. C9orf72 binds SMCR8, localizes to lysosomes, and regulates mTORC1 signaling. *Molecular Biology of the Cell* **2016**, 27 (20), 3040.
 - (43) Sellier, C.; Campanari, M.-L.; Julie Corbier, C. *et al.* Loss of C9ORF72 impairs autophagy and synergizes with polyQ Ataxin-2 to induce motor neuron dysfunction and cell death. *The EMBO Journal* **2016**, 35 (12), 1276.
 - (44) Babi, #x; Leko, M. *et al.* Molecular Mechanisms of Neurodegeneration Related to C9orf72 Hexanucleotide Repeat Expansion. *Behav. Neurol.* **2019**, 2019, 18.
 - (45) Webster, C. P.; Smith, E. F.; Bauer, C. S. *et al.* The C9orf72 protein interacts with Rab1a and the ULK1 complex to regulate initiation of autophagy. *The EMBO Journal* **2016**, 35 (15), 1656.
 - (46) Xiao, S.; MacNair, L.; McGoldrick, P. *et al.* Isoform-specific antibodies reveal distinct subcellular localizations of C9orf72 in amyotrophic lateral sclerosis. *Ann. Neurol.* **2015**, 78 (4), 568.
 - (47) Sareen, D.; O'Rourke, J. G.; Meera, P. *et al.* Targeting RNA Foci in iPSC-Derived Motor Neurons from ALS Patients with a C9ORF72 Repeat Expansion. *Sci. Transl. Med.* **2013**, 5 (208), 208ra149.
 - (48) Haeusler, A. R.; Donnelly, C. J.; Periz, G. *et al.* C9orf72 nucleotide repeat structures initiate molecular cascades of disease. *Nature* **2014**, 507 (7491), 195.
 - (49) Van Blitterswijk, M.; Gendron, T. F.; Baker, M. C. *et al.* Novel clinical associations with specific C9ORF72 transcripts in patients with repeat expansions in C9ORF72. *Acta Neuropathol* **2015**, 130 (6), 863.
 - (50) Xi, Z.; Zinman, L.; Moreno, D. *et al.* Hypermethylation of the CpG Island Near the G₄C₂ Repeat in ALS with a C9orf72 Expansion. *The American Journal of Human Genetics* **2013**, 92 (6), 981.
 - (51) Gijssels, I.; Van Mossevelde, S.; van der Zee, J. *et al.* The C9orf72 repeat size correlates with onset age of disease, DNA methylation and transcriptional downregulation of the promoter. *Mol. Psychiatry* **2016**, 21 (8), 1112.
 - (52) Belzil, V. V.; Bauer, P. O.; Gendron, T. F. *et al.* Characterization of DNA hypermethylation in the cerebellum of c9FTD/ALS patients. *Brain Res.* **2014**, 1584,

- 15.
- (53) Xi, Z.; Zhang, M.; Bruni, A. C. *et al.* The C9orf72 repeat expansion itself is methylated in ALS and FTLN patients. *Acta Neuropathol* **2015**, 129 (5), 715.
- (54) Donnelly, Christopher J.; Zhang, P.-W.; Pham, Jacqueline T. *et al.* RNA Toxicity from the ALS/FTD C9ORF72 Expansion Is Mitigated by Antisense Intervention. *Neuron* **2013**, 80 (2), 415.
- (55) Zu, T.; Liu, Y.; Bañez-Coronel, M. *et al.* RAN proteins and RNA foci from antisense transcripts in C9ORF72 ALS and frontotemporal dementia. *Proceedings of the National Academy of Sciences* **2013**, 110 (51), E4968.
- (56) Lagier-Tourenne, C.; Baughn, M.; Rigo, F. *et al.* Targeted degradation of sense and antisense C9orf72 RNA foci as therapy for ALS and frontotemporal degeneration. *Proc. Natl. Acad. Sci. U. S. A.* **2013**, 110 (47), E4530.
- (57) Reddy, K.; Schmidt, M. H. M.; Geist, J. M. *et al.* Processing of double-R-loops in (CAG)·(CTG) and C9orf72 (GGGGCC)·(GGCCCC) repeats causes instability. *Nucleic Acids Res.* **2014**, 42 (16), 10473.
- (58) Xu, Z.; Poidevin, M.; Li, X. *et al.* Expanded GGGGCC repeat RNA associated with amyotrophic lateral sclerosis and frontotemporal dementia causes neurodegeneration. *Proceedings of the National Academy of Sciences* **2013**, 110 (19), 7778.
- (59) Zhang, K.; Donnelly, C. J.; Haeusler, A. R. *et al.* The C9orf72 repeat expansion disrupts nucleocytoplasmic transport. *Nature* **2015**, 525, 56.
- (60) Mori, K.; Nihei, Y.; Arzberger, T. *et al.* Reduced hnRNPA3 increases C9orf72 repeat RNA levels and dipeptide-repeat protein deposition. *EMBO reports* **2016**, 17 (9), 1314.
- (61) Mori, K.; Weng, S. M.; Arzberger, T. *et al.* The C9orf72 GGGGCC repeat is translated into aggregating dipeptide-repeat proteins in FTLN/ALS. *Science* **2013**, 339 (6125), 1335.
- (62) Zu, T.; Gibbens, B.; Doty, N. S. *et al.* Non-ATG-initiated translation directed by microsatellite expansions. *Proc. Natl. Acad. Sci. U. S. A.* **2011**, 108 (1), 260.
- (63) Nguyen, L.; Cleary, J. D.; Ranum, L. P. W. Repeat-Associated Non-ATG Translation: Molecular Mechanisms and Contribution to Neurological Disease. *Annu. Rev. Neurosci.* **2019**, 42 (1), 227.
- (64) Freibaum, B. D.; Taylor, J. P. The Role of Dipeptide Repeats in C9ORF72-Related ALS-FTD. *Front. Mol. Neurosci.* **2017**, 10 (35).
- (65) Mizielinska, S.; Grönke, S.; Niccoli, T. *et al.* C9orf72 repeat expansions cause neurodegeneration in *Drosophila* through arginine-rich proteins. *Science* **2014**, 345 (6201), 1192.

- 
- (66) Wen, X.; Tan, W.; Westergard, T. *et al.* Antisense proline-arginine RAN dipeptides linked to *C9ORF72*-ALS/FTD form toxic nuclear aggregates that initiate in vitro and in vivo neuronal death. *Neuron* **2014**, *84* (6), 1213.
- (67) Lee, K. H.; Zhang, P.; Kim, H. J. *et al.* C9orf72 Dipeptide Repeats Impair the Assembly, Dynamics, and Function of Membrane-Less Organelles. *Cell* **2016**, *167* (3), 774.
- (68) Gendron, T. F.; Chew, J.; Stankowski, J. N. *et al.* Poly(GP) proteins are a useful pharmacodynamic marker for *C9ORF72*-associated amyotrophic lateral sclerosis. *Sci. Transl. Med.* **2017**, *9* (383), eaai7866.
- (69) Kwon, I.; Xiang, S.; Kato, M. *et al.* Poly-dipeptides encoded by the *C9orf72* repeats bind nucleoli, impede RNA biogenesis, and kill cells. *Science* **2014**, *345* (6201), 1139.
- (70) Molliex, A.; Temirov, J.; Lee, J. *et al.* Phase Separation by Low Complexity Domains Promotes Stress Granule Assembly and Drives Pathological Fibrillization. *Cell* **2015**, *163* (1), 123.
- (71) Lin, Y.; Mori, E.; Kato, M. *et al.* Toxic PR Poly-Dipeptides Encoded by the C9orf72 Repeat Expansion Target LC Domain Polymers. *Cell* **2016**, *167* (3), 789.
- (72) Brangwynne, Clifford P.; Tompa, P.; Pappu, Rohit V. Polymer physics of intracellular phase transitions. *Nature Physics* **2015**, *11* (11), 899.
- (73) Mier, P.; Paladin, L.; Tamana, S. *et al.* Disentangling the complexity of low complexity proteins. *Brief. Bioinform.* **2019**, *21* (2), 458.
- (74) Shi, K. Y.; Mori, E.; Nizami, Z. F. *et al.* Toxic PRn poly-dipeptides encoded by the C9orf72 repeat expansion block nuclear import and export. *Proc. Natl. Acad. Sci. U. S. A.* **2017**, *114* (7), E1111.
- (75) Lopez-Gonzalez, R.; Lu, Y.; Gendron, Tania F. *et al.* Poly(GR) in *C9ORF72*-Related ALS/FTD Compromises Mitochondrial Function and Increases Oxidative Stress and DNA Damage in iPSC-Derived Motor Neurons. *Neuron* **2016**, *92* (2), 383.
- (76) Chang, Y.-J.; Jeng, U.-S.; Chiang, Y.-L. *et al.* The Glycine-Alanine Dipeptide Repeat from C9orf72 Hexanucleotide Expansions Forms Toxic Amyloids Possessing Cell-to-Cell Transmission Properties. *J. Biol. Chem.* **2016**, *291* (10), 4903.
- (77) Guo, Q.; Lehmer, C.; Martínez-Sánchez, A. *et al.* In Situ Structure of Neuronal C9orf72 Poly-GA Aggregates Reveals Proteasome Recruitment. *Cell* **2018**, *172* (4), 696.
- (78) Zhang, Y.-J.; Jansen-West, K.; Xu, Y.-F. *et al.* Aggregation-prone c9FTD/ALS poly (GA) RAN-translated proteins cause neurotoxicity by inducing ER stress. *Acta Neuropathol* **2014**, *128* (4), 505.
- (79) May, S.; Hornburg, D.; Schludi, M. H. *et al.* C9orf72 FTLD/ALS-associated Gly-Ala

- 
- dipeptide repeat proteins cause neuronal toxicity and Unc119 sequestration. *Acta Neuropathol* **2014**, 128 (4), 485.
- (80) Zhang, Y.-J.; Gendron, T. F.; Grima, J. C. *et al.* C9ORF72 poly(GA) aggregates sequester and impair HR23 and nucleocytoplasmic transport proteins. *Nat. Neurosci.* **2016**, 19, 668.
 - (81) Lee, S. J. C.; Nam, E.; Lee, H. J. *et al.* Towards an understanding of amyloid- β oligomers: characterization, toxicity mechanisms, and inhibitors. *Chemical Society Reviews* **2017**, 46 (2), 310.
 - (82) Lee, S. M.; Asress, S.; Hales, C. M. *et al.* TDP-43 cytoplasmic inclusion formation is disrupted in C9orf72-associated amyotrophic lateral sclerosis/frontotemporal lobar degeneration. *Brain Communications* **2019**, 1 (1).
 - (83) Khosravi, B.; Hartmann, H.; May, S. *et al.* Cytoplasmic poly-GA aggregates impair nuclear import of TDP-43 in C9orf72 ALS/FTLD. *Hum. Mol. Genet.* **2016**, 26 (4), 790.
 - (84) Nonaka, T.; Masuda-Suzukake, M.; Hosokawa, M. *et al.* C9ORF72 dipeptide repeat poly-GA inclusions promote intracellular aggregation of phosphorylated TDP-43. *Hum. Mol. Genet.* **2018**, 27 (15), 2658.
 - (85) Bamford, C. H.; Norrish, R. G. W. 359. Primary photochemical reactions. Part VII. Photochemical decomposition of isovaleraldehyde and di-n-propyl ketone. *Journal of the Chemical Society (Resumed)* **1935**, 1504.
 - (86) Rich, D. H.; Gurwara, S. K. Removal of protected peptides from an ortho-nitrobenzyl resin by photolysis. *J. Chem. Soc., Chem. Commun.* **1973**, 610.
 - (87) Rich, D. H.; Gurwara, S. K. Preparation of a new o-nitrobenzyl resin for solid-phase synthesis of tert-butyloxycarbonyl-protected peptide acids. *Journal of the American Chemical Society* **1975**, 97 (6), 1575.
 - (88) Lu, H.; Wang, J.; Bai, Y. *et al.* Ionic polypeptides with unusual helical stability. *Nat. Commun.* **2011**, 2, 206.
 - (89) Chen, W.-S.; Chen, Y.-J.; Huang, Y.-A. *et al.* Ran-dependent TPX2 activation promotes acentsosomal microtubule nucleation in neurons. *Sci. Rep.* **2017**, 7 (1), 42297.
 - (90) Chen, W.; Young, L. J.; Lu, M. *et al.* Fluorescence Self-Quenching from Reporter Dyes Informs on the Structural Properties of Amyloid Clusters Formed in Vitro and in Cells. *Nano Lett.* **2017**, 17 (1), 143.
 - (91) Chou, C.-C.; Zhang, Y.; Umoh, M. E. *et al.* TDP-43 pathology disrupts nuclear pore complexes and nucleocytoplasmic transport in ALS/FTD. *Nat. Neurosci.* **2018**, 21 (2), 228.
 - (92) Kinoshita, Y.; Ito, H.; Hirano, A. *et al.* Nuclear Contour Irregularity and Abnormal

- Transporter Protein Distribution in Anterior Horn Cells in Amyotrophic Lateral Sclerosis. *J. Neuropathol. Exp. Neurol.* **2009**, 68 (11), 1184.
- (93) Liu, K.-Y.; Shyu, Y.-C.; Barbaro, B. A. *et al.* Disruption of the nuclear membrane by perinuclear inclusions of mutant huntingtin causes cell-cycle re-entry and striatal cell death in mouse and cell models of Huntington's disease. *Hum. Mol. Genet.* **2015**, 24 (6), 1602.
- (94) Paonessa, F.; Evans, L. D.; Solanki, R. *et al.* Microtubules Deform the Nuclear Membrane and Disrupt Nucleocytoplasmic Transport in Tau-Mediated Frontotemporal Dementia. *Cell Reports* **2019**, 26 (3), 582.
- (95) Diez, L.; Wegmann, S. Nuclear Transport Deficits in Tau-Related Neurodegenerative Diseases. *Front. Neurol.* **2020**, 11 (1056).
- (96) Freibaum, B. D.; Lu, Y.; Lopez-Gonzalez, R. *et al.* GGGGCC repeat expansion in C9orf72 compromises nucleocytoplasmic transport. *Nature* **2015**, 525 (7567), 129.
- (97) Chew, J.; Gendron, T. F.; Prudencio, M. *et al.* C9ORF72 repeat expansions in mice cause TDP-43 pathology, neuronal loss, and behavioral deficits. *Science* **2015**, 348 (6239), 1151.
- (98) Fusco, G.; Chen, S. W.; Williamson, P. T. F. *et al.* Structural basis of membrane disruption and cellular toxicity by α -synuclein oligomers. *Science* **2017**, 358 (6369), 1440.
- (99) Westergard, T.; Jensen, Brigid K.; Wen, X. *et al.* Cell-to-Cell Transmission of Dipeptide Repeat Proteins Linked to C9orf72-ALS/FTD. *Cell Reports* **2016**, 17 (3), 645.

Chapter 2 : Developing the Auto-releasing Peptide Probe for Protein Fragment Aggregation Studies



I. Introduction

1-1 Amyloidogenic sequence of TDP-43 in ALS

In most ALS patients, cytoplasmic protein inclusions present a significant pathological hallmark and their correlation with disease progression is yet to be determined.¹ However, accumulating studies have shown transactive response DNA-binding protein 43 (TDP-43), a 45 kDa protein, is the main component within these cytosolic inclusions.² As a nuclear abundant protein, the detailed functions of TDP-43 are majorly involving in DNA transcriptional regulation, RNA splicing, and translational regulation.³ However, in tissue samples from ALS patients, TDP-43 was hyper-ubiquitinated, hyper-phosphorylated, truncated into C-terminal fragments, and tended to accumulate in cytoplasm.^{2,4,5} Our group have previously demonstrated that a fragment in C-terminus domain of TDP-43 was capable of forming amyloidogenic fibrils and seeding the full-length TDP-43.^{6,7} This fragment, named as D1core, has been proved to form amyloid oligomers and ThT-positive fibrils *in vitro*; nevertheless, its cytotoxicity is less clear. In order to properly address toxicity, one must efficiently deliver the D1core peptides into the cell models. The high molecular weight and poor solubility of D1core, however, has impeded the passive diffusion of D1core fragments into the cytoplasm.

1-2 Delivery of peptides and proteins into cytoplasm

Cytoplasmic membranes protect cells from the outer toxins and only permit the small molecules to transverse freely via protein channels or passive diffusion.^{8,9} Thus, macromolecules, such as DNA, peptides, proteins, and antibodies, are usually excluded outside of cytoplasmic membranes. In order to efficiently deliver macromolecules, several methods based on different principles have already been developed.

Microinjection is a widely-used tool for intracellular delivery of molecules including small-molecule drugs and even antibodies.¹⁰ Our group has applied the microinjection method to enable releasing another amyloidogenic peptide, QN1, in the cells, which allowed us to monitor the aggregation process in real-time.¹¹ Nevertheless, it is not practical to investigate cytotoxicity and detailed mechanism in a large scale with statistical analysis through the microinjection method due to technical issues.

As a commonly used transfection tool, electroporation has been intensively surveyed as a platform to transport proteins or peptides into cells.^{12,13} Through the transient enhancement of membrane permeability, macromolecules were permitted to transverse the stubborn plasma membrane. It is critical to note that fine adjustment was required in electroporation for different cell lines due to disparate membrane composition and membrane potential.

Another common strategy to transport peptides or proteins is to decorate

macromolecules with cell-penetrating peptide (CPPs) sequence.¹⁴⁻¹⁸ These CPPs are usually comprising hydrophobic and positive amino acid residues, which results in a positive net charge of these sequences at physiological conditions. Though the detailed mechanism is yet to be determined, studies have suggested that CPPs may first bind to the glycan on the membrane surface or negatively-charged phosphate group on lipid via electrostatic force, then enter the cell via endocytosis, and finally release the cargoes in the cytoplasm through endosomal escape.^{19,20} It has been shown fluorescent proteins and nanobodies can thus be transported to cytoplasm through conjugation to CPPs.²¹ Unfortunately, some CPPs may affect the localization of cargoes in cells, leading them to accumulate in the nucleus or other cellular compartments; therefore, CPPs that attached to cargoes must be selected with caution.

1-3 Research aim and experimental design

In order to comprehensively elucidate D1core toxicity in cells, we attempted to deliver D1core peptides without the further interference from CPPs after releasing from the endosome. Therefore, we inserted a disulfide bond spacer composed in the bridge of CPPs and D1core, which will be reduced and cleaved in the reducing environment to release the D1core fragments in the cytoplasm (Figure 17).

To prepare the peptide probe, we aim to conjugate two cysteines through the thiol

groups on their side chain. Several reagents have been reported to catalyze the formation of disulfide bond between cysteines in the solution.^{22,23} Among them, Ellman's reagent represents a catalyzer with a fast reaction rate and high yield since it allows the further disulfide exchange reaction.²² However, normal disulfide exchange reactions activated by Ellman's reagent in solution will inevitably generate byproducts from homo-coupling and the quantity of product from a single batch is limited,²⁴ we thus introduced the solid-phase synthesis combining with Ellman's reagent to minimize the homo-coupling mislocalization byproducts and provide large scale preparation.

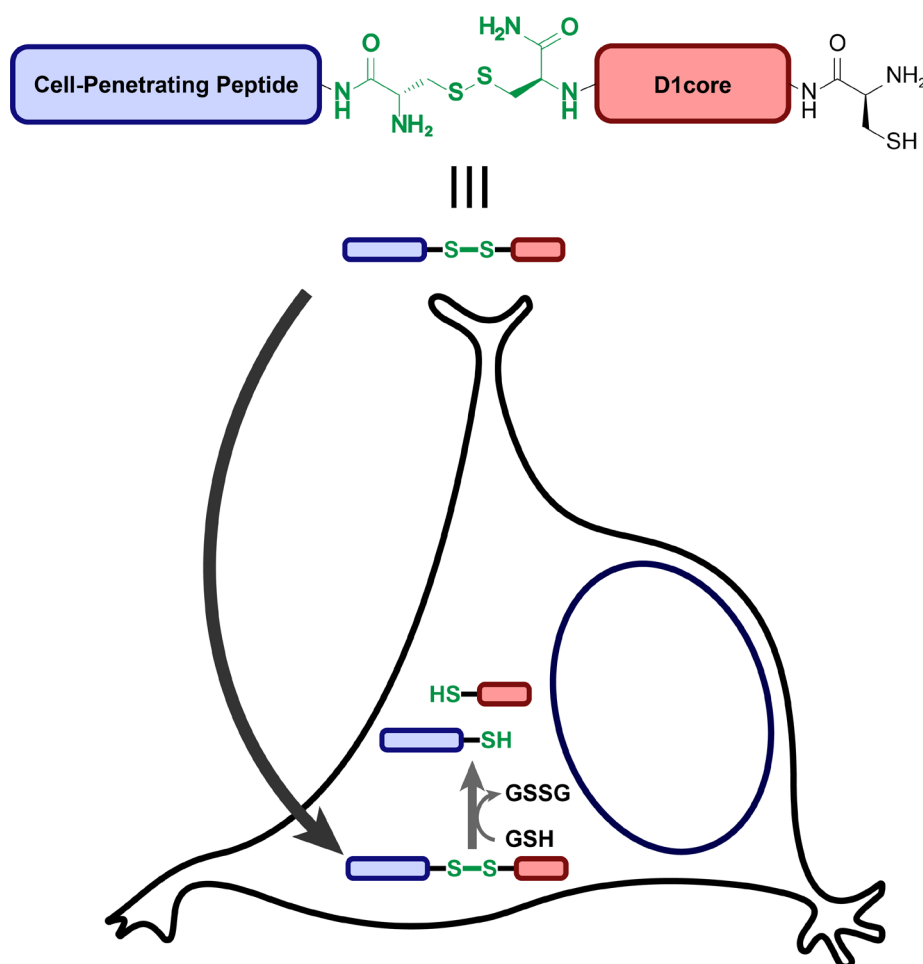


Figure 17. Model of auto-releasing probe and its anticipated reaction in cells.

II. Material and Methods



2-1 Material and instruments list

Material list

Reagents	CAS no.	Suppliers
Fmoc-Arg(Pbf)-OH	154445-77-9	AnaSpec
Fmoc-Cys(Mmt)-OH	177582-21-7	AnaSpec
Fmoc-Cys(Trt)-OH	103213-32-7	AnaSpec
Fmoc-Met-OH	71989-28-1	AnaSpec
Fmoc-Gly-OH	29022-11-5	AnaSpec
Fmoc-Asn(Trt)-OH	132388-59-1	AnaSpec
Fmoc-Phe-OH	35661-40-6	AnaSpec
Fmoc-Ala-OH	35661-39-3	AnaSpec
Fmoc-Ser(tBu)-OH	71989-33-8	AnaSpec
Fmoc-Ile-OH	71989-23-6	AnaSpec
Fmoc-Pro-OH	71989-31-6	AnaSpec
5,5' -Dithiobis(2-nitrobenzoic acid)	69-78-3	Sigma-Aldrich
Rink Amide AM Resin (200-400 mesh)	<i>None</i>	Merck-Millipore
Acetonitrile	75-05-8	Fisher Scientific
Dichloromethane	75-09-2	Seedchem
Ethanol	64-17-5	J.T. Baker
N,N-Dimethylformamide	68-12-2	ECHO Chemicals
Methyl tert-butyl ether	1634-04-4	TEDIA
2-(1H-Benzotriazole-1-yl)-1,1,3,3-tetramethyluronium hexafluorophosphate	94790-37-1	Alfa Aesar
N,N-Diisopropylethylamine	7087-68-5	Sigma-Aldrich
Piperidine	110-89-4	ECHO Chemicals
Trifluoroacetic Acid	76-05-1	Sigma-Aldrich
Triisopropylsilane	6485-79-6	Sigma-Aldrich
1,2-Ethanedithiol	540-63-6	Sigma-Aldrich
Sodium chloride	7647-14-5	TCI Chemicals
Potassium chloride	7447-40-7	TCI Chemicals
Sodium phosphate dibasic	7558-79-4	Fisher Scientific
Alexa Fluor™ 568 C5 Maleimide		Thermo-Fisher
Thioflavin T	2390-54-7	Sigma-Aldrich
Uranyl acetate	541-09-3	Provide by IMB,AS

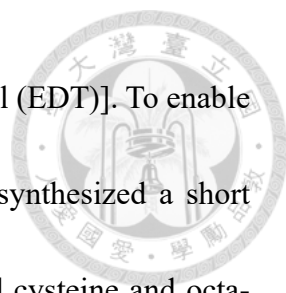
Paraformaldehyde	30525-89-4	Thermo-Fisher
Tris(hydroxymethyl)aminomethane	77-86-1	Sigma-Aldrich
Dulbecco's modified Eagle's medium	None	Invitrogen
Glutamine	56-85-9	Thermo-Fisher
Fetal bovine serum	9014-81-7	Thermo-Fisher
Penicillin-Streptomycin	None	Invitrogen

Instrument list

Instruments	Model	Company
Automated peptide synthesizer	Liberty Blue™	CEM Corporation, U.S.A.
High-performance liquid chromatography	1260 Infinity LC System	Agilent, U.S.A.
HPLC Column	Spolar C18	Shiseido, Japan
Lyophilizer	CoolSafe 4-15L	LaboGene, Denmark
Mass spectrometer	New ultrafleXtreme™	Bruker, U.S.A.
Circular dichroism spectrophotometer	J-815	JASCO, Japan
Fluorescence spectrophotometer	F-4500	Hitachi, Japan
UV-Vis spectrophotometer	DU 800	Beckman, U.S.A.
Electron microscope	JEM-2011	JEOL, Japan
Confocal microscope	LSM 880	Zeiss, Germany
Eppendorf mixer/ incubator	Thermomixer	Eppendorf, Germany

2-2 Synthesis and characterization of auto-releasing probe

Peptides were synthesized by the Fmoc-protecting polyamide chemistry on Rink Amide AM resin using the microwave-assisted automated peptide synthesizer Liberty Blue™ [Activator: 2-(1H-Benzotriazole-1-yl)-1,1,3,3-tetramethyluronium hexafluorophosphate (HBTU) ; Activator base: N,N-Diisopropylethylamine (DIEA) ; Deprotection: 20% Piperidine in N,N-Dimethylformamide (DMF) ; Main solvent: DMF]. Sequence Cys-D1core (CMGGGMNFGAFSINPAM) was first synthesized using liberty blue and cleaved from the resin by cleavage cocktail [90 % Trifluoroacetic Acid (TFA) /



2.5 % water / 2.5 % Triisopropylsilane (TIPS) / 5 % 1,2-Ethanedithiol (EDT)]. To enable on-beads synthesis of disulfide bond containing peptide, we then synthesized a short fragment of cell-penetrating sequence, monomethoxytrityl-protected cysteine and octa-arginine [(MMT)-CR₈], on the resin. 2% TFA solution was used to deprotect MMT group for the following disulfide bond formation. The **Resin-R₈-Cys** was then activated by 10 equivalent of Ellman's reagent [5,5'-dithiobis-(2-nitrobenzoic acid)] in 60 °C overnight to form a stable disulfide bond intermediate, **Resin-R₈-Cys-TNB**. The complete of this reaction is by monitoring the absorbance at 412 nm. After wash with DMF (3 × 10 mL), the resin attached with TNB-Cys-R₈ was then immersed in a DMF solution containing 2 equivalent of Cys-D1core and agitated for 12 hours at room temperature. The resulting peptide was cleaved from the resin by cleavage cocktail [95 % Trifluoroacetic Acid (TFA) / 2.5 % water / 2.5 % Triisopropylsilane (TIPS)]. The cocktail solution was then mixed with methyl t-butyl ether for precipitation of peptides which was later purified by high-performance liquid chromatography (HPLC) equipped with a C18 reverse-phase semi-preparative column (Shiseido, Japan). Gradient separation of peptides was accomplished by mixing buffer A (5 % Acetonitrile (ACN) / 0.1 % TFA / 94.9 % water) and buffer B (0.1 % TFA / 99.9 % acetonitrile). Collecting purified peptides was analyzed and identified by matrix-assisted laser desorption/ionization - time of flight (MALDI-TOF) mass spectroscopy (New ultrafleXtreme™).

2-3 General sample preparation for *in vitro* measurements

Peptides (50 μM) was prepared in deionized water. For the test of peptide release in the presence of reducing agent, peptide solution (50 μM) was prepared in the solution containing 5 equivalent of glutathione (250 μM). Resulting peptide samples were incubated at 37 $^{\circ}\text{C}$ for *in vitro* characterization.

2-4 UV-Vis spectroscopy

The measurements of DNB^{2-} ion in DMF was achieved with 1 cm quartz cuvette on UV-Vis spectrophotometer.

2-5 Transmission electron microscopy

5 μL aliquot of peptides solution was applied on the grow-charged 300 mesh Formvar- and carbon-coated copper grids, and then stained with 2 % uranyl acetate. After drying overnight, grid samples were analyzed by electron microscope.

III. Results



3-1 Preparation of probe JJS-4 & JJS-5

To enable the large-quantity and high purity preparation of disulfide bond-conjugated probes, we employed on-resin synthesis rather than solution-based reaction. We first synthesized the cargo peptide, Cys-D1core (CMGGGMNFGAFSINPAM), via automated microwave-assisted peptide synthesizer (Liberty Blue, CEM Corporation, U.S.A.) with Fmoc-protecting chemistry method (Figure 18). Next, to couple the cargo peptide, **Cys-D1core**, with the cell-penetrating sequence on the resin through disulfide bond. Here, octaarginine was chosen for its high solubility and endocytosis efficiency.²⁵ The octaarginine with a cysteine carrying monomethoxytrityl (Mmt) protective group onside-chain was prepared then (Figure 18). The purpose of using Mmt-protective cysteine here is to enable deprotection of thiol on the side chain at mild acidic condition while the peptides were still attached to resins. Accordingly, we used 2 % trifluoroacetic acid in water to remove the Mmt protecting group. Next, **Resin-Arg₈-Cys** was activated by Ellman's reagent, namely 5,5'-dithiobis-(2-nitrobenzoic acid), through disulfide bond exchange to obtain the stable intermediate **Resin-Arg₈-Cys-TNB**. Given that this disulfide exchange reaction is stoichiometric and it released an equivalent of 2-nitro-5-thiobenzoate (TNB) ions with the highest UV-Vis absorbance at 484 nm with molar

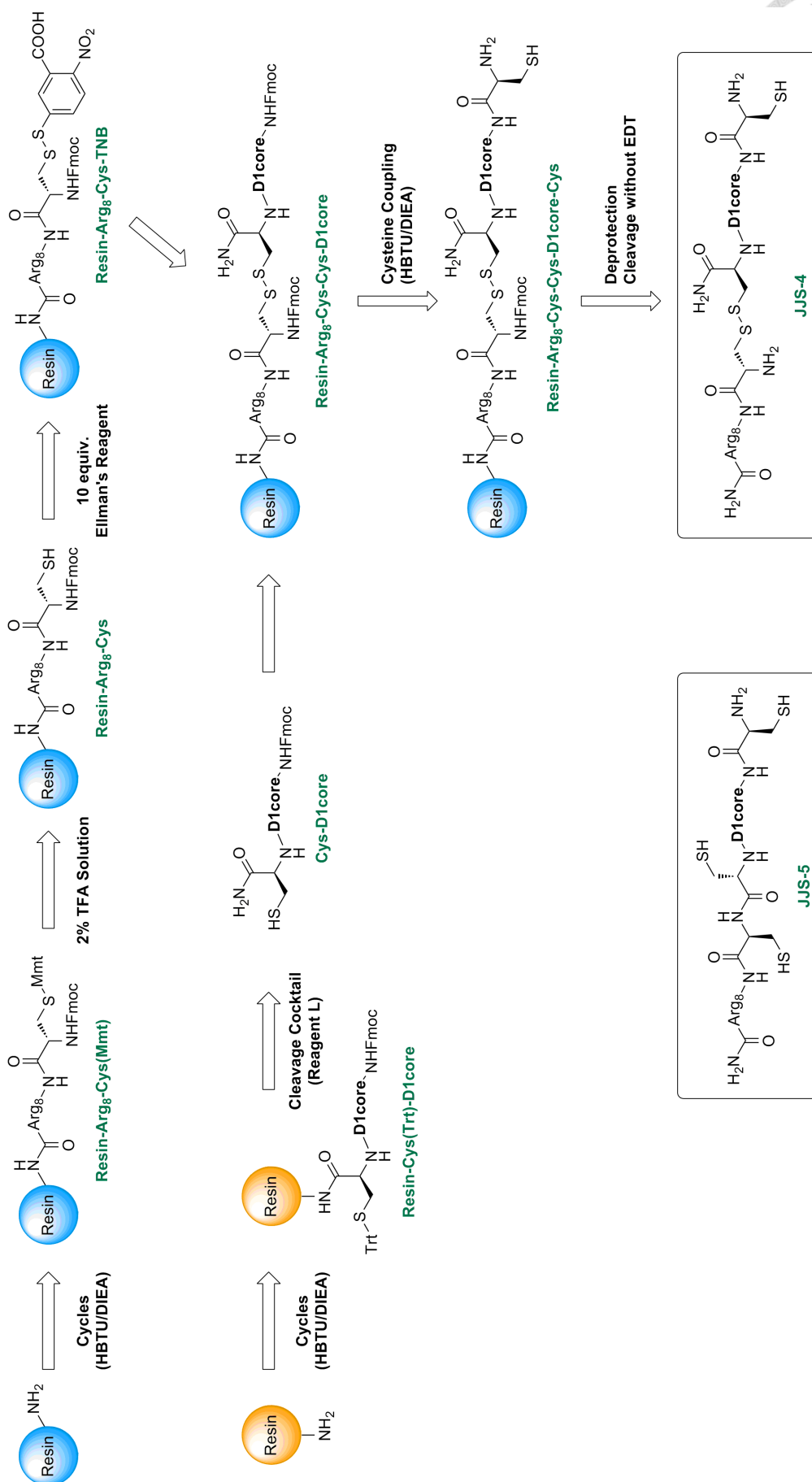


Figure 18. Synthesis scheme of JJS-4 and JJS-5.

attenuation coefficient around 14150 M^{-1} in DMF, so we can easily monitor the disulfide bond exchange reaction by measuring diluted reaction solution. As we depicted in Figure 19, the disulfide exchange from **Resin-Arg₈-Cys** to **Resin-Arg₈-Cys-TNB** is saturated within an hour. With **Resin-Arg₈-Cys-TNB** at hand, we next attempted to couple it with our cargo peptide, **Cys-D1core**. The **Resin-Arg₈-Cys-TNB** was immersed in dimethylformamide solution containing 2 equivalent of Cys-D1core and agitated for 12

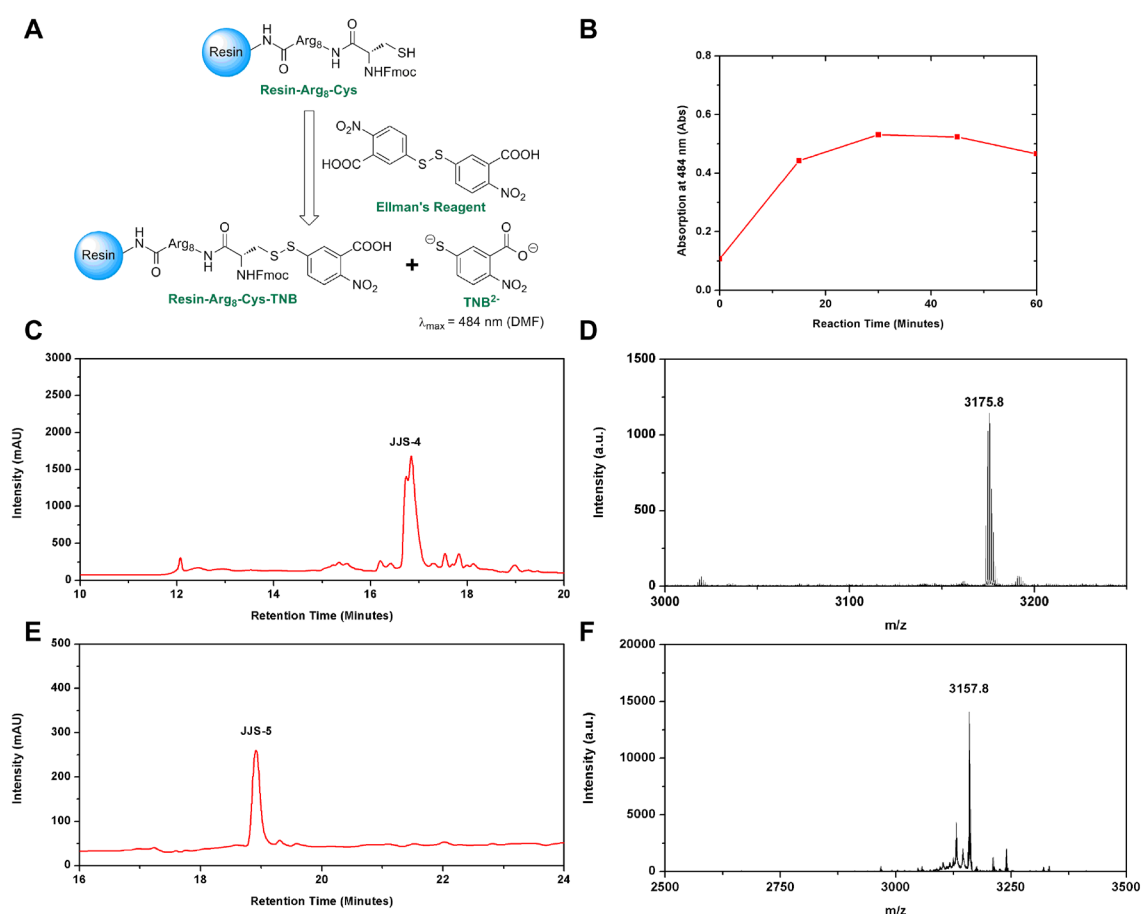
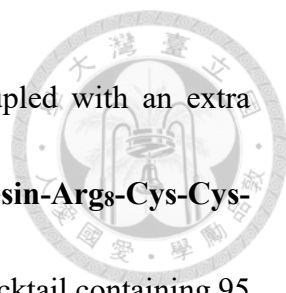


Figure 19. Disulfide bond exchange reaction monitoring and identification of JJS-4 and JJS-5. (A) Scheme of Ellman's reagent activated disulfide bond exchange reaction. **(B)** The time-course absorption spectra (484 nm) of TNB^{2-} ion in DMF. Data were collected at 0th, 15th, 30th, 45th, and 60th minutes after mixing of Resin-Arg₈-Cys with Ellman's reagent. **(C)** HPLC spectrum of JJS-4. **(D)** MALDI-TOF mass spectrum of JJS-4, calc. mass: 3176.6; observed: 3175.8 ($[M]^+$). **(E)** HPLC spectrum of JJS-5. **(F)** MALDI-TOF mass spectrum of JJS-5, calc. mass: 3158.5; observed: 3157.8 ($[M]^+$).



hours to obtain **Resin-Arg₈-Cys-Cys-D1core** which was later coupled with an extra cysteine on the end of peptide for fluorophore labeling. The **Resin-Arg₈-Cys-Cys-D1core-Cys** was then deprotected by piperidine and cleaved by cocktail containing 95 % trifluoroacetic acid, 2.5 % triisopropylsilane, and 2.5 % water to get the peptide crude. For cleaving the peptides from resin, one has to note that thiols like 1,2-ethylenedithiol must be excluded for their ability to reduce the disulfide bond. The resulting peptide, **JJS-4**, was later purified with high-performance liquid chromatography and identified by mass spectroscopy (Figure 19). In parallel, we also synthesized the control peptide, **JJS-5**, which shared the same sequence in **JJS-4** but differed in their cysteine bonding. **JJS-5** used amide bond to couple cell-penetrating sequence and cargo peptide instead of disulfide bond.

3-2 *In vitro* characterization of auto-releasing probes

With the JJS-4 in hand, we next aim to understand whether JJS-4 can successfully release the cargo peptide in a reducing environment. As mentioned earlier that the cytoplasm is enriched with reducing agents like glutathione, we accordingly mixed our probes with 5 equivalents of glutathione in water at 37 °C to test the cleavage efficiency. From our reaction kinetic analysis through HPLC and mass spectroscopy (Figure 20A), we confirmed that JJS-4 can be cleaved into cargo peptide, Cys-D1core-Cys, and the cell-

penetrating peptide, Cys-Arg8, within 90 minutes.

We next would like to examine whether the cargo peptide, Cys-D1core-Cys, can form amyloid fibrils after releasing from probe in the reducing environment. Through transmission electron microscopy (Figure 20B), we found JJS-4 treated with glutathione formed fibrillar structure after 2 days incubation. Instead, neither JJS-4 without glutathione treatment nor JJS-5 failed to form any fibrillar-like structure.

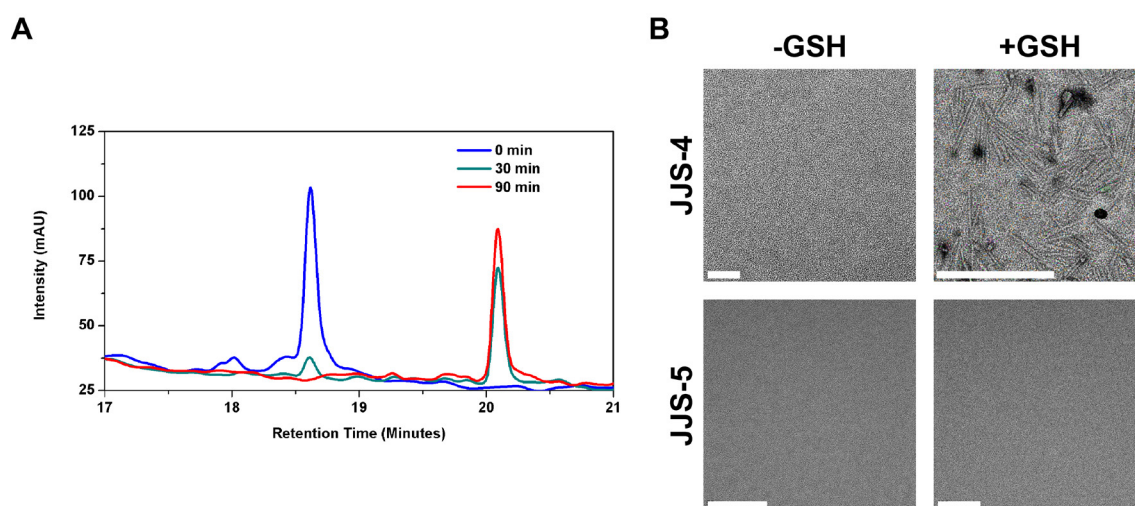


Figure 20. GSH mediated reductive cleavage of JJS-4. (A) The HPLC spectra of JJS-4 (100 μ M) in the presence of GSH (500 μ M) under different reaction time points. (B) TEM images of JJS-4 and JJS-5 in the presence or absence of GSH. Scale bar indicates 200 nm.

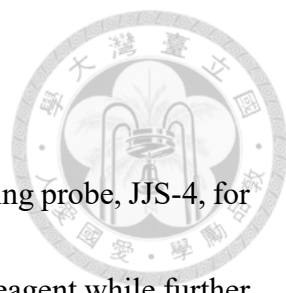
IV. Discussion



4-1 Comparison between photoinducible probe and auto-releasing probe

Previously, our group has developed a photoinducible probe to deliver amyloidogenic fragments into cells via methoxynitrobenzene chemistry.²⁶ However, the photoinitiation condition may cause DNA damage in some fragile cells such as neurons. Therefore, we would like to develop an alternative strategy to deliver amyloid fragments in a milder condition. As the cleavage efficiency of JJS-4 in the reducing environment and some of its biophysical properties were examined, we will test our auto-releasing probe in a cell model. Comparing to the rapid photolysis reaction of the photoinducible probe, the cleavage reaction of JJS-4 apparently took a longer time to release the cargo. We surmised that the difference may correlate with the multiple steps in the cleavage reaction of JJS-4 in the presence of GSH. Usually, the reduction of disulfide bond by GSH involved an exchange mechanism. The thiol on GSH can undergo a substitution reaction with $R_1-S-S-R_2$ to form $R_1-S-S-GSH$ and $R_2-S-S-GSH$ intermediates, another GSH molecule can subsequently react with these intermediates to form oxidized glutathione disulfide (GSSG) and simultaneously release R_1 and R_2 . The two steps intermolecular reaction of reductive cleavage may be the main reason behind its slower releasing efficiency.

4.2 Conclusion and prospect

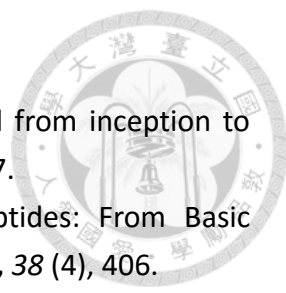


In summary, we have developed a method to prepare auto-releasing probe, JJS-4, for peptide aggregation studies via solid-state synthesis using Ellman's reagent while further optimization of reaction is underway. Through the HPLC and mass spectroscopy, we carefully examined the reductive cleavage condition of JJS-4 by glutathione *in vitro* and monitored its cleavage kinetics overtime. In addition, the released D1core is capable of forming fibrils under a glutathione-rich environment. With JJS-4 at our hand, we will directly focus on the practice of reductive cleavage of the probe in cells and the investigation of releasing amyloidogenic peptide aggregation studies *in vivo*. We expected that the auto-releasing probe may serve to provide more insight into the pathological roles of amyloidogenic peptides in diseases in the future.



V. Reference

- (1) Brown, R. H.; Al-Chalabi, A. Amyotrophic Lateral Sclerosis. *New England Journal of Medicine* **2017**, 377 (2), 162.
- (2) Neumann, M.; Sampathu, D. M.; Kwong, L. K. *et al.* Ubiquitinated TDP-43 in Frontotemporal Lobar Degeneration and Amyotrophic Lateral Sclerosis. *Science* **2006**, 314 (5796), 130.
- (3) Prasad, A.; Bharathi, V.; Sivalingam, V. *et al.* Molecular Mechanisms of TDP-43 Misfolding and Pathology in Amyotrophic Lateral Sclerosis. *Frontiers in Molecular Neuroscience* **2019**, 12 (25).
- (4) Arai, T.; Hasegawa, M.; Akiyama, H. *et al.* TDP-43 is a component of ubiquitin-positive tau-negative inclusions in frontotemporal lobar degeneration and amyotrophic lateral sclerosis. *Biochemical and Biophysical Research Communications* **2006**, 351 (3), 602.
- (5) Kametani, F.; Hasegawa, M.; Nonaka, T. *et al.* Truncation and pathogenic mutations facilitate the formation of intracellular aggregates of TDP-43. *Hum. Mol. Genet.* **2009**, 18 (18), 3353.
- (6) Chen, A. K. H.; Lin, R. Y. Y.; Hsieh, E. Z. J. *et al.* Induction of Amyloid Fibrils by the C-Terminal Fragments of TDP-43 in Amyotrophic Lateral Sclerosis. *Journal of the American Chemical Society* **2010**, 132 (4), 1186.
- (7) Liu, G. C.-H.; Chen, B. P.-W.; Ye, N. T.-J. *et al.* Delineating the membrane-disrupting and seeding properties of the TDP-43 amyloidogenic core. *Chemical Communications* **2013**, 49 (95), 11212.
- (8) Stewart, M. P.; Langer, R.; Jensen, K. F. Intracellular Delivery by Membrane Disruption: Mechanisms, Strategies, and Concepts. *Chemical Reviews* **2018**, 118 (16), 7409.
- (9) Fu, A.; Tang, R.; Hardie, J. *et al.* Promises and Pitfalls of Intracellular Delivery of Proteins. *Bioconjugate Chemistry* **2014**, 25 (9), 1602.
- (10) Zhang, Y.; Yu, L.-C. Microinjection as a tool of mechanical delivery. *Current Opinion in Biotechnology* **2008**, 19 (5), 506.
- (11) He, R.-Y.; Huang, Y.-C.; Chiang, C.-W. *et al.* Characterization and real-time imaging of the FTLD-related protein aggregation induced by amyloidogenic peptides. *Chemical Communications* **2015**, 51 (41), 8652.
- (12) Gehl, J. Electroporation: theory and methods, perspectives for drug delivery, gene therapy and research. *Acta Physiologica Scandinavica* **2003**, 177 (4), 437.
- (13) Cao, Y.; Ma, E.; Cestellos-Blanco, S. *et al.* Nontoxic nanopore electroporation for effective intracellular delivery of biological macromolecules. *Proceedings of the*

- 
- National Academy of Sciences* **2019**, 116 (16), 7899.
- (14) Magzoub, M.; Gräslund, A. Cell-penetrating peptides: small from inception to application. *Quarterly Reviews of Biophysics* **2004**, 37 (2), 147.
 - (15) Guidotti, G.; Brambilla, L.; Rossi, D. Cell-Penetrating Peptides: From Basic Research to Clinics. *Trends in Pharmacological Sciences* **2017**, 38 (4), 406.
 - (16) Allolio, C.; Magarkar, A.; Jurkiewicz, P. *et al.* Arginine-rich cell-penetrating peptides induce membrane multilamellarity and subsequently enter via formation of a fusion pore. *Proceedings of the National Academy of Sciences* **2018**, 115 (47), 11923.
 - (17) Derakhshankhah, H.; Jafari, S. Cell penetrating peptides: A concise review with emphasis on biomedical applications. *Biomedicine & Pharmacotherapy* **2018**, 108, 1090.
 - (18) Dougherty, P. G.; Sahni, A.; Pei, D. Understanding Cell Penetration of Cyclic Peptides. *Chemical Reviews* **2019**, 119 (17), 10241.
 - (19) Ruseska, I.; Zimmer, A. Internalization mechanisms of cell-penetrating peptides. *Beilstein Journal of Nanotechnology* **2020**, 11, 101.
 - (20) Yesylevskyy, S.; Marrink, S.-J.; Mark, A. E. Alternative Mechanisms for the Interaction of the Cell-Penetrating Peptides Penetratin and the TAT Peptide with Lipid Bilayers. *Biophysical Journal* **2009**, 97 (1), 40.
 - (21) Herce, H. D.; Schumacher, D.; Schneider, A. F. L. *et al.* Cell-permeable nanobodies for targeted immunolabelling and antigen manipulation in living cells. *Nature Chemistry* **2017**, 9 (8), 762.
 - (22) Ellman, G. L. Tissue sulfhydryl groups. *Archives of Biochemistry and Biophysics* **1959**, 82 (1), 70.
 - (23) Mandal, B.; Basu, B. Recent advances in S–S bond formation. *RSC Advances* **2014**, 4 (27), 13854.
 - (24) Riddles, P. W.; Blakeley, R. L.; Zerner, B. Reassessment of Ellman's reagent. *Methods in Enzymology* **1983**, 91, 49.
 - (25) Nakase, I.; Noguchi, K.; Aoki, A. *et al.* Arginine-rich cell-penetrating peptide-modified extracellular vesicles for active macropinocytosis induction and efficient intracellular delivery. *Scientific Reports* **2017**, 7 (1), 1991.
 - (26) He, R.-Y.; Chao, S.-H.; Tsai, Y.-J. *et al.* Photocontrollable Probe Spatiotemporally Induces Neurotoxic Fibrillar Aggregates and Impairs Nucleocytoplasmic Trafficking. *ACS Nano* **2017**, 11 (7), 6795.